UNCLASSIFIED
SECURITY CLASSIFICATION OF THIS PAGE (When Data Entered)

REPORT DOCUMENTATION PAGE		READ INSTRUCTIONS BEFORE COMPLETING FORM
1. REPORT NUMBER AFFDL-TR-75-47	2. GOVT ACCESSION NO.	3. RECIPIENT'S CATALOG NUMBER
4. TITLE (and Subtitle) Application of Differential Games to Air-To-Air Combat Problems		5. TYPE OF REPORT & PERIOD COVERED Final Report April 1973 to February 1974 6. PERFORMING ORG. REPORT NUMBER
7. AUTHOR(s) L. Earl Miller		8. CONTRACT OR GRANT NUMBER(s)
9. PERFORMING ORGANIZATION NAME AND ADDRESS Air Force Flight Dynamics Laboratory Wright-Patterson Air Force Base, Ohio 45433		10. PROGRAM ELEMENT, PROJECT, TASK AREA & WORK UNIT NUMBERS 13660213 & 13660214
11. CONTROLLING OFFICE NAME AND ADDRESS Air Force Flight Dynamics Laboratory Wright-Patterson Air Force Base, Ohio 45433		12. REPORT DATE July 1975 13. NUMBER OF PAGES 169
14. MONITORING AGENCY NAME & ADDRESS(if different from Controlling Office)		15. SECURITY CLASS. (of this report) Unclassified 15a. DECLASSIFICATION/DOWNGRADING SCHEDULE

16. DISTRIBUTION STATEMENT (of this Report)

Approved for public release; distribution unlimited.

17. DISTRIBUTION STATEMENT (of the abstract entered in Block 20, if different from Report)

18. SUPPLEMENTARY NOTES

Doctor of Philosophy Dissertation

19. KEY WORDS (Continue on reverse side if necessary and identify by block number)

Differential Games
Optimal Control
Differential Game Barriers
Air-to-Air Combat
Tactics Optimization
Maneuvering Analysis
Zero-Sum Games

20. ABSTRACT (Continue on reverse side if necessary and identify by block number)

Differential game barrier theory was applied to three pursuit-evasion problems. For the first problem the solution involving the angle-off constraint was directly determined from the natural barrier solution. For the second problem the capture range was relatively insensitive to the angle-off. The solution to the third problem which approximates the terminal part of air-to-air combat showed that an increase in the pursuer's speed or a decrease in his minimum radius of turn resulted in a decrease in the capture range.

DD FORM 1 JAN 73 1473 EDITION OF 1 NOV 65 IS OBSOLETE

UNCLASSIFIED
SECURITY CLASSIFICATION OF THIS PAGE (When Data Entered)

FOREWORD

This report was prepared by personnel of the High Speed Aero Performance Branch, Flight Mechanics Division of the Air Force Flight Dynamics Laboratory (AFFDL/FXG), Wright-Patterson Air Force Base, Ohio. This research was accomplished under Task 13660213, "Application of Differential Game Theory to Combat Aircraft Design and Synthesis of Combat Tactics," and Task 13660214, "Air-to-Air Combat Differential Game Computer Program."

The effort reported here covered the period from April 1973 to February 1974. Acknowledgment is made to Professor A. B. Bishop of The Ohio State University who served as the adviser for this research which culminated in the award of Doctorate of Philosophy in March 1974. Special acknowledgment is extended to Lt Col Bill Othling and Lt Jim Rader for their review of this report.

TABLE OF CONTENTS

LIST OF ILLUSTRATIONS

LIST OF TABLES

LIST OF SYMBOLS AND ABBREVIATIONS

a_N	normal acceleration
a_Y	acceleration component along the velocity vector
A_1, B_1, C_o	integration constants
A,B	control functions
BUP	boundary of the usable part
C	control function, acceleration ratio, or terminal surface
C_D	aerodynamic drag coefficient
C_L	aerodynamic lift coefficient
C_T	engine control function
C_4, C_5	Problem III performance parameters
D	aerodynamic drag
$\bar{e}$	unit vector
E	evader
f	differential state vector function or barrier closure equation
F	Problem III barrier closure equation
g	acceleration of gravity
h_i	i^{th} component of terminal surface
k	induced drag factor
$\bar{L}$	nondimensional capture range
L	capture range
n	nondimensional normal acceleration

NUP	nonusable part
P	pursuer
Q	dynamic pressure
R	minimum radius of turn or ratio of minimum turning radii
s, s^*, s_1, s_2	terminal surface parameters
S	terminal surface parameter, reference area, or sensitivity parameters
t	time
T	thrust or Laplace transform
UP	usable part
$u, \bar{u}$	pursuer's nondimensional speed and pursuer's vector control function
u_K, v_K	k^{th} components of pursuer's and evader's vector control functions
u^*, v^*	optimal pursuer and evader control vectors
$v, \bar{v}$	evader's nondimensional speed and evader's vector control function
v_1, v_2	control functions in Problem III particular solution
V	speed
W	weight
$\bar{x}$	state vector
x, y	reduced coordinate frame components
X, Y	nondimensional coordinates
z	reduced coordinate component or Laplace transform
α	turning performance control variable
$\alpha_1, \ldots, \alpha_5$	performance parameters
β	nondimensional time

$\bar{\beta}$	barrier nondimensional closure time
$\delta_1, \gamma, \Delta, \sigma$	angular displacements
δ_2	pursuer's control variable
ϵ, $\bar{\epsilon}$	evader's speed/pursuer's speed
θ	angle-off constraint
$\lambda_0, \ldots, \lambda_6$	Problem III performance parameters
$\wedge$	Problem II parameter
$\wedge_0, \wedge_1, \wedge_2$	Problem III performance parameters
$\nu_1, \ldots, \nu_6$	components of vector normal to barrier
$\bar{\nu}$	normal vector to barrier
ρ	atmospheric density
τ	nondimensional time
ϕ	control variable
ψ	angular displacement or control variable
ω	angular velocity

Subscripts

a_N	normal acceleration
A	artificial barrier
c	barrier closure condition
C	corner condition
C_L	lift coefficient condition
E	evader
f	final
H	homogeneous solution

MAX	maximum value
MIN	minimum value
N	natural barrier
o	terminal surface or singular arc condition
P	pursuer or particular solution
V_P	pursuer speed
W/S	weight/reference area
x,y,z	reduced coordinate frame
θ	angle-off

Superscripts

($\cdot$)	derivative of ( ) with respect to time
( )'	derivative of ( ) with respect to β
( )*	optimal value of ( )

SECTION I

INTRODUCTION

Historical Background

It was during World War I that the first air-to-air engagements between friendly and enemy aircraft took place. Initially aircraft were used only for reconnaissance purposes. Their role was to fly over the enemy lines, determine the enemy deployments and strengths, and then relay this information to the Army. Eventually aircraft from each side came into visual contact. This resulted in the observers' carrying rifles or handguns with which they fired at the enemy whenever the opportunity arose. Since this type of armament was ineffective, the observers started carrying machine guns.

Aircraft of this period were of two types, either tractors or pushers. Tractors had their engines mounted in the front whereas the pushers had their engines located at the rear of the fuselage. Consequently, the pushers could fire straight ahead, but they were less maneuverable than the tractors. The problem with the tractors was the danger of the machine gun bullets hitting the propeller and thereby shooting their own plane down. There were four ways of averting this catastrophe. The first way was to not fire the machine gun; this obviously was an unacceptable solution. The second way was to fire forward. (Obviously the gunner's cockpit was situated behind the pilot.) For the third way the gunner was ahead of the pilot and stood up in his

seat firing over the top wing of the biplane or triplane. The problem here was that while the bullets missed the propeller, the gunner was forced to stand in a slip stream of fifty to sixty miles per hour. In addition the pilot was maneuvering the aircraft to get into position for an effective shot, consequently there existed the hazard for the gunner of maintaining his position in the aircraft. If he did not, there was the risk of falling out of the aircraft. The fourth way consisted of the gunner seated behind the pilot with the machine gun attached to the coaming of the gunner's cockpit. The gun could be aimed upwards or sideways in addition to backwards. The problem with this approach was that when approaching the enemy from the rear the pilot had to turn the aircraft away from the other plane or attempt to fly alongside the enemy.

Until 1915, the most advantageous position was a position ahead of the enemy plane. This corresponded to firing the gun in either the second or fourth way, and resulted in both a good offensive and defensive position. The enemy could not fire for fear of his bullets striking the blades of his propeller. Since the lead aircraft was firing backwards, there was no danger of hitting its own propeller.

Early in 1915 the French developed a gun which could fire through the propeller. Imagine the consternation of the German crews when they managed to reach a position ahead of the French fighters thinking they were in a favorable tactical position only to be shot down by the French crews. At this point in the war the air struggle swung in favor of the French. Unfortunately for the Allies, a French

fighter equipped with the device for firing through the propeller made a forced landing behind the German lines. The pilot was captured before he could destroy his machine. The machine was taken to Berlin and turned over to a Dutch airplane designer, Anthony Fokker. His instructions were to adapt the French idea to the German Parabellum machine gun. Fokker received the French invention and the German machine gun on a Tuesday evening and by the following Friday had adapted an improved version to a German airplane. The French version had deflector plates attached to the propeller blades. Consequently there was risk of shooting off the blades or the inherent danger of ricochets from the blades hitting the pilot. Fokker designed an interrupter gear that resulted in the bullets passing between the blades, that is, he synchronized the propeller and machine gun.

These inventions resulted in the eventual disappearance of the two man fighters. There was no need for an additional crew member to fire the gun. The pilot flew the aircraft, aimed it at the enemy, and fired the gun. This also led to a change in fighter tactics. Two or more aircraft flew in formation. In pairs one fighter directed his search in finding the enemy while the other's duty was to protect his partner. Today the situation remains essentially the same.

Starting with World War I, aerial combatants attempted to defeat their adversaries, either through exploitation of their superior skill or superior aircraft over the other's capability or aircraft. History shows a small handful of fighter pilots were successful in achieving a significant number of kills. These fantastic pilots were able to meet and defeat the enemies with aircraft in which other

pilots either failed or had only moderate success. Thus only a small fraction were able to operate their systems in a way which appears to have approached optimal control. A fighter ace is defined to be a pilot that had five or more aerial kills. In this century, out of 45,000 pilots in World Wars I and II and the Korean conflict, there are only 1300 aces. This amounts to approximately three per cent.

There seem to be several characteristics common among these aces. Shooting ability rather than pilot skill was a pilot's most important asset. Few pilots achieved the ability of shooting from a moving platform at a moving target. Good eyesight was an attribute that resulted in attaining a favorable tactical position. This was more true in World War I where the speeds were slower than those in World War II and the Korean conflict. The best fighter pilots knew the strengths and weaknesses of their opponents as well as of their own aircraft. In addition they were generally successful in escaping if they were attacked. This could come about by their being taken by surprise or by overshooting a target and thereby becoming the pursued rather than the pursuer. As an example, the American Volunteer Group known as the Flying Tigers in World War II achieved an exchange ratio of fifteen to one, fifteen Japanese aircraft shot down for each U. S. loss. The Flying Tigers flew P40's which fared poorly against the Germans in North Africa. The P40 was a poor fighter in a dogfight, which is the way that it was used in Africa. A dogfight is defined as aerial combat involving many maneuvers between two or more aircraft. In China, the Flying Tigers would make a high speed pass and then run away rather than engage in a dogfight. Consequently it was unlikely

that they could be placed in an unfavorable tactical position. Another example of the significance of good tactics occurred when the P38 was first introduced in World War II. P38 pilots that attempted to dogfight with Japanese Zeros were shot down. The Zero had better turning performance, thus the U. S. losses were significant until different tactics were employed. This led to climbing to a higher speed and altitude relative to the Zero. The P38 pilots then made high speed dives and passes at the Zeros. It was due to the P38's dive superiority and higher altitude ceiling over the Zero that resulted in U. S. pilots turning the tables on the Zeros.

Another characteristic of the fighter aces was their aggressiveness. This proved to be one of the fighter aces' greatest psychological weapons. A common denominator for a large fraction of the fighter aces was that they had multiple kills in a single engagement. As examples, Fred Christenson shot down six aircraft on one mission, Glenn Eagleston shot down three ME-109's in one day, Francis Gerad shot down four planes in one aerial battle, David Campbell had nine confirmed and two probable kills in a single mission, Kenneth Dahms scored five victories in one mission, Stanley Vejtasa shot down seven enemy planes in one engagement, Robert Murray shot down four aircraft in one engagement, Kenneth Hippe shot down five aircraft in one mission. Four Navy aces, Eugene Valencia, Harris Mitchell, James French, and Clinton Smith achieved the pinnacle of success when they took on approximately forty Japanese fighters on one single mission. The result was sixteen Japanese kills and no U. S. losses. The number of kills might have been higher if the Navy aces had not run low on fuel

and therefore were unable to chase the enemy when they broke off the engagement. Thus history shows that only a few achieved success while many had limited success or completely failed.

Aerial Combat State-of-the-Art

Examination of the development of fighter weapon systems shows that new systems designs either attempted to eliminate or improve some aircraft deficiency. The methods that were employed were based strictly on experience and judgment factors. Consequently there was a great deal of uncertainty as far as how well the system would perform when it entered into air-to-air combat. Obviously the final test was which system, friendly or enemy, came out the winner.

One of the fundamental problems associated with new fighter designs past and present is the lack of analytical tools for assessing how well the system would do in air-to-air combat. There was no attempt, up until approximately ten years ago, to formulate the engagement problem as consisting of two or more opposing aircraft. Within the past decade, however, considerable amounts of money and time have been directed at developing methods for predicting the outcome of aircraft engaged in air-to-air combat. By and large, emphasis has been placed on the development of digital combat simulation and ground based simulators. In the former the pilot's capability is ignored or at best grossly approximated. The ground based simulators on the other hand do include pilots and are reasonable representations of cockpits and displays incorporated in fighters. The pilots employ typical fighter controls and attempt to engage and defeat each other. The problems

associated with the ground based simulators are attributed to their high cost and the uncertainty relative to the pilots' learning period.

Today a majority of the aircraft companies, several research companies, and many organizations within the department of defense have produced digital air combat simulations. A common denominator among these different groups is the belief that their simulation is the best. A little reflection on the developments along this line, however, makes one wonder if any of the simulations are any good. First it should be pointed out that the major differences between the various simulations can be related directly to the assumptions regarding the tactics employed by each fighter. The fundamental problem is that the controls are continuous functions over a relatively large range; hence there is literally an infinite choice of controls at any time during the course of the engagement. There seems to be two approaches for reaching or defining appropriate controls. The first is based on past pilot experience, consequently tactics are formulated which were used in previous air-to-air engagements. The problem here is that the development of a new fighter system ends up being evaluated based on old tactics. The second approach for formulating the controls is an iterative approach which also is employed in the first approach. A tactic or guidance scheme is selected, the results of the simulation are analyzed, and the tactics are then revised based on the outcome of the engagement. This is strictly a trial and error method with the result that the revisions in the tactics invariably end up showing that the aircraft thought initially to be the best does indeed come out on top. Consequently digital air-to-air combat simulations end up

favoring the new proposed fighter system. Although the new fighter is probably superior to existing fighters there must be some suspicion as far as the degree of improvement is concerned.

Another point about digital simulations, and probably the most significant one, has to do with the pilot's representation. It was mentioned previously that the pilot's capability is either ignored or grossly approximated. In general the constraints are either not present or at best a maximum normal acceleration for the pilot. In real engagements, maneuvers are limited by both the pilot's physical ability and the fighter performance constraints. All pilots are treated as being equal. Since the pilot constraints are often the same or nearly the same as the aircraft, the pilot ends up at the top or close to it as far as fighter skills are concerned. Thus every simulation tends to be flown by a superior pilot. This clearly contradicts history which shows that only three per cent of the fighter pilot force were aces.

The question then is, if ground based simulators are expensive as design tools and the results of digital simulations are questionable, what other approaches are there for determining the characteristics and tactics for new fighter systems? There are several which should be considered. The first is to take two existing aircraft, slightly modify them, and let them engage in air-to-air combat. There are several reasons why this approach is unsatisfactory. It is expensive since several pilots would be needed in order to obtain a representative sample. Also, one of the aircraft should be an enemy aircraft or at least be representative. Clearly the likelihood of acquiring an

enemy aircraft is minimal. Obviously neither aircraft could use its armament, hence the measure of effectiveness would have to be related to the number of firing opportunities or the time during which one aircraft fell inside the other's firing envelope. The paramount reason why this approach would probably be unsuccessful is due to the problem of applying the results to new conceptual systems. Therefore the approach of employing airborne systems can be dropped from further consideration.

Another approach and the one that will be considered in this endeavor is the analytical treatment of the significant factors in air-to-air combat problems. These factors consist of the aircraft system parameters and the tactics employed in air-to-air combat. The difference between this approach and those using digital simulations is that the goal will be to determine optimal system parameters in addition to the optimal tactics that a pilot should employ in air-to-air combat. Implementing these tactics is another problem which will not be considered here.

Examination of the technology available for addressing the tactics optimization problem reveals that the developments of Isaacs (1) in differential game theory are well suited to the problems to be addressed here. That only a small number of problems have received attention to date can be attributed to the observation that the developments by Isaacs occurred only within the past decade and that two-player differential games are significantly different from one-player games or optimal control problems. In games of two or more players each player in making a decision must take into account his

opponent's portending action and his opponent's similar wariness of the first player's actions. This situation has resulted in difficulty in obtaining correct analytical or numerical solutions.

A differential game approach is appropriate since the motions of the players are described by differential equations. The advantages of addressing the air-to-air combat problem as a differential game are twofold. If a solution can be obtained, then optimal tactics are defined for each player. In addition the characteristics of one player necessary to counter or capture the second player are defined.

Isaacs (1) considered only deterministic zero-sum two-player games. Deterministic implies perfect information. Zero sum means one player's loss is the other player's gain. Subsequent to Isaacs' efforts, one can now find in the literature both theoretical developments and applications of differential games for zero sum games, non-zero sum games, games with more than two players, and stochastic games. The latter corresponds to games of imperfect information. Some of the studies employing differential game theory as related to air-to-air combat will now be briefly discussed.

Two problems both of which are gross approximations of the air-to-air combat have been studied by Isaacs (1), Breakwell and Merz (2), Miller (3) and Lynch (4). The utility of these problems is that the description of the motion and the performance characteristics results in linear differential equations. Consequently analytical solutions were obtained. The problems are related to aerial combat in the sense that the players have conflicting goals. The two problems were originally called by Isaacs the homocidal chauffeur game and the game

of two cars. In the former game a chauffeur in a car traveling faster than a pedestrian attempts to run down the pedestrian. The pedestrian's goal is to avoid the car. The pedestrian can change his direction instantaneously, whereas the car is limited by its minimum turning radius. Both pedestrian and car speeds remain constant during the engagement. The car has higher speed but less maneuverability relative to the pedestrian.

The game of two cars is similar to the homocidal chauffeur game. The difference is that the pedestrian is replaced with a car of finite turning rate. Changing directions instantaneously corresponds to an infinite turning rate. Thus a maximum finite turning rate corresponds to a nonzero minimum radius of turn. Like the homocidal chauffeur game both cars remain at constant speeds.

The dominant assumptions in both games are constant speeds for each player and two dimensional engagements. Lynch (4), however, has addressed the variable speed case and some three dimensional engagement problems. Lynch concluded that constant speed engagements are good first order approximations to the variable speed case. For the homocidal chauffeur game, Lynch showed that the optimal trajectories are the same for both two and three dimensional engagements. For the three dimensional version of the game of two cars, Lynch derived approximate closed form control logic.

The previous references were concerned with solving two types of problems. The first problem was the determination of the characteristics of both players which would result in the pursuer capturing the evader. Capture occurred if the separation between pursuer and evader

ever reached a value less than some prescribed range. The utility of the solutions was the delineation between the sets of initial positions for capture and escape in the playing space. The respective objectives of the pursuer and evader were to minimize and maximize the final separation range. Isaacs (1) derived the solution for the homocidal chauffeur game. Miller (3), later verified by Lynch (4), derived the minimax range solution for the three dimensional constant speed case.

The second type of problem was concerned with determining optimal controls for minimax time given that capture could occur. For this problem the pursuer attempted to minimize the capture time while the evader attempted to maximize it. Breakwell and Merz (2) have essentially solved the homocidal chauffeur game. Lynch (4) has studied the two dimensional and three dimensional cases.

Othling (5) and Miller (6) studied two dimensional engagements with variable speed aircraft. The former effort assumed that the engagement took place in the vertical plane, whereas the second effort considered only the constant altitude or horizontal plane case. Othling was able to synthesize closed loop optimal or near optimal control laws for deterministic two player games. Miller determined optimal controls near the end of the game for the minimax range problem.

As far as nonzero sum games are concerned, Starr (7), Case (8), Prasad (9), and Leatham (10) are worth mentioning. A nonzero sum game differs from a zero sum game in that each player generally attempts to minimize a performance function which is not related to the other player's objective function. Starr demonstrated that analytical and conceptual features are evident in nonzero sum games that are not

found in zero sum games. He discussed at length the Nash equilibrium, minimax, and noninferior or Pareto optimal strategies. He further proved that the principle of optimality of optimal control theory does not generalize in an obvious way to the nonzero sum game. Case, in addition to Starr, was one of the first to explore the extension of the zero sum game to the N player nonzero sum game. Case developed necessary and sufficient conditions for the nonzero sum games. Prasad related N person games to problems of vector programming and decision making under uncertainty. In addition, Prasad dealt at length with the special switching surfaces which seem to be characteristic of differential games. Leatham extended the theory of nonzero sum games in which the nonlinear system equations have bounded linear controls. He solved two aerial combat problems formulated as nonzero sum games. Both were interceptor problems with the first involving two players and the second three players. In addition, Leatham studied pursuit-evasion problems with different pay-offs for each player.

Application of differential game theory to stochastic problems or incomplete information problems has been very limited. The only problems to date are classified as linear quadratic cases. The descriptions of the system dynamics are linear in the controls and the state variables. The performance function to be optimized is quadratic in both the state and control variables. There has been no attempt to address the air-to-air combat problem as a stochastic game.

There have been efforts at extending the numerical algorithms developed for solving optimal control problems to two player zero sum games with perfect information. Noteworthy examples are due to the efforts of Roberts and Montgomery (11), Graham (12), Lin (13), and McFarland (14). Montgomery and Roberts developed a gradient technique for numerically solving differential games and applied it to pursuit-evasion problems with control and state variable inequality constraints.

Lin developed a neighboring extremal method for solving pursuit-evasion problems. McFarland applied a differential dynamic programming method for determining minimax and maximin solutions. These methods involve the solution of the linearized forms of the state differential equations and influence functions. The latter are like Lagrange multipliers in the calculus of variations. All are iterative numerical techniques. They differ primarily in the assumptions concerning the state differential equations, the derivatives of the influence functions, the control optimality conditions, and the boundary conditions. These methods are particularly useful for solving differential games when the system differential equations are nonlinear.

Purpose of this Research

The purpose of this research is to address an area which has not been presented anywhere in the literature to date. The differential games that have been solved have not considered the limitations imposed by fighter weapons limitations, namely relative positions, rather than separation range alone. One way of handling the weapon, whether it be guns or air-to-air missiles, is to define the weapon envelope within which it is possible to kill a target. In other words, if a pursuer can maneuver such that the evader enters the pursuer's launch envelope, then the evader can be killed.

The objective of this research is to determine the relationship between the system performance characteristics that separates the playing space into two distinct parts - a capture area and an escape area. This is called the barrier solution. The shape of the barrier and the pursuer's weapon envelope provides the information necessary for determining kill or escape.

The utility of the barrier solution is twofold. Imagine an aircraft armed with machine guns attempting to shoot down an opponent. Clearly the former attempts to maneuver such that the separation range

is a minimum since the gun effectiveness increases with decreasing range. The aircraft under attack desires the opposite. For initial separations falling in the escape area, which in general will be the case, the barrier solution provides the minimum separation range under optimal play by both aircraft. If the minimum separation range exceeds the lethal gun range, then the likelihood of a kill is negligible. If on the other hand the lethal range is greater, then the chances of a kill are improved. Consequently the barrier solution along with the weapon's capability determines those engagements wherein the aggressor is successful or unsuccessful.

The second utility of the barrier solution is that of defining the sensitivity of the minimum separation range to small changes in the performance characteristics. As a consequence those performance characteristics which yield the biggest improvement are identified.

Three problems will be studied. The first problem is like the homocidal chauffeur game, the second is like the game of two cars, and the third is a two dimensional engagement between variable speed aircraft. The first two problems differ from the homocidal chauffeur game and the game of two cars in the definition of the terminal surface, that is, the surface on which the game ends. Previous studies treated the terminal surface as a circle and a cylinder for the homocidal chauffeur game and the game of two cars, respectively. This research will assume more realistic terminal surfaces as exemplified by guns and air-to-air missile envelopes.

In Section II, the background for the mathematical necessary conditions for zero sum differential games is presented. In Section III, the three problems are formulated. Sections IV, V, and VI present the solutions of these problems. The optimal tactics and performance characteristics are developed in these sections. Section VII discusses the significant results.

SECTION II

ZERO SUM DIFFERENTIAL GAME THEORY

Differential Games and Optimal Control Problems

The primary difference between optimal control problems and differential games is in the number of players involved. In optimal control problems one player selects his controls so as to optimize his performance function. There may be two or more participants but only one is free as far as selecting his optimal controls. In differential games at least two players select their controls optimally. Their respective performance functions which each seeks to optimize are not necessarily the same.

A simple example illustrates the difference between the optimal control problem and a differential game. Consider the situation depicted in Figure 1. Assume that a vehicle (such as a bomber) at point A desires to reach a target area in minimum time or come as close to the target area as possible. In the absence of an interceptor vehicle at point B, the vehicle at A should fly the path AC which is the perpendicular distance between A and the target area. This is the solution to the optimal control problem. If an interceptor initially at point B attempts to intercept the bomber initially at point A then the bomber should fly the path AO. The line OO" is the locus of intercept points between the two vehicles. If the

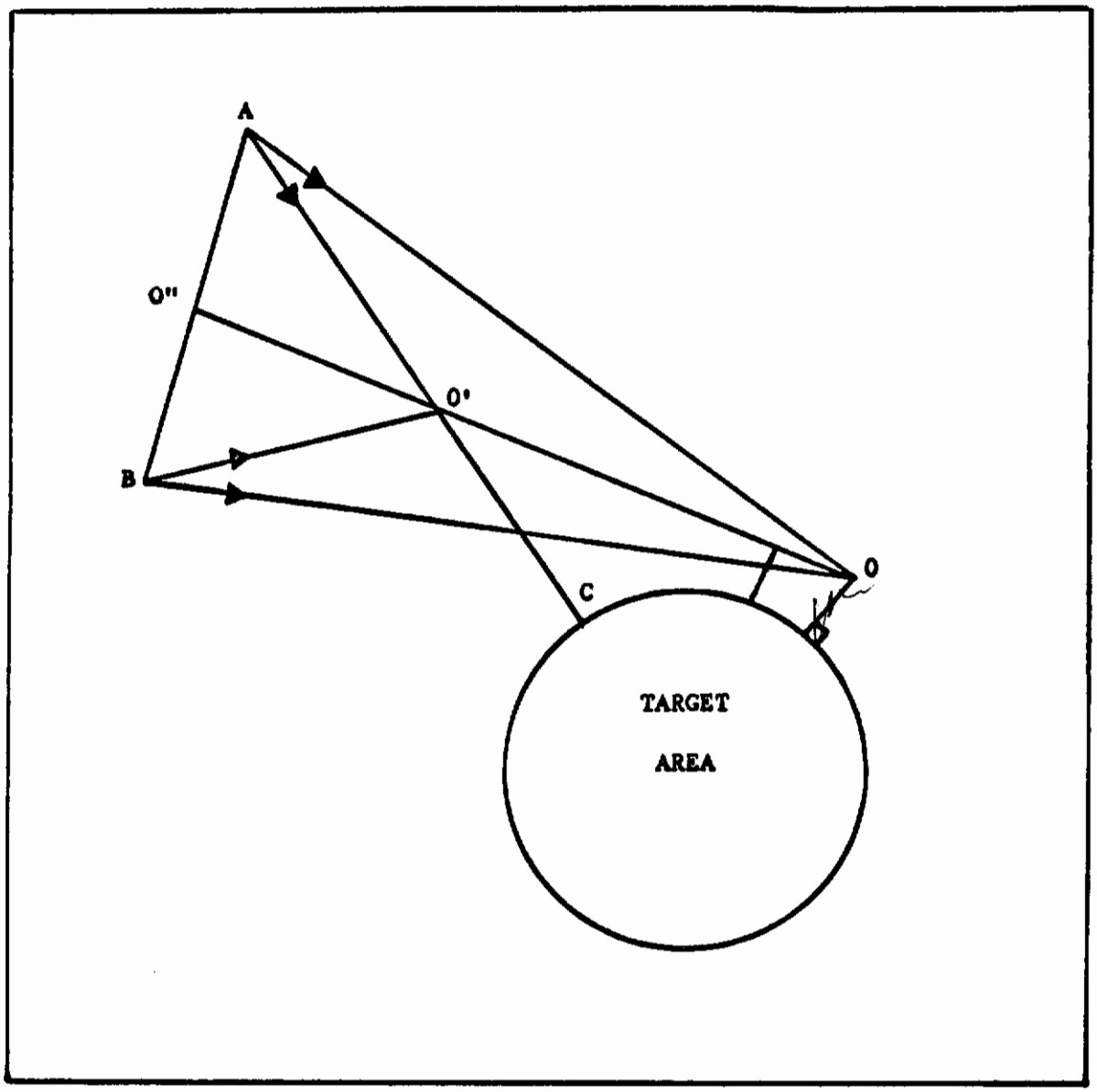

Fig. 1.--An Optimal Control Problem and a Differential Game

bomber flew along the path AC, it would be intercepted by the interceptor at point O'. Consequently, the closest that the bomber could come to the target area is point O if both vehicles flew optimally. This situation corresponds to a differential game, in which the bomber attempts to come as close as possible to the target area defined by an interceptor.

Recall that the objective of this research is to determine the relationship between the system performance characteristics which separates the playing space into a capture area and an escape area. By definition, capture occurs if the terminal surface is crossed or penetrated during the play of the game. The game ends when the terminal surface is reached. Capture range is defined by the radius of curvature of the terminal surface.

The answer to the question of a kill of the evader by the pursuer is dependent upon the initial state of the game and the shapes of the terminal surface and pursuer's weapon envelope. If the initial state is in the escape area (generally it will be) and the weapon envelope falls within the capture area, then no kill can occur under optimal evader play. On the other hand, if part of the weapon envelope is in the escape area, then the pursuer may be able to achieve a kill.

Hereafter we refer to the pursuing player as P and the evading player as E. It is necessary therefore to determine the hypersurface in the playing space that delineates starting points from which capture or escape occurs. This hypersurface is called the barrier by Isaacs (1). We now turn our attention to the necessary conditions for determining the barrier.

The Barrier

As an introduction to the concept of a differential game barrier, consider the following simple example. Imagine an air-to-air engagement between two aircraft where one aircraft reaches a position directly behind another aircraft. Thus, a tail chase situation ensues. Assume P has machine guns for weapons and his goal is to shoot down E. To do this requires that P bring his guns to bear on E; that is, E must fall within the lethal volume of his guns. The lethal volume can be thought of as the volume inside a cone with P at the apex and the base at the maximum effective range of the guns. Assume that E detects P before P can bring his guns to bear on E. E's objective is to escape; that is, stay outside of the gun's lethal volume. Consequently E escapes if he can stay outside the lethal volume; if not, he is shot down or captured. Thus their roles are well defined.

Let the initial time correspond to the time that E starts his evasive maneuvers. Assume that are no constraints other than each aircraft has a minimum radius of turn. If P has faster speed and smaller turning radius, then P can capture E for all initial positions. If the opposite holds and E is initially outside the lethal volume, P can never capture E. The outcome is the same if E is faster and has the larger minimum turning radius since E can simply run away from P. If P has a speed advantage and E a smaller minimum turning radius, then the outcome is not as clear. If E is initially very close to the lethal volume, P will probably capture E. If E is far ahead of P, then E may be able to force P into an overshoot and thereby escape. Capture or escape is dependent upon the speeds, the minimum turning radii, the

initial positions, and the lethal volume. Between those initial points which lead to capture or escape are initial points which result in E only grazing the terminal surface. This set of initial points is the barrier. This is the type of problem to be addressed in this research.

Another illustration of the barrier concept is the encounter between a bull and a bullfighter. The bull is much faster but less maneuverable. If the bullfighter waits too long he is gored. If he moves too soon he may also be gored. There are, however, separations for which he can escape. Thus, there is a set of initial points for which the bull only grazes the bullfighter. This corresponds to the barrier.

As a third example, consider the bomber-interceptor example discussed earlier. The bomber is the evader and the interceptor is the pursuer. Assume that the initial interceptor position is fixed at point B in Figure 2. The barrier then is the locus of the bomber initial positions that results in the bomber and interceptor reaching the boundary of the target area simultaneously. If the interceptor is faster, the barrier is like that illustrated in Figure 2. For bomber starting points outside the barrier, the interceptor reaches the bomber before the bomber reaches the target area. The opposite occurs for initial bomber points between the barrier and the target area.

The barrier has the following characteristics. It is never crossed during optimal play. If it forms a closed surface in the playing space, then the playing space is divided into two parts - a capture set and an escape set. If the barrier forms a closed surface, then initial states on the barrier lead to a neutral outcome. That is, the terminal surface (the surface on which the game ends) is only grazed and not penetrated under optimal play.

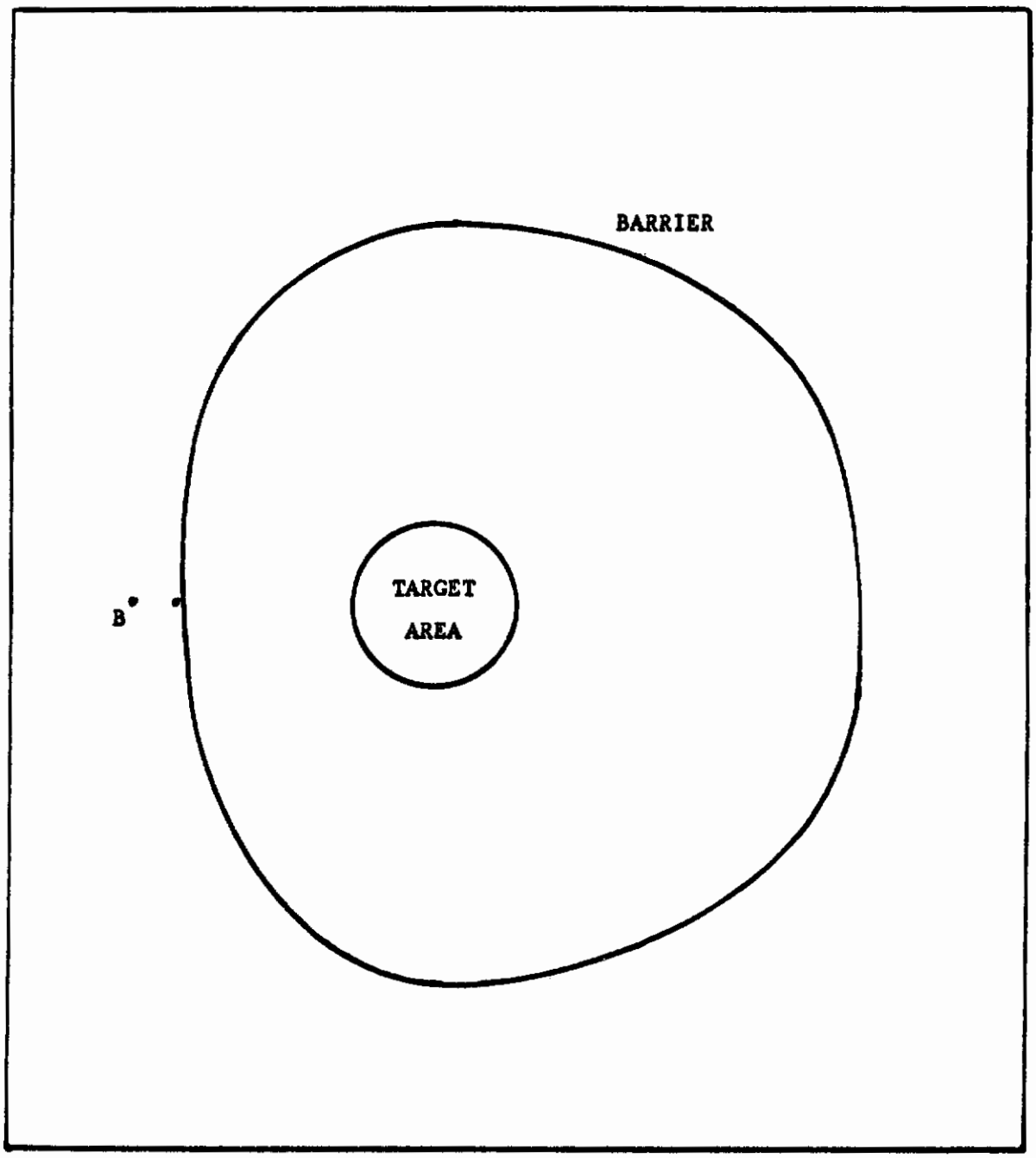

Fig. 2.--The Barrier for the Bomber-Interceptor Problem

Thus the closed barrier divides the playing space in two parts. Outside the barrier E can escape and inside E is captured. As a consequence, the barrier solution leads to the relationship between the terminal surface, both relative range and angle-off, the speeds of the two players, and their minimum turning radii. If the terminal range exceeds the lethal range of the pursuer's weapon, then the pursuer can not destroy the evader under optimal evader play. If the terminal range falls within the pursuer's weapon envelope, then the pursuer may be able to kill the evader.

A reduced playing space will be considered for the problems to be addressed in this research. This is a coordinate space where the states are measured relative to P. The justification for this is that relative positions between P and E are important in air-to-air combat problems. As a consequence, the playing space and the dimension of the space is reduced relative to an inertial coordinate frame.

There are several problems associated with determining the barrier surface. The first has to do with finding the proper terminal conditions where the barrier meets the terminal surface. The second problem is the evaluation of the necessary conditions which define the barrier at the points where it grazes the terminal surface. The derivation of the necessary conditions for the barrier follows.

Construction of the Barrier

The reduced playing space has dimension n. Let C denote the terminal surface which has dimension n-1 since it is a surface within the playing space. As mentioned earlier, for pursuit-evasion problems such as air-to-air combat problems, the terminal surface is an envelope measured relative to the pursuer's position. Let the inside of the terminal surface, the shaded area in Figure 3, correspond to the volume inside the terminal surface containing the pursuer's position. The pursuer's (P) objective is to force the evader (E) across the terminal surface C from evader positions outside the

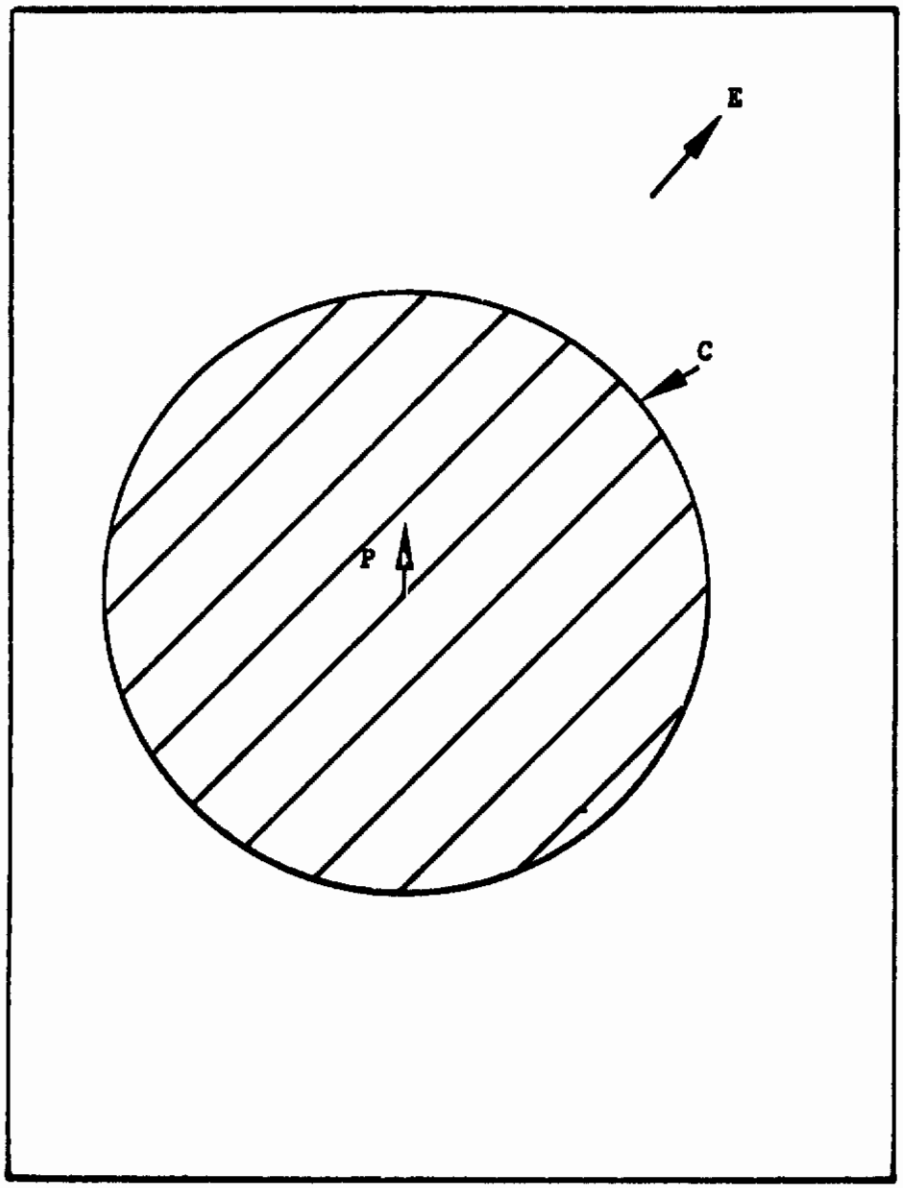

Fig. 3.--The Smooth Terminal Surface

terminal surface. The evader seeks the opposite. Both natural and artificial barriers will be defined and the necessary conditions for their solutions established.

The natural barrier corresponds to smooth terminal surfaces, e. g. a spherical terminal surface with the pursuer located at the origin of the sphere. An artificial barrier can result if the terminal surface is not smooth, e. g. the intersection between a cone and spherical surface with the apex of the cone and the center of the sphere colocated at the pursuer's position as illustrated in Figure 4. An example of an artificial barrier is a fighter armed with a machine gun which is not steerable. The gun is effective only within a small cone relative to the fighter's direction.

The state of the system is described by a system of first order differential equations

$$\dot{\bar{x}} = f(\bar{x},\bar{u},\bar{v}) \qquad (1)$$

where $\bar{x}$ is an n-dimensional state vector, $\bar{u}$ and $\bar{v}$ are m-dimensional control vectors, $f(\bar{x},\bar{u},\bar{v})$ is a vector function of the state and controls, and $\dot{x}$ is the time rate of change x. Hereafter, $(\dot{})$ means the time derivative of ( ). If $\bar{u}$ and $\bar{v}$ are known functions of the time or state and n boundary conditions are specified for the state vector $\bar{x}$, then Eq (1) can be integrated if $f(\bar{x},\bar{u},\bar{v})$ is continuous and single valued. It may be extremely difficult to do so, however, if the boundary conditions are split, i.e., some boundary conditions are specified initially and the remaining boundary conditions are

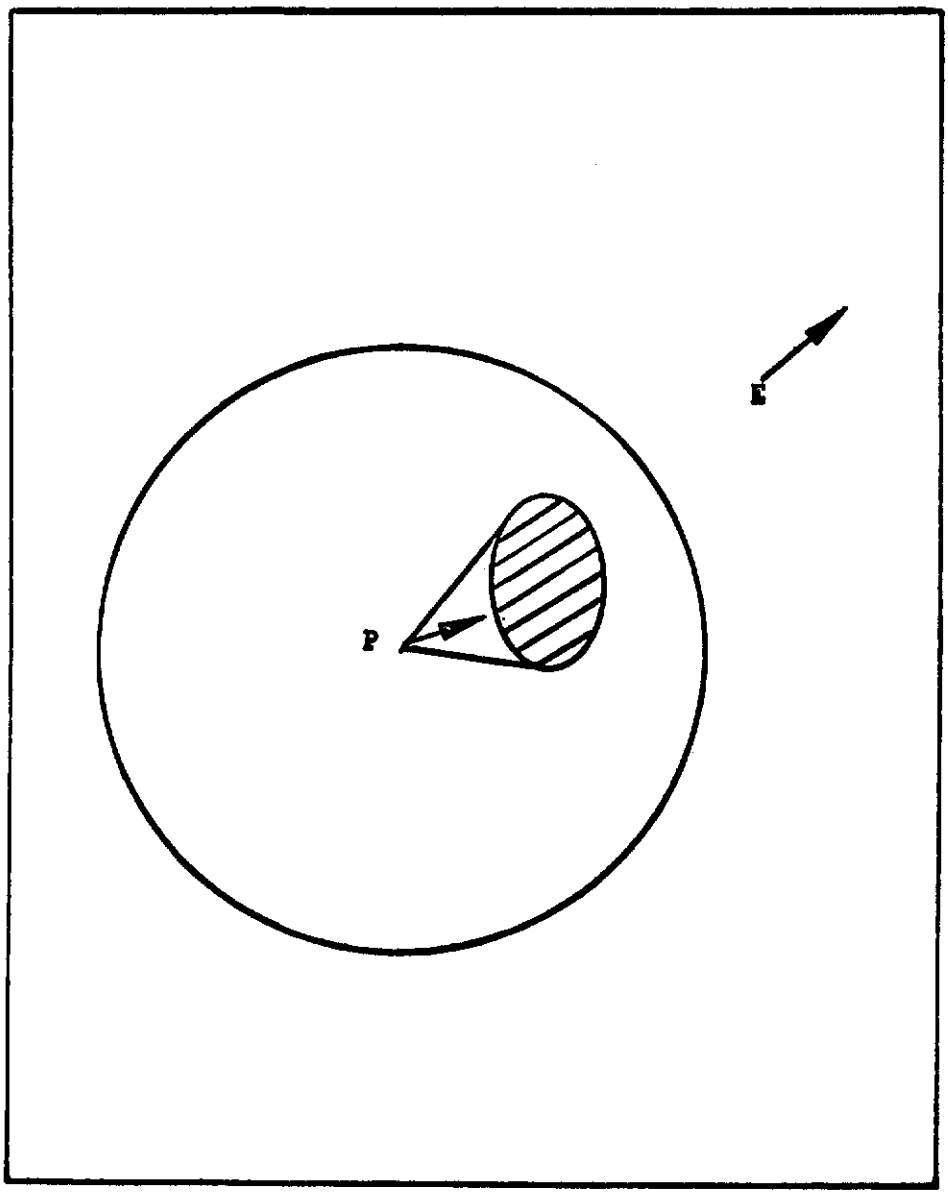

Fig. 4.--The Restricted Terminal Surface

specified terminally. Fortunately, for the pursuit-evasion problems to be addressed here, the boundary conditions are specified on the terminal surface. Thus the problems are terminal boundary value problems.

The concept of the barrier is fundamentally quite simple. Its construction, however, can be very difficult. Recall that one characteristic of the barrier is that it is not crossed under optimal play. Thus, if the barrier is closed, then it delineates between the capture and escape sets. Let the vector $\bar{\nu}$ define the vector normal to the barrier and extending into the escape set as illustrated in Figure 5. If the pursuer can force the evader into the shaded region in Figure 5, then the pursuer will capture the evader, i.e., the pursuer can force the evader to penetrate the terminal surface. Recall that the terminal surface corresponds to the relative positions at the end of the game and is defined by the radius of curvature and an angle-off-constraint. If the evader can stay outside the shaded region, he can prevent capture no matter what the pursuer does. Since Eq (1) defines the rate-of-change of the state E relative to the state of P, then the scalar product

$$\bar{\nu} \cdot f\ (\bar{x},\bar{u},\bar{v}) \tag{2}$$

represents the rate of change of E's state normal to and away from the barrier. Thus in the neighborhood of the barrier, P desires for any E control $\bar{v}$

$$\min_{u} \bar{\nu} \cdot f\ (\bar{x},\bar{u},\bar{v}) < 0$$

which corresponds to relative motion towards the capture set.

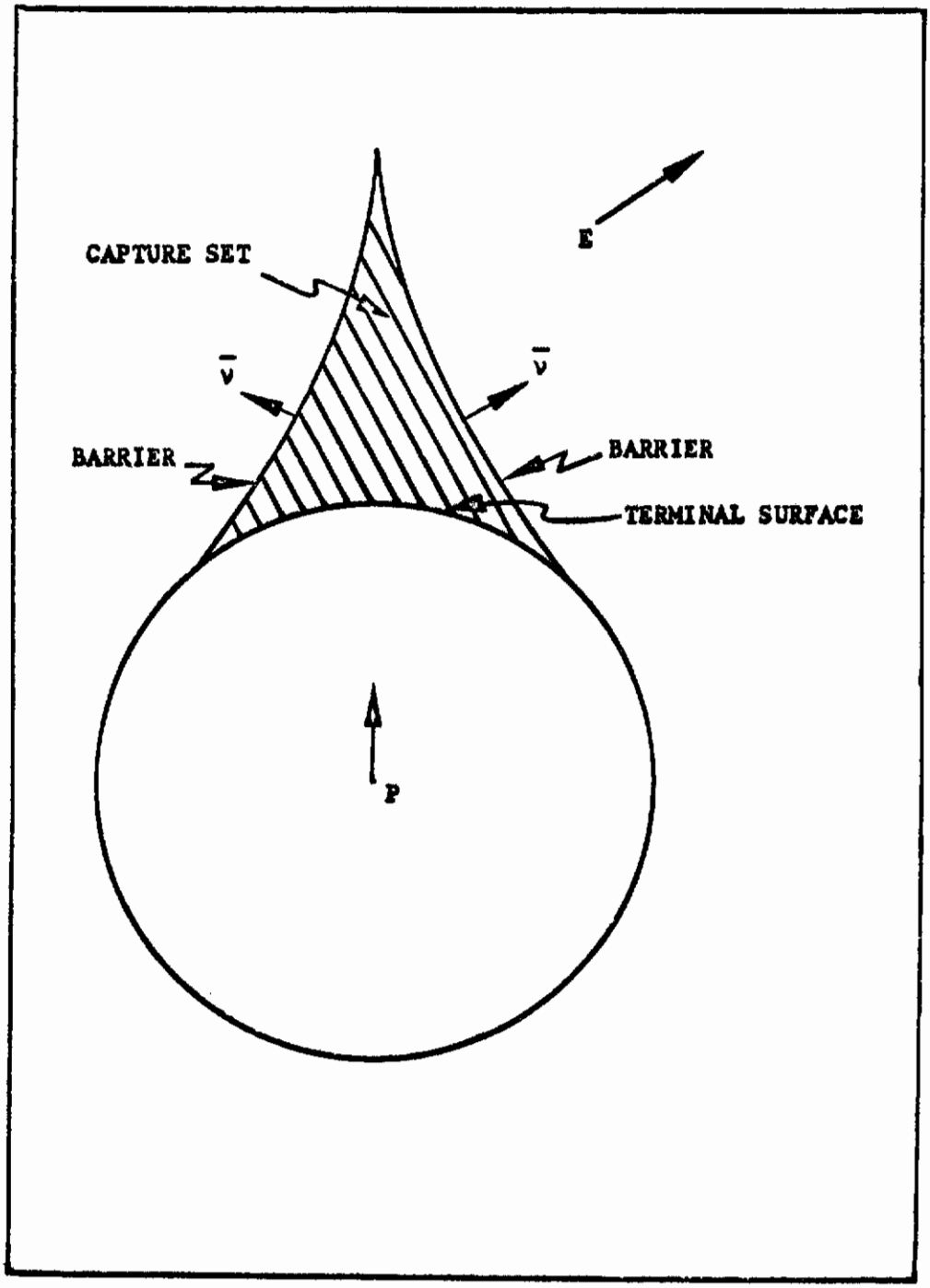

Fig. 5.--The Natural Barrier

Contrarily, E seeks for any P control $\bar{u}$

$$\max_{v} \bar{\nu} \cdot f(\bar{x},\bar{u},\bar{v}) > 0$$

which corresponds to relative motion away from the capture set. It follows that on the barrier for optimal play by both players

$$\min_{u} \max_{v} \bar{\nu} \cdot f(\bar{x},\bar{u},\bar{v}) = 0 \tag{3}$$

If the differential equations are separable relative to $\bar{u}$ and $\bar{v}$ controls, then Eq (3) is equivalent to

$$\max_{v} \min_{u} \bar{\nu} \cdot f(x,u,v) = 0 \tag{4}$$

For the problems to be studied in this effort, the differential equations will be separable in $\bar{u}$ and $\bar{v}$. Eq (3) or Eq (4) then provides the relation for determining optimal P and E controls, u* and v*, respectively, in terms of the state $\bar{x}$ and the normal vector $\bar{\nu}$, namely

$$u^* = u^*(\bar{x},\bar{\nu}) \tag{5}$$

$$v^* = v^*(\bar{x},\bar{\nu}) \tag{6}$$

At this point the differential equations have been defined and the necessary conditions for optimal play, Eqs (5) and (6), have been determined. The remaining steps involve derivation of a relation for determining $\bar{\nu}$ and definition of the boundary conditions. The necessary condition for $\bar{\nu}$ will be determined first. Substitution of Eqs (5) and (6) into Eq (3) gives

$$\min_{u} \max_{v} \bar{v} \cdot \bar{f} = \sum_{i=1}^{n} v_i f_i(x,u^*,v^*) = 0 \tag{7}$$

Although the bars have been dropped from x, u*, and v* for convenience it should be understood that they are vectors. In Eq (7) v_i and f_i are the scalar components of $\bar{v}$ and f. If any component of $\bar{u}$, say u_k, is interior then

$$\frac{\partial}{\partial u_k} \sum_{i=1}^{n} v_i f_i \ (x,u^*,v^*) = \sum_{i=1}^{n} v_i \frac{\partial f_i}{\partial u_k} = 0 \tag{8}$$

A similar expression holds for any component of $\bar{v}$ which is interior. If any component of $\bar{u}$, u_k, is on the boundary of the control region and the boundaries are constant as they are in the problems to be addressed here, then

$$\dot{u}_k = 0 \tag{9}$$

A similar relation holds for any component of $\bar{v}$ which falls on the control boundary. Now differentiation of Eq (7) with respect to time gives

$$\sum_{i=1}^{n} \dot{v}_i f_i + \sum_{i=1}^{n} v_i \sum_{j=1}^{n} \frac{\partial f_i}{\partial x_j} \dot{x}_j + \sum_{i=1}^{n} v_i \sum_{k=1}^{m} \left(\frac{\partial f_i}{\partial u_k} \dot{u}_k + \frac{\partial f_i}{\partial v_k} \dot{v}_k \right) = 0 \tag{10}$$

Rewriting the last two series gives

$$\sum_{k=1}^{m} \left(\sum_{i=1}^{n} v_i \frac{\partial f_i}{\partial u_k} \right) \dot{u}_k + \sum_{k=1}^{m} \left(\sum_{i=1}^{n} v_i \frac{\partial f_i}{\partial v_k} \right) \dot{v}_k \tag{11}$$

In light of Eqs (8) and (9) and similar forms for v_k, Eq (11) is zero. Changing indices on the second series in Eq (10) and substituting Eq (1), $\dot{x}_i = f_i$, gives

$$\sum_{i=1}^{n} \left(\dot{v}_i + \sum_{j=1}^{n} v_j \frac{\partial f_j}{\partial x_i} \right) f_i = 0 \qquad (12)$$

If the f_i are linearly independent as they are for the problems to be studied here, then the equations for determining the components of $\bar{v}$ are

$$\dot{v}_i = - \sum_{j=1}^{n} v_j \frac{\partial f_j}{\partial x_i} \qquad i=1,\ldots,n \qquad (13)$$

The final step is the derivation of the boundary conditions on the terminal surface. The region on the terminal surface bordering the capture set as illustrated in Figure 5 is called the usable part (UP) by Isaacs. The intersection between the barrier and the terminal surface is called the boundary of the usable part (BUP). The remaining part of the terminal surface is called the nonusable part (NUP). The UP, BUP, and NUP are important in the construction of the barrier in that points in the neighborhood and close to the terminal surface lead to either capture, a neutral outcome, or escape.

Let the terminal surface, which has dimension n-1, be written in the following parametric form

$$x_i = h_i (s_1,\ldots,s_{n-1}) , \quad i = 1,\ldots,n \qquad (14)$$

where the parameters s_i designate points on the terminal surface.

From Eq (14)

$$\frac{\partial x_i}{\partial s_k} = \frac{\partial h_i}{\partial s_k} \quad , \; i=1,\ldots,n \; ; \; k=1,\ldots,n-1$$

which are the components of the tangent plane to the terminal surface at the intersection of the barrier and the terminal surface. If the terminal surface is smooth and has no discontinuities in its slope, then the tangent plane is defined at every point on the terminal surface. Since $\bar{\nu}$ is normal to the barrier and the barrier can not penetrate the terminal surface, the following normality condition holds

$$\sum_{i=1}^{n} \nu_i \frac{\partial h_i}{\partial s_k} = 0 \; , \; k=1,\ldots,n-1 \qquad (15)$$

These n-1 equations and Eq (7) provide n equations in the n variables ν_i and the parameters $s_1,\ldots,s_n$. This then determines the boundary conditions on the terminal surface and defines the boundary of the usable part (BUP) since the barrier meets the terminal surface at the BUP.

The conditions for barrier closure are problem dependent, hence these conditions will be established when each specific problem is addressed. Barrier closure results when the barriers meet and separate the playing space in two parts.

Consider next the artificial barrier. The artificial barrier may result if the terminal surface has discontinuities in its slope. The discontinuities result from angle-off constraints. Gun firing

envelopes fall in this category since the gun is effective only within a specified range of the target and within a small angle-off of the target relative to the fighter's direction. Figure 6 illustrates the two dimensional example where the barrier passes through a corner of the terminal surface. If the barrier is tangent to the terminal surface like that in Figure 5, then the barrier is natural and the preceding equations hold. Eqs (7) and (13) must hold for both natural and artificial barriers since the barrier is never crossed under optimal play.

The difference between the natural and artificial barriers is due to the boundary conditions for $\bar{v}$ on the terminal surface. The tangent plane to the terminal surface is undefined at the corner. This can be circumvented by a construction whereby the corner is replaced with a circular surface of infinitesimal radius tangent to the terminal surface. The terminal surface now is continuous in its slope and the tangent plane is defined. The boundary conditions on the terminal surface are the same as for the natural barrier. If the barrier is tangent to the terminal surface at points other than the corner, we treat the barrier as a natural barrier. If not, we replace the corner with a smooth surface, employ natural barrier analysis, and then let the infinitesimal radius approach zero.

In summary, the construction of the barrier involves the solution of the state equations,

$$\dot{\bar{x}} = f\ (\bar{x},\bar{u}^*,\bar{v}^*) \tag{1}$$

the necessary conditions on the barrier,

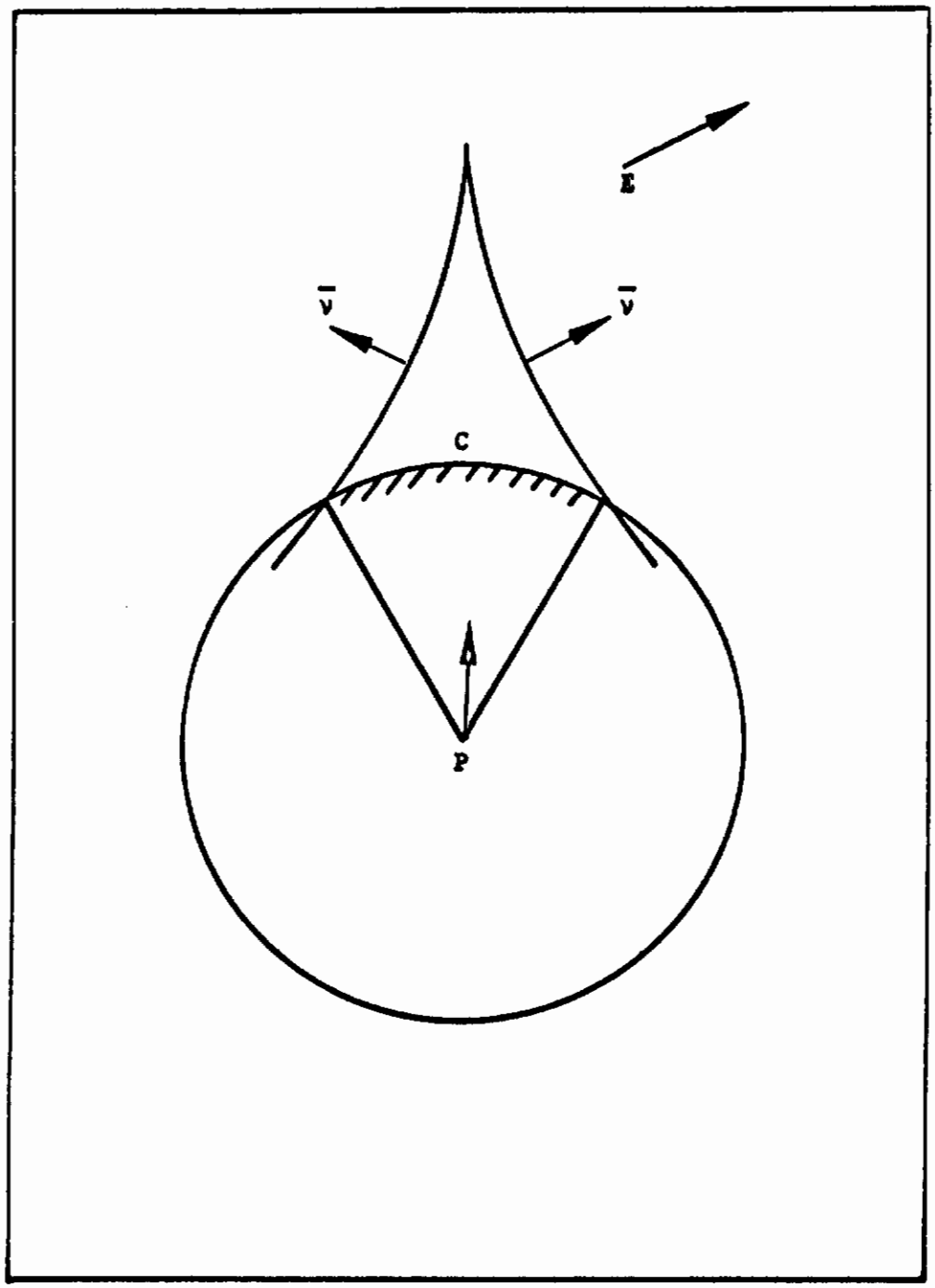

Fig. 6.--The Artificial Barrier

$$\sum_{i=1}^{n} \nu_i f_i \ (x,u^*,v^*) = 0 \tag{7}$$

$$\dot{\nu}_i = - \sum_{j=1}^{n} \nu_j \frac{\partial f_j}{\partial x_i} \ , \ i=1,\ldots,n \tag{13}$$

and the boundary conditions on the terminal surface

$$\sum_{i=1}^{n} \nu_i \ \frac{\partial h_i}{\partial s_k} = 0 \ , \ \ k=1,\ldots,n-1 \tag{15}$$

The solution to these equations gives the relationship between the range (the radius of curvature of the terminal surface), the final separation between P and E, the speeds of both players, the minimum turning radii, and the angle-off constraint.

We now turn our attention to the formulation of the problems to be addressed in this research.

SECTION III

PROBLEM FORMULATION

Three problems will be addressed in this research. They differ primarily in the number of variables required to describe the systems and the controls available to each player. The procedure will be to start with the problem that has the lowest dimension and then add additional state variables and controls in order to add more realism in the system description. The first problem, Problem I, will be referred to as the limited pursuer simple motion evader. The problem description follows.

Problem I

Both pursuer (P) and evader (E) have constant speeds with the pursuer's speed V_P greater than the evader's speed V_E. The play is in a two dimensional plane. The evader can change directions instantaneously. The pursuer's maneuvering is limited by his minimum radius of turn. Consequently P can turn anywhere between a hard right and a hard left turn. This includes flying straight ahead. The geometry of the engagement is illustrated in Figure 7. The X'Y' coordinate system is a fixed nonrotating frame. The xy coordinate frame is a relative frame attached to the pursuer with the y axis always directed in the same direction as P's velocity vector $\overline{V}_P$. The vectors $\overline{X}_P$, $\overline{X}_E$, and $\overline{X}$ correspond to the position of P and E in the X'Y' coordinate frame

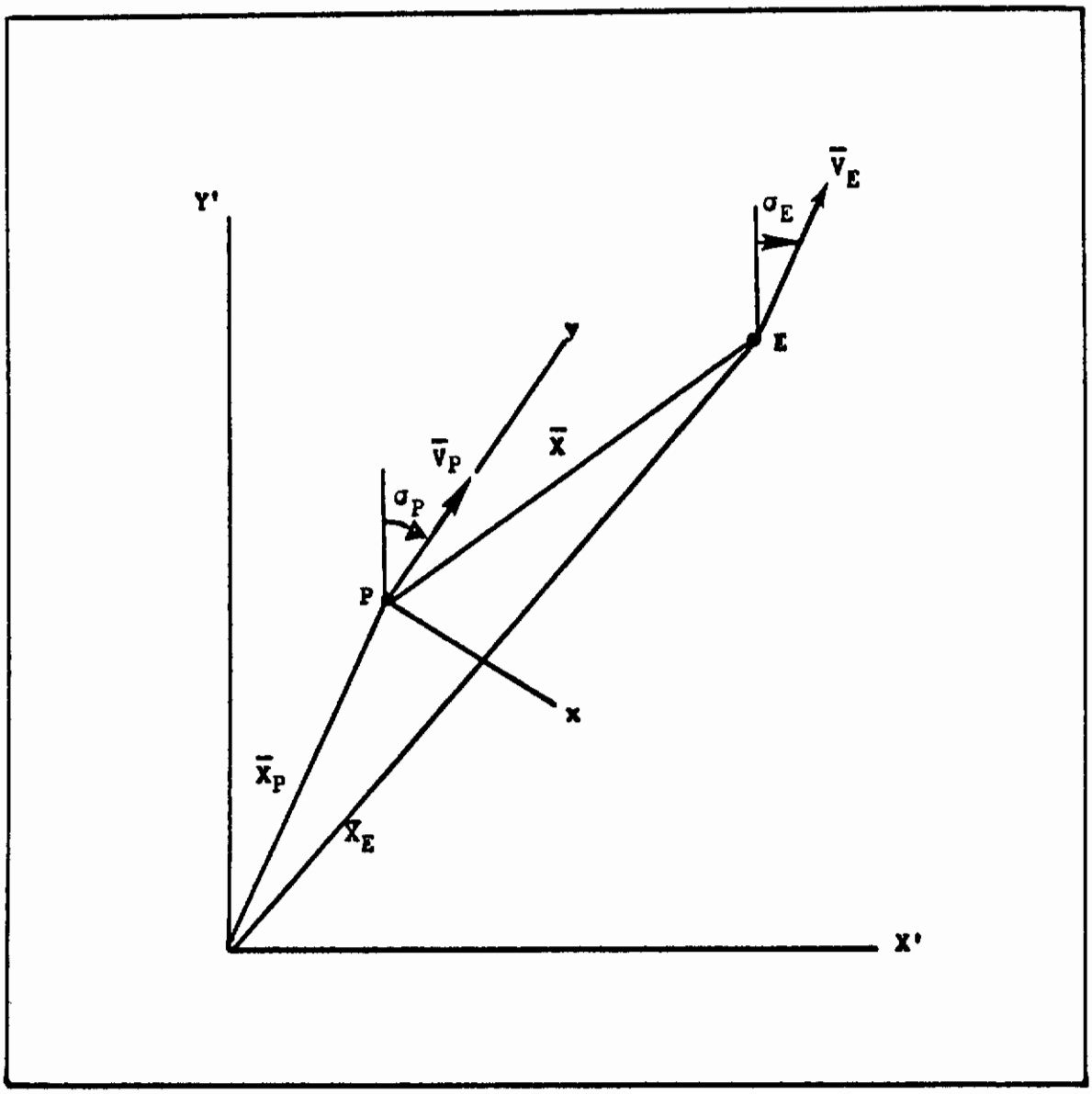

Fig. 7.--The Geometry for Problems I and II

and the position of E relative to P, respectively. The reason for introducing a relative coordinate system is simply that only relative positions are important in air-to-air combat. The directions of the velocities $\bar{V}_P$ and $\bar{V}_E$ are defined by the angles σ_P and σ_E. The differential equations of state describing the motion of E relative to P are derived in Appendix A. The differential equations and the control constraint are:

$$\dot{x} = V_E \sin \psi - \frac{V_P}{R_P} \alpha_P \, y \tag{16}$$

$$\dot{y} = V_E \cos \psi - V_P + \frac{V_P}{R_P} \alpha_P \, x \tag{17}$$

$$-1 \leq \alpha_P \leq 1 \tag{18}$$

where ψ is defined by

$$\psi = \sigma_E - \sigma_P$$

and is the evader's control; α_P is the pursuer's control, and R_P is P's minimum radius of turn. Thus for Problem I there are two states and two controls.

By introducing nondimensional variables it is possible to study a class of problems rather than a single problem. The nondimensional transformations are as follows

$$X = \frac{x}{R_P} \tag{19}$$

$$Y = \frac{y}{R_P} \tag{20}$$

$$\epsilon = \frac{V_E}{V_P} \tag{21}$$

$$\tau = \frac{V_P t}{R_P} \tag{22}$$

where X and Y are nondimensional state variables, ϵ is a nondimensional parameter, and τ is the independent nondimensional variable time. Substitution of Eqs (19) through (22) into Eqs (16) through (18) and then rearranging gives

$$\dot{X} = \epsilon \sin \psi - \alpha_p Y \tag{23}$$

$$\dot{Y} = \epsilon \cos \psi - 1 + \alpha_p X \tag{24}$$

$$-1 \leq \alpha_p \leq 1 \tag{25}$$

where derivatives are with respect to τ. The solution to these differential equations, Eqs (23) through (25), represents the solution to a class of dimensional problems. That is, one solution of Eqs (23) through (25) is the solution of all problems represented by Eqs (16) through (18) if the value of ϵ and the boundary conditions are the same.

In addition to the description of the motion of E relative to P the formulation requires the definition of the terminal surface. The surface is illustrated in Figure 8. The terminal surface C is a circular arc of radius L (nondimensional radius $\bar{L} = L/R_p$) constrained by a maximum angle-off relative to the pursuer's velocity of θ. In Chapter IV the solution of Problem I will be addressed.

Problem II

In this problem both evader and pursuer have limited turning capability. Neither player can turn instantaneously. Consequently ψ becomes a state variable rather than E's control. In Appendix A it

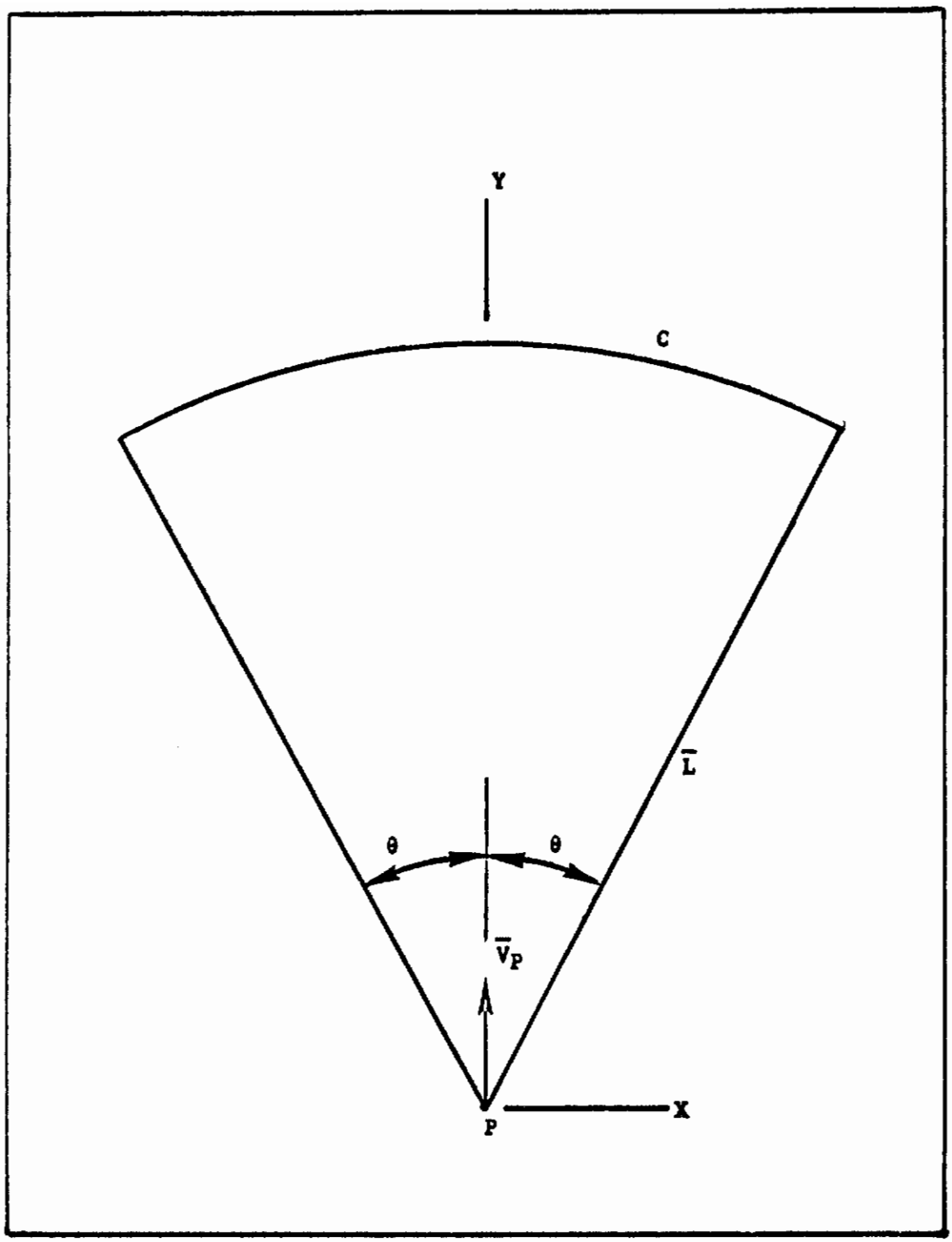

Fig. 8.--The Terminal Surface for Problem I

is shown that the state differential equations and controls are

$$\dot{x} = V_E \sin\psi - \frac{V_P}{R_P}\alpha_P\, y \tag{26}$$

$$\dot{y} = V_E \cos\psi - V_P + \frac{V_P}{R_P}\alpha_P\, x \tag{27}$$

$$\dot{\psi} = \frac{V_E}{R_E}\alpha_E - \frac{V_P}{R_P}\alpha_P \tag{28}$$

$$-1 \le \alpha_P \le 1 \tag{29}$$

$$-1 \le \alpha_E \le 1 \tag{30}$$

where α_E is E's control. In comparison with Problem I it is seen that one additional state variable results, namely ψ, and a different control for E appears, namely α_E. Substitution of the nondimensional variables, Eqs (19) through (22) into Eqs (26) through (30) gives the following nondimensional state differential equations and constraints

$$\dot{X} = \epsilon \sin\psi - \alpha_P\, Y \tag{31}$$

$$\dot{Y} = \epsilon \cos\psi - 1 + \alpha_P\, X \tag{32}$$

$$\dot{\psi} = -\alpha_P + \epsilon R\, \alpha_E \tag{33}$$

$$-1 \le \alpha_P \le 1 \tag{34}$$

$$-1 \le \alpha_E \le 1 \tag{35}$$

where R is an additional nondimensional parameter defined by

$$R = \frac{R_P}{R_E}$$

The terminal surface for Problem II is similar to Problem I except that ψ ranges from 0 to 2π. The surface is illustrated in Fig. 9.

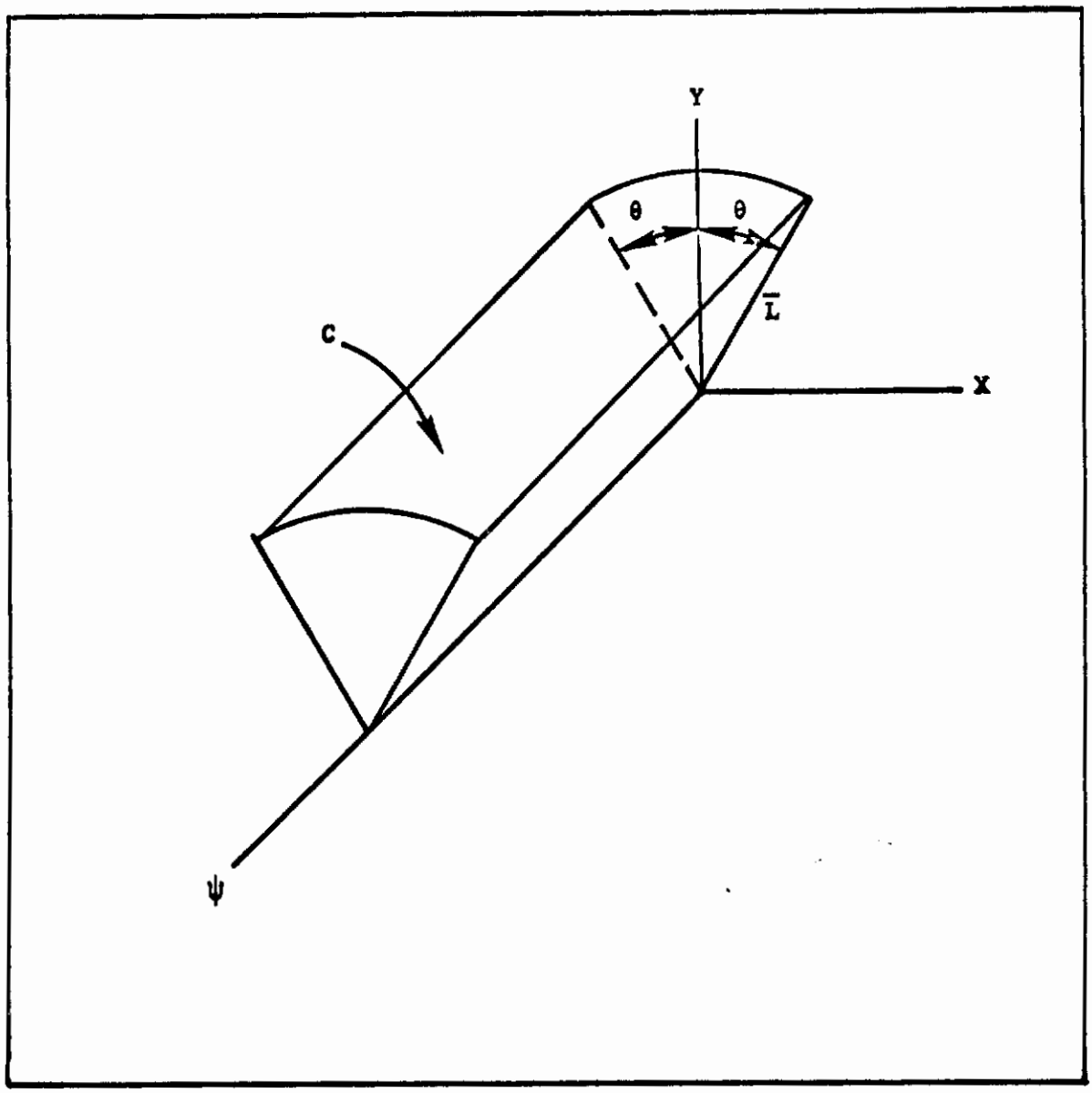

Fig. 9.--The Terminal Surface for Problem II

Problem III

The third problem adds considerably more realism to the description of the air-to-air combat problem. For this problem each player is able to maneuver in three dimensional space. In addition, each player has the potential for accelerating or decelerating. Consequently the speeds vary with time. It will be seen that more state variables and control variables enter this problem relative to the two previous problems.

The derivation of the state differential equations is dependent upon the velocity of the reduced coordinate (equal to the pursuer's velocity) and the external forces experienced by each system. In Figure 10 is illustrated the normal $\bar{a}_N$ and tangential acceleration $\bar{a}_V$ components, the angular velocity $\bar{\omega}$, and the control angle ϕ. In Figure 11 is illustrated the geometry for Problem III. The difference between this problem and the previous two problems is that $\bar{X}_P$, $\bar{X}_E$, and $\bar{X}$ are measured in a three dimensional space.

In Appendix A are presented the details of the derivation of the state differential equations. The velocity vectors $\bar{V}_P$ and $\bar{V}_E$ and the angular velocity of the relative $\bar{\omega}$ coordinate frame are

$$\bar{V}_P = V_P \bar{e}_y \tag{36}$$

$$\bar{V}_E = V_E(\bar{e}_x \sin\gamma \cos\sigma + \bar{e}_y \cos\gamma + \bar{e}_z \sin\gamma \sin\sigma) \tag{37}$$

$$\bar{\omega} = \frac{V_P}{R_P} \alpha_P (\bar{e}_x \cos\phi_P + \bar{e}_z \sin\phi_P) \tag{38}$$

The position of E relative to P, namely $\bar{X}$, can be written as

$$\bar{X} = \bar{y} + \bar{r} \tag{39}$$

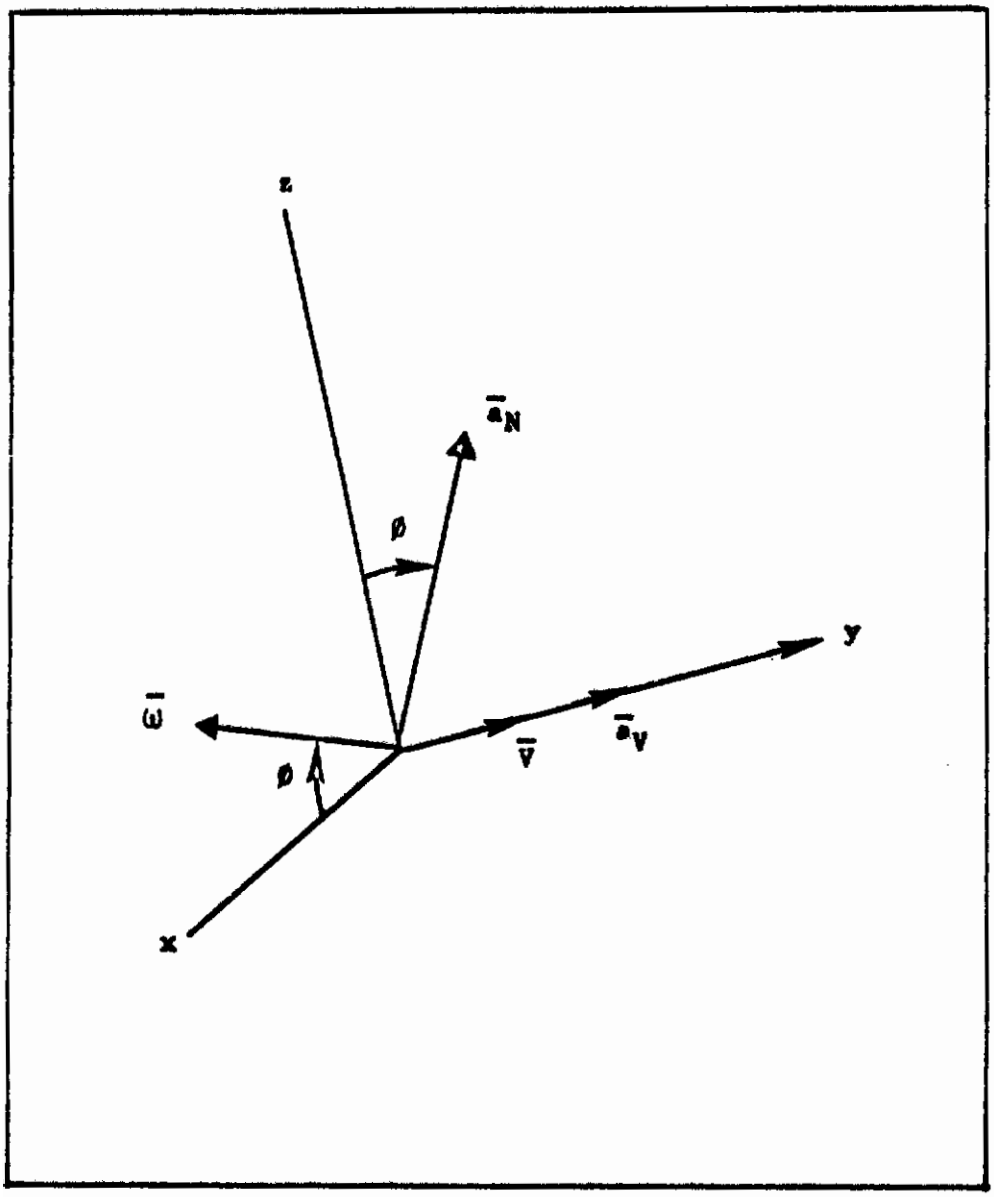

Fig. 10.--Problem III Vectors

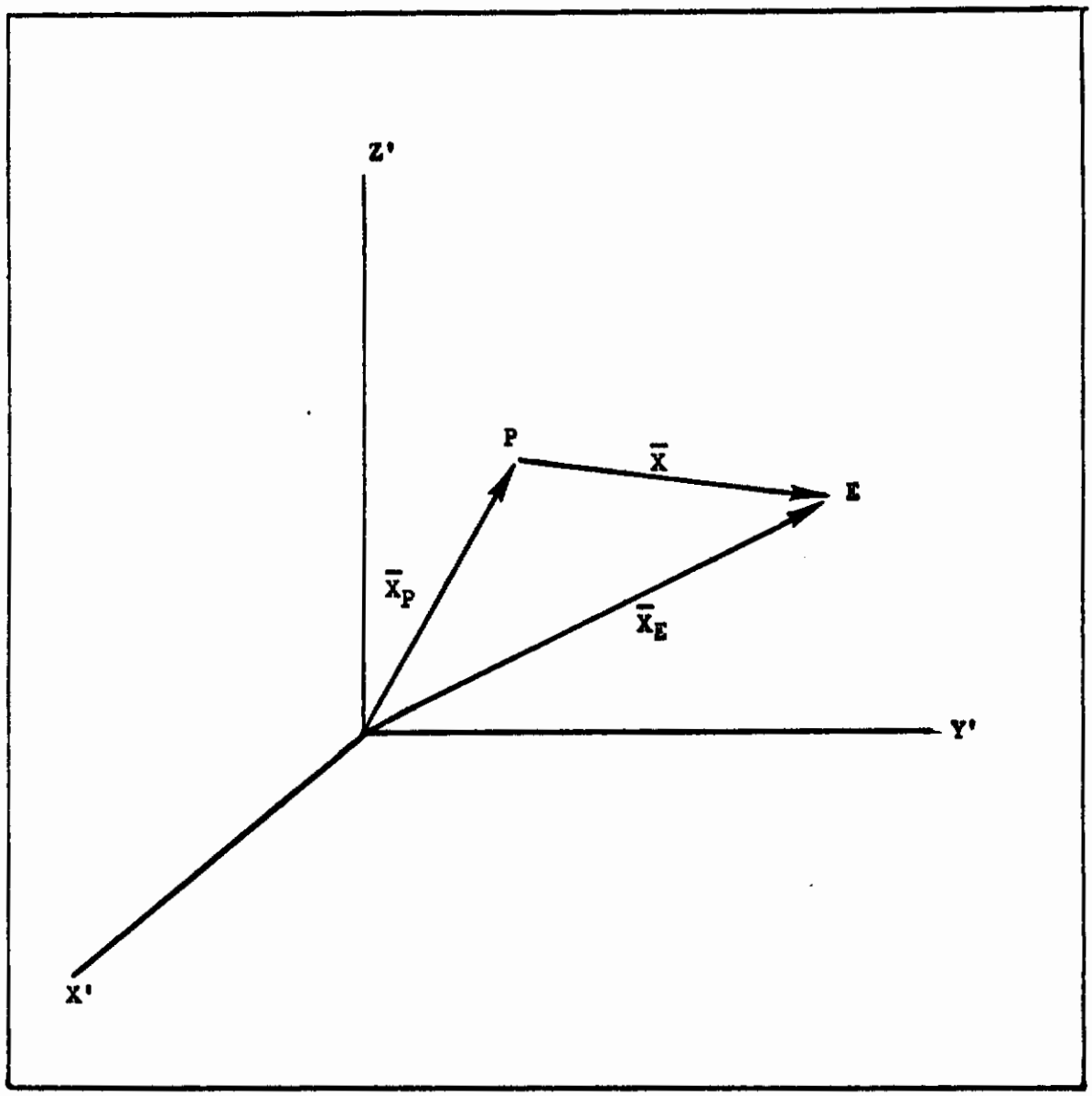

Fig. 11.--The Geometry for Problem III

where $\bar{r}$ is the component of $\bar{x}$ in the xz plane. The vector $\bar{r}$ makes an angle Δ with the x axis. Introduce δ_1 and δ_2 defined by

$$\delta_1 = \sigma - \Delta \tag{40}$$

$$\delta_2 = \phi_P - \Delta \tag{41}$$

Through evaluation of the acceleration components normal to and parallel to $\bar{V}_P$, the following differential equations are derived in Appendix A

$$\dot{r} = V_E \sin\gamma \cos\delta_1 + \frac{a_{N_P}}{V_P} y \sin\delta_2 \tag{42}$$

$$\dot{y} = V_E \cos\gamma - V_P - \frac{a_{N_P}}{V_P} r \sin\delta_2 \tag{43}$$

$$\dot{\gamma} = -\frac{a_{N_E}}{V_E} \sin\phi_E + \frac{a_{N_P}}{V_P} \sin(\delta_2 - \delta_1) \tag{44}$$

$$\dot{\delta}_1 = \frac{a_{N_E}}{V_E} \sin\gamma \cos\phi_E - \frac{1}{r}\left(V_E \sin\gamma \sin\delta_1 - \frac{a_{N_P}}{V_P} y \cos\delta_2\right) \tag{45}$$

$$\dot{V}_E = g\, C_{T_E} - \frac{K_E W_E}{g\, Q_E S_E}\, a_{N_E}{}^2 \tag{46}$$

$$\dot{V}_P = g\, C_{T_P} - \frac{K_P W_P}{g\, Q_P S_P}\, a_{N_P}{}^2 \tag{47}$$

where P's controls are a_{N_P}, δ_2, and C_{T_P}; E's controls are a_{N_E}, ϕ_E, and C_{T_E}; g is the acceleration of gravity; K is an aerodynamic drag parameter; W is the weight; Q is the dynamic pressure and S is the reference area for the aerodynamic drag parameters. The coefficient C_T is defined by

$$C_T = \frac{T}{W} - \frac{D_o}{W} \tag{48}$$

where T is the engine thrust and D_o is the zero lift aerodynamic drag. The control constraints are

$$0 \leq a_N \leq a_{N_{MAX}} \tag{49}$$

$$C_{T_{MIN}} \leq C_T \leq C_{T_{MAX}} \tag{50}$$

Consequently a_N and C_T are bounded for both P and E. Eqs (42) through (47), (49) and (50) define the state differential equations and control constraints for Problem III.

Some comments are in order relative to the comparison between Problems II and III. If the speeds are constant and the motions are two dimensional, then it should be possible to reduce Problem III to Problem II. First the magnitude of the normal acceleration vector is related to α in Eqs (26) through (30) by

$$a_N = -\frac{V^2}{R}\alpha \tag{51}$$

The negative sign results from the difference in the direction of the normal acceleration in the two problems. Equating the variables in Problem III to corresponding variables in Problem II in the following manner

$$(r, y, \phi_E, \delta_1, \delta_2, \gamma)_{III} = (x, y, \frac{\pi}{2}, 0, \frac{\pi}{2}, \psi)_{II}$$

shows that Problem III reduces directly to Problem II. Also, whereas Problem II has three state variables and two controls, Problem III has six state variables and six controls.

As in Problems I and II, nondimensional variables are introduced in order to study a class of problems. Similar to Eqs (19) through (22), let

$$X = r/R_o \tag{52}$$

$$Y = y/R_o \tag{53}$$

$$\tau = gt/V_o \tag{54}$$

$$u = V_P/V_o \tag{55}$$

$$v = V_E/V_o \tag{56}$$

$$\alpha_1 = V_o^2/g\ R_o \tag{57}$$

$$\alpha_2 = \frac{2K_E\ W_E}{\rho_E\ V_o^2\ S_E} \tag{58}$$

$$\alpha_3 = \frac{2K_P\ W_P}{\rho_P\ V_o^2\ S_P} \tag{59}$$

where R_o and V_o are a characteristic length and speed which will be defined later. Substitution of Eqs (52) through (59) gives

$$\dot{X} = \alpha_1\ V \sin\gamma \cos\delta_1 + \frac{n_P Y}{u} \sin\delta_2 \tag{60}$$

$$\dot{Y} = \alpha_1\ V \cos\gamma - \alpha_1\ u - \frac{n_P X}{u} \sin\delta_2 \tag{61}$$

$$\dot{\gamma} = -\frac{n_E}{V} \sin\phi_E + \frac{n_P}{u} \sin(\delta_2 - \delta_1) \tag{62}$$

$$\dot{\delta}_1 = \frac{n_E}{V} \sin\gamma \cos\phi_E - \alpha_1 \frac{V}{X} \sin\gamma \sin\delta_1 + \frac{n_P}{u} \frac{Y}{X} \cos\delta_2 \tag{63}$$

$$\dot{v} = C_{T_E} - \alpha_2 \frac{n_E^2}{V^2} \tag{64}$$

$$\dot{u} = C_{T_P} - \alpha_3 \frac{n_P^2}{u^2} \tag{65}$$

where differentiation is with respect to τ. The control constraints are

$$C_{T_{E_{MIN}}} \leq C_{T_E} \leq C_{T_{E_{MAX}}} \tag{66}$$

$$C_{T_{P_{MIN}}} \leq C_{T_P} \leq C_{T_{P_{MAX}}} \tag{67}$$

$$0 \leq n_E \leq n_{E_{MAX}} \tag{68}$$

$$0 \leq n_P \leq n_{P_{MAX}} \tag{69}$$

The terminal surface has dimension five. The constraint is on the angle-off of the evader relative to the pursuer's velocity vector.

Finally a comment on the significance of the introduction of the relative coordinate frame attached to the pursuer's position is in order. In Problems I, II, and III, two, three, and six state variables resulted. If the descriptions were based upon a fixed non-rotating coordinate frame, then five state variables would have resulted in Problem I, two spatial coordinates each for P and E plus the heading angle for P. In Problem II, six state variables would have resulted, those in Problem I plus E's heading angle. In Problem III twelve states would have occurred, six for each player. The six variables are the three spatial coordinates, the speed, and two angular displacements for defining the orientation of the velocity vector in the

playing space. Clearly the introduction of a relative coordinate frame results in a significant decrease in the number of variables required to define the state.

Having formulated the three problems, we can now turn our attention to obtaining their solutions. Sections IV, V, and VI will be concerned with solving Problems I, II and III respectively.

SECTION IV

PROBLEM I SOLUTION

Problem Definition

The differential equations of state and the control constraint were derived in Appendix A and presented in Chapter III. Eqs (23), (24), and (25) define the nondimensional state differential equations and the control constraint, respectively:

$$\dot{X} = \epsilon \sin \psi - \alpha_p Y \tag{23}$$

$$\dot{Y} = \epsilon \cos \psi - 1 + \alpha_p X \tag{24}$$

$$-1 \leq \alpha_p \leq 1. \tag{25}$$

P's control variable is α_p and ψ is E's control variable.

The Approximation of the Terminal Surface

The terminal surface is illustrated in Figure 8. The corners between the terminal surface and the two rays from the origin at the angle-off θ are smoothed like that illustrated in Figure 12. The rays are perpendicular to the terminal surface and the terminal surface has a constant radius of curvature $\bar{L}$ between the corners. Let the coordinates X_o, Y_o correspond to the center of either circle which is tangent to both the ray from the origin and the terminal surface. The radius of the circle is r which is assumed to be much smaller than $\bar{L}$.

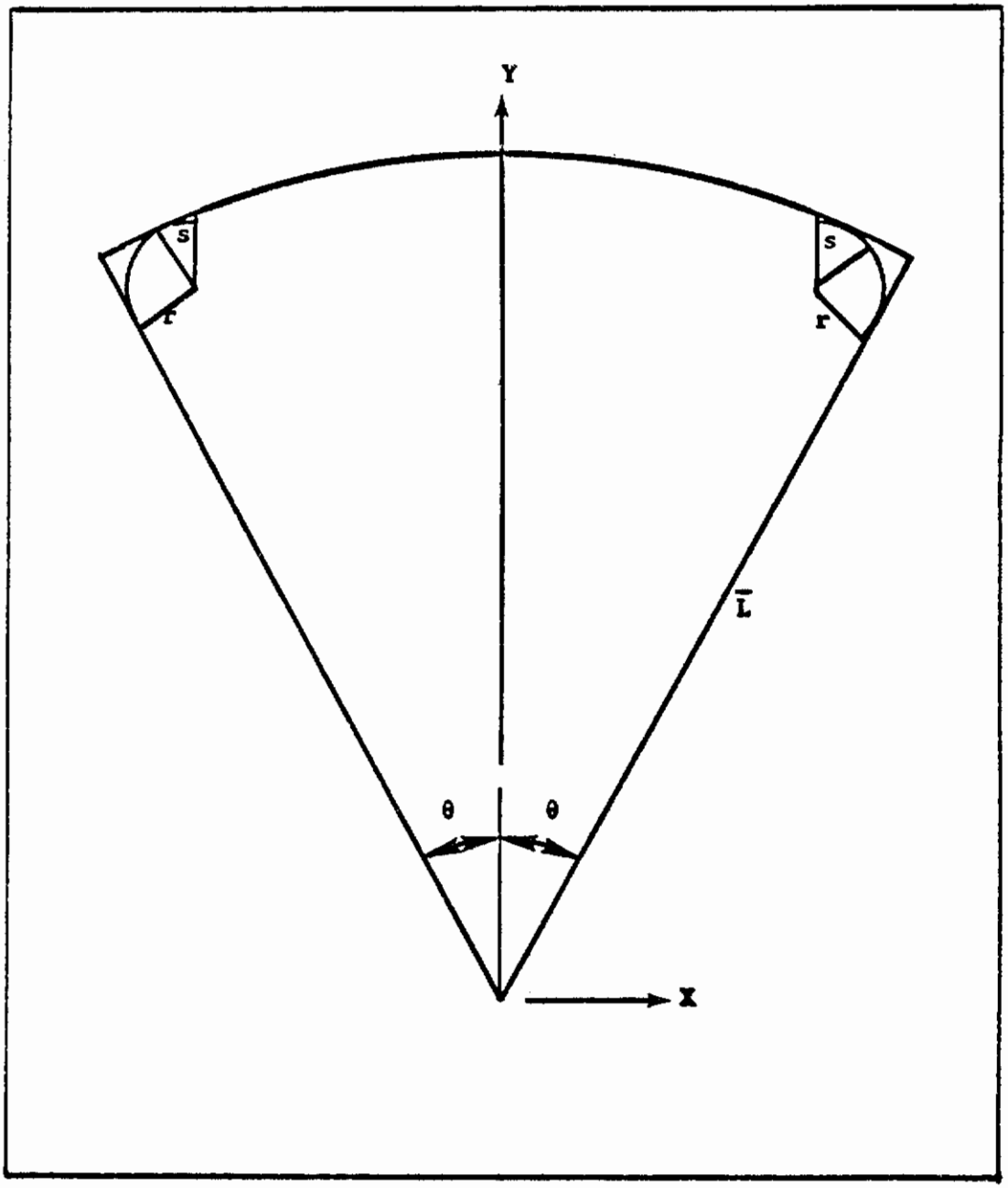

Fig. 12.--The Smooth Terminal Surface

It is easily shown that the center for the right circle is located at

$$X_o = \bar{L} \sin\theta - r(\sin\theta + \cos\theta)$$

$$Y_o = \bar{L} \cos\theta - r(\cos\theta - \sin\theta).$$

Similarly for the left circle

$$X_o = -\bar{L} \sin\theta + r(\cos\theta + \sin\theta)$$

$$Y_o = \bar{L} \cos\theta - r(\cos\theta - \sin\theta).$$

Any point on the arc of the right circle is defined by

$$X = \bar{L} \sin\theta + r(\sin s - \sin\theta - \cos\theta) \qquad (70)$$

$$Y = \bar{L} \cos\theta + r(\cos s + \sin\theta - \cos\theta) \qquad (71)$$

where s is the angular displacement on the circles measured relative to the Y axis. On the left circle

$$X = -\bar{L} \sin\theta + r(-\sin s + \sin\theta + \cos\theta) \qquad (72)$$

$$Y = \bar{L} \cos\theta + r(\cos s + \sin\theta - \cos\theta). \qquad (73)$$

The necessary conditions for the barrier will be established next, then the limit determined as r goes to zero.

The Necessary Conditions

The first necessary condition is the optimality condition, Eq (7). Substitution of Eqs (23) and (24) gives

$$\min_{\alpha_p} \max_{\psi} \left[\nu_1(\epsilon \sin\psi - \alpha_p Y) + \nu_2(\epsilon \cos\psi - 1 + \alpha_p X)\right] = 0. \tag{74}$$

The optimal controls for P and E are

$$\sin\psi^* = \nu_1 \qquad \cos\psi^* = \nu_2 \tag{75}$$

$$\alpha_p^* = \operatorname{sgn} A \quad ; \quad A = \nu_1 Y - \nu_2 X. \tag{76}$$

where sgn is the sign function defined by

$$\begin{aligned} \operatorname{sgn} A &= 1 \quad \text{if} \quad A > 0 \\ &= -1 \quad \text{if} \quad A < 0. \end{aligned}$$

Eq (15) defines a necessary condition for the intersection of the barrier and the terminal surface. The parametric representation of the terminal surface is defined by Eqs (70) through (73) where s is the parameter which defines the normal to the terminal surface. On the right side of the terminal surface, substitution of Eqs (70) and (71) into Eq (15) gives

$$r(\nu_1 \cos s - \nu_2 \sin s) = 0. \tag{77}$$

Since $\bar{\nu}$ points away from the terminal surface, select

$$\begin{aligned} \nu_1 &= \sin s \\ \nu_2 &= \cos s. \end{aligned} \tag{78}$$

On the left side of the terminal surface, Eqs (15), (72), and (73) give

$$r(-\nu_1 \cos s - \nu_2 \sin s) = 0. \tag{79}$$

For the proper orientation, select

$$\begin{aligned} \nu_1 &= -\sin s \\ \nu_2 &= \cos s. \end{aligned} \tag{80}$$

Eqs (78) and (80) define boundary conditions for the barriers on the terminal surface. According to Eq (76), P's optimal control is dependent upon the sign of A. On the right side of the terminal surface ($X > 0$)

$$A = \bar{L} \sin (s-\theta) + r \left[\cos (s-\theta) - \sin (s-\theta)\right] \tag{81}$$

On the left side of the terminal surface ($X < 0$)

$$A = -\bar{L} \sin (s-\theta) - r \left[\sin (s-\theta) + \cos (s-\theta)\right] \tag{82}$$

In the limit as r goes to zero, then

$$A \rightarrow \pm \bar{L} \sin (s-\theta)$$

If $s \leq \theta$, then the corner conditions do not hold and we set $\theta = s$. In this case

$$A = 0 \tag{83}$$

and P's controls are undefined. We will come back to this situation later. If $\theta < s$, then A is positive on the right corner and negative on the left corner. Consequently P's controls on the terminal surface are +1 on the right corner and -1 on the left corner.

The boundary of the usable part (BUP) is obtained from Eqs (7), (70) through (73), (78), and (80). Substitution of the optimal

controls and Eqs (23) and (24) into Eq (7) gives

$$\epsilon - \nu_2 - \alpha_p^* A = 0 \tag{84}$$

On the right corner in the limit as r goes to zero

$$\epsilon - \cos s - \bar{L} \sin (s-\theta) = 0. \tag{85}$$

Similarly for the left corner

$$\epsilon - \cos s - \bar{L} \sin (s-\theta) = 0 \tag{86}$$

The usable part (UP) of the terminal surface is obtained from

$$\min_{\alpha_p} \max_{\psi} \bar{\nu} \cdot \bar{f} < 0$$

or

$$\epsilon - \nu_2 - \alpha_p^* A < 0. \tag{87}$$

This inequality is satisfied by any point between the corners. Thus the UP is the arc between the corners.

It will be convenient at this point to introduce a new non-dimensional time defined by

$$\beta = \tau_f - \tau \tag{88}$$

where τ_f denotes the nondimensional time on the terminal surface. Through the introduction of β, the terminal boundary conditions with respect to τ are initial boundary conditions with respect to β. In addition the differential equations of state are integrated in a

retrogressive sense, that is, backwards in time. The transformed differential equations of state become upon substitution of the optimal controls for E

$$X' = -\epsilon \nu_1 + \alpha_P^* Y \tag{89}$$

$$Y' = -\epsilon \nu_2 + 1 - \alpha_P^* X \tag{90}$$

$$\alpha_P^* = \text{sgn } A$$

where the primes imply differentiation with respect to β. The differential equations for ν_1 and ν_2 are obtained from Eq (13). Introducing the new time variable results in a positive sign on the right side of Eq (13). The differential equations for ν_1 and ν_2 are therefore

$$\nu_1' = \alpha_P^* \nu_2 \tag{91}$$

$$\nu_2' = -\alpha_P^* \nu_1. \tag{92}$$

The boundary conditions are as follows with respect to β

$$X(0) = \bar{L} \sin\theta \quad \text{right corner} \tag{93}$$

$$= -\bar{L} \sin\theta \quad \text{left corner}$$

$$Y(0) = \bar{L} \cos\theta \tag{94}$$

$$\nu_1(0) = \sin s \quad \text{right corner} \tag{95}$$

$$= -\sin s \quad \text{left corner}$$

$$\nu_2(0) = \cos s. \tag{96}$$

If $\theta \geq s$, then θ is replaced with s. In this case Eq (83) shows that P's control is undefined. Through differentiation of A, it can be

shown that

$$A' = \nu_1 \tag{97}$$

Consequently on the right side of the terminal surface

$$A' = \sin s > 0$$

and on the left side

$$A' = -\sin s < 0.$$

Therefore

$$\alpha_p^* = +1 \qquad \text{right barrier} \tag{98}$$

$$= -1 \qquad \text{left barrier} \tag{99}$$

P's controls are constant as long as A does not change sign. Thus the boundary value problem for the two barriers is defined by Eqs (89) through (96), (98), and (99).

The Trajectory Solution

The differential equations are linear with constant coefficients. They are, therefore, well suited to solution by means of Laplace transforms. Let $T(\cdot)$ denote the Laplace transform of $(\cdot)$ and z the Laplace transform variable. The transformed problem becomes

$$zT(X) - \alpha_p^* \bar{L} \sin\theta = -\epsilon T(\nu_1) + \alpha_p^* T(Y)$$

$$zT(Y) - \bar{L}\cos\theta = -\epsilon T(\nu_2) + \frac{1}{z} - \alpha_p^* T(X)$$

$$zT(\nu_1) - \alpha_p^* \sin s = \alpha_p^* T(\nu_2)$$

$$zT(\nu_2) - \cos s = -\alpha_p^* T(\nu_1)$$

Four linear algebraic equations result. The latter two equations are independent of T(X) and T(Y). Therefore, we solve for $T(\nu_1)$ and $T(\nu_2)$ and then substitute the solutions into the first two equations and solve for T(X) and T(Y). The result is

$$T(\nu_1) = \frac{z}{z^2 + \alpha_p^{*2}} \cdot \alpha_p^* \sin s + \frac{\alpha_p^*}{z^2 + \alpha_p^{*2}} \cos s$$

$$T(\nu_2) = \frac{z}{z^2 + \alpha_p^{*2}} \cos s - \frac{\alpha_p^*}{z^2 + \alpha_p^{*2}} \cdot \alpha_p^* \sin s$$

$$T(X) = \frac{z}{z^2 + \alpha_p^{*2}} \left[\alpha_p^* \bar{L} \sin\theta - \epsilon T(\nu_1)\right] + \frac{\alpha_p^*}{z^2 + \alpha_p^{*2}} \left[\bar{L} \cos\theta - \epsilon T(\nu_2) + \frac{1}{z}\right]$$

$$T(Y) = \frac{z}{z^2 + \alpha_p^{*2}} \left[\bar{L} \cos\theta - \epsilon T(\nu_2) + \frac{1}{z}\right] - \frac{\alpha_p^*}{z^2 + \alpha_p^{*2}} \left[\alpha_p^* \bar{L} \sin\theta - \epsilon T(\nu_1)\right]$$

The inverse transformations are easily obtained by means of Laplace transform tables and the convolution property of Laplace transforms. The solution for the dependent variables is

$$\nu_1(\beta) = \sin \alpha_p^* (s + \beta)$$

$$\nu_2(\beta) = \cos \alpha_p^* (s + \beta)$$

$$X(\beta) = \bar{L} \sin \alpha_p^*(\theta + \beta) + \alpha_p^*(1 - \cos \alpha_p^* \beta) - \epsilon\beta \sin \alpha_p^*(s + \beta)$$

$$Y(\beta) = \bar{L} \cos \alpha_p^*(\theta + \beta) + \alpha_p^* \sin \alpha_p^* \beta - \epsilon\beta \cos \alpha_p^*(s + \beta)$$

where s is the solution of Eqs (85) and (86). If $\theta \geq s$, then we set $\theta = S$ where

$$S = \cos^{-1} \epsilon$$

Since $\alpha_p^* = 1$ on the right barrier and $\alpha_p^* = -1$ on the left barrier, we see immediately that the barriers are symmetric about the Y-axis.

The solution for the values of the parameters $\bar{L}$ and ϵ which separate the playing region into two parts is determined from

$$X(\bar{\beta}) = 0$$

$$X'(\bar{\beta}) = 0$$

where $\bar{\beta}$ is the nondimensional time that the barrier reaches the Y-axis. An alternative to using the rate equation $X'(\bar{\beta}) = 0$ is to use $v_2(\bar{\beta}) = 0$ since $\bar{v}(\beta)$ is perpendicular to the barrier which is tangent to the Y-axis at time $\bar{\beta}$. Three unknowns $\bar{L}$, S, and $\bar{\beta}$ result. They are obtained from the previous two equations and Eq (85), thus for the right barrier

$$\bar{L} \sin (\theta + \bar{\beta}) + 1 - \cos \bar{\beta} - \epsilon\bar{\beta} \sin (s + \bar{\beta}) = 0 \qquad (100)$$

$$\bar{L} \cos (\theta + \bar{\beta}) + \sin \bar{\beta} - \epsilon \sin (s + \bar{\beta}) - \epsilon\bar{\beta} \cos (s + \bar{\beta}) = 0 \qquad (101)$$

$$\epsilon - \cos s - \bar{L} \sin (s - \theta) = 0. \qquad (85)$$

Consider first the natural barrier, i.e., $\theta > S$. For this case

$$\cos S = \epsilon. \tag{102}$$

Eqs (100) and (101) become upon substitution of $\theta = S$

$$(\bar{L} - \epsilon\bar{\beta}) \sin (S + \bar{\beta}) + 1 - \cos \bar{\beta} = 0 \tag{103}$$

$$(\bar{L} - \epsilon\bar{\beta}) \cos (S + \bar{\beta}) + \sin \bar{\beta} - \epsilon \sin (S + \bar{\beta}) = 0. \tag{104}$$

Expansion of the last two terms in the latter equation and substitution of Eq (102) gives

$$\begin{aligned} \sin \bar{\beta} - \epsilon \sin (S + \bar{\beta}) &= \sin \bar{\beta} - \cos S(\sin S \cos \bar{\beta} + \cos S \sin \bar{\beta}) \\ &= \sin \bar{\beta} \sin^2 S - \sin S \cos S \cos \bar{\beta} \\ &= - \sin S \cdot \cos (S + \bar{\beta}). \end{aligned}$$

Substitution into Eq (104) and rearranging gives

$$(\bar{L} - \epsilon\bar{\beta}) \cos (S + \bar{\beta}) - \sin S \cdot \cos (S + \bar{\beta}) = 0$$

or

$$(\bar{L} - \epsilon\bar{\beta} - \sin S) \cos (S + \bar{\beta}) = 0.$$

The solution is

$$S + \bar{\beta} = \frac{\pi}{2}$$

which also agrees with $\nu_2(\bar{\beta}) = 0$. Substitution into Eq (103) gives

$$\bar{L} - \epsilon \left(\frac{\pi}{2} - S\right) + 1 - \cos \left(\frac{\pi}{2} - S\right) = 0.$$

Solving for $\bar{L}$ gives

$$\bar{L} = \epsilon \left(\frac{\pi}{2} - \cos^{-1} \epsilon \right) - 1 + \sin S$$

$$= \epsilon \sin^{-1} \epsilon - 1 + \sqrt{1 - \epsilon^2} \qquad (105)$$

Eq (105) defines the relationship between the capture range $\bar{L}$ and the speed ratio ϵ. Figures 13, 14, and 15 depict the natural barriers for $\epsilon = 0.5$, 0.9, and 0.999, respectively. With respect to the non-dimensional time τ, the barrier trajectory starts on the Y-axis and ends on the terminal surface.

The situation for the artificial barrier, $\theta < S$, is clearly more complicated relative to the natural barrier problem. From Eq (85)

$$\cos s = \epsilon - \bar{L} \sin (s - \theta) < \epsilon$$

since $S > \theta$. Therefore

$$s > \cos^{-1} \epsilon$$

Recall that s defines the unit vector $\bar{v}$ normal to the terminal surface. On the natural barrier the unit vector eventually rotates away from the Y-axis. At the tangency point between the barrier and the Y-axis the vector is normal to the Y-axis. Therefore, we consider the possibility that the artificial barrier falls upon the natural barrier. If so, the natural barrier is determined from the intersection of the ray from the origin at the angle θ and the natural barrier as illustrated in Figure 16. If this is the case, then the time to

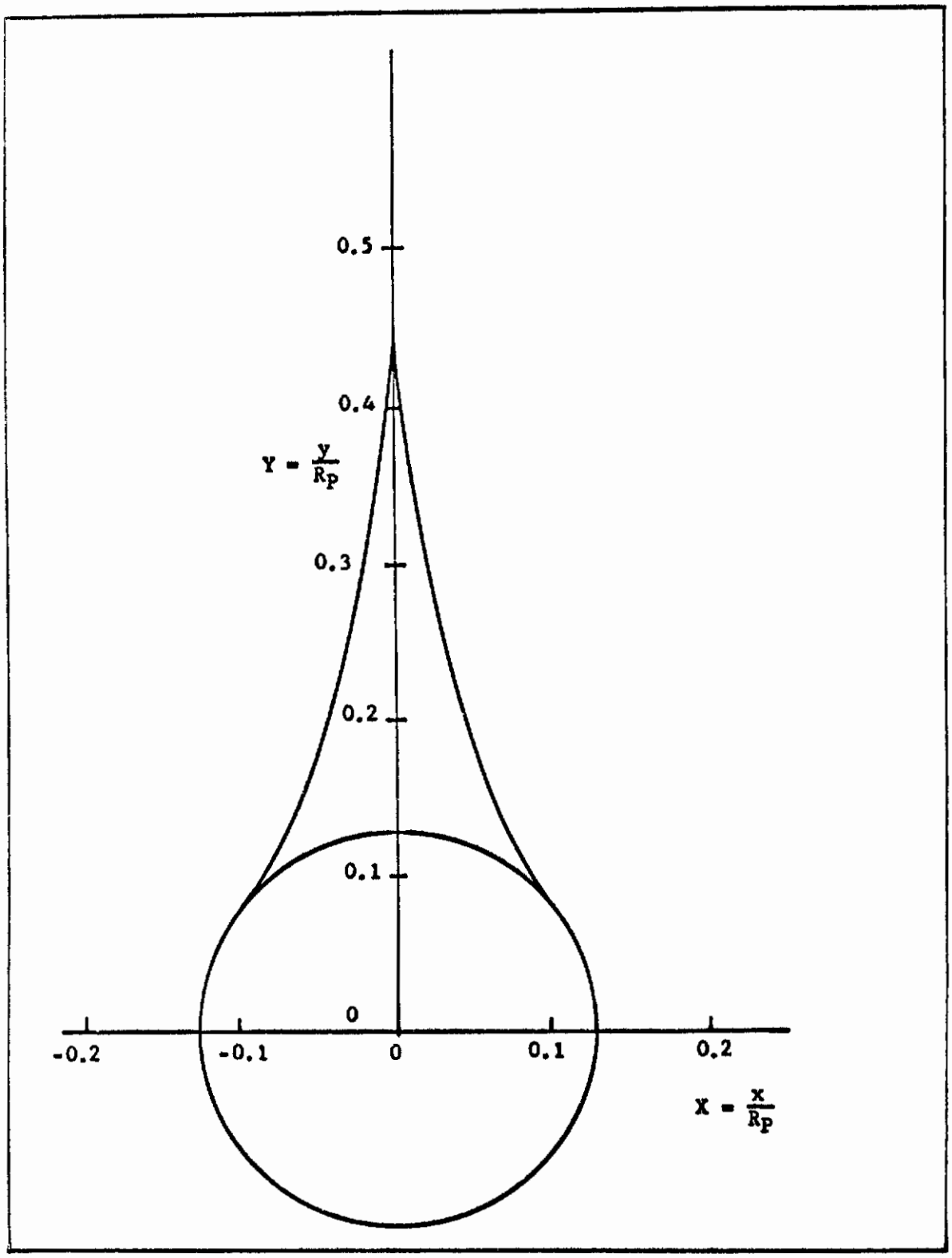

Fig. 13.--Natural Barriers for $\epsilon = 0.5$

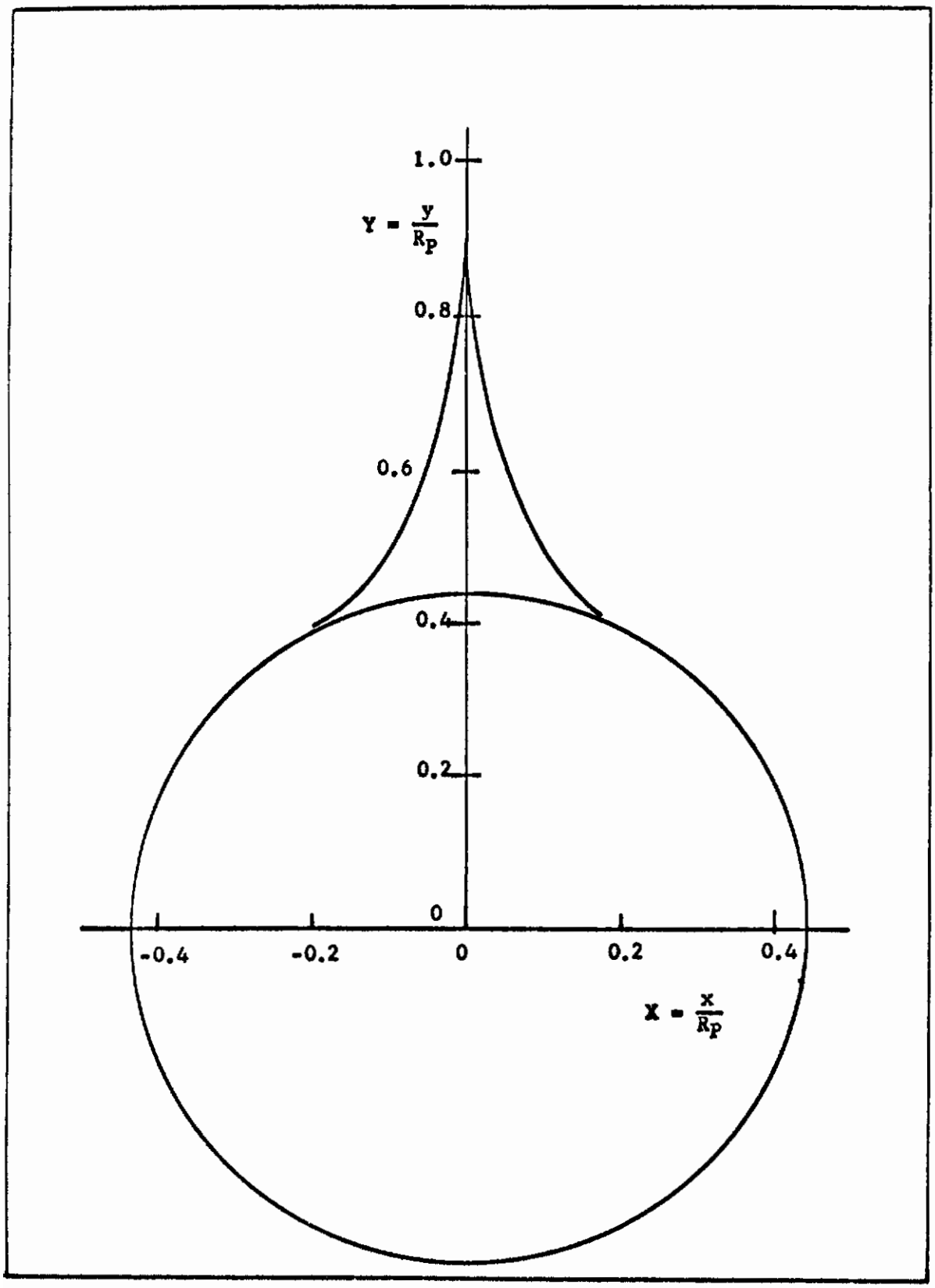

Fig. 14.--Natural Barriers for $\epsilon = 0.9$

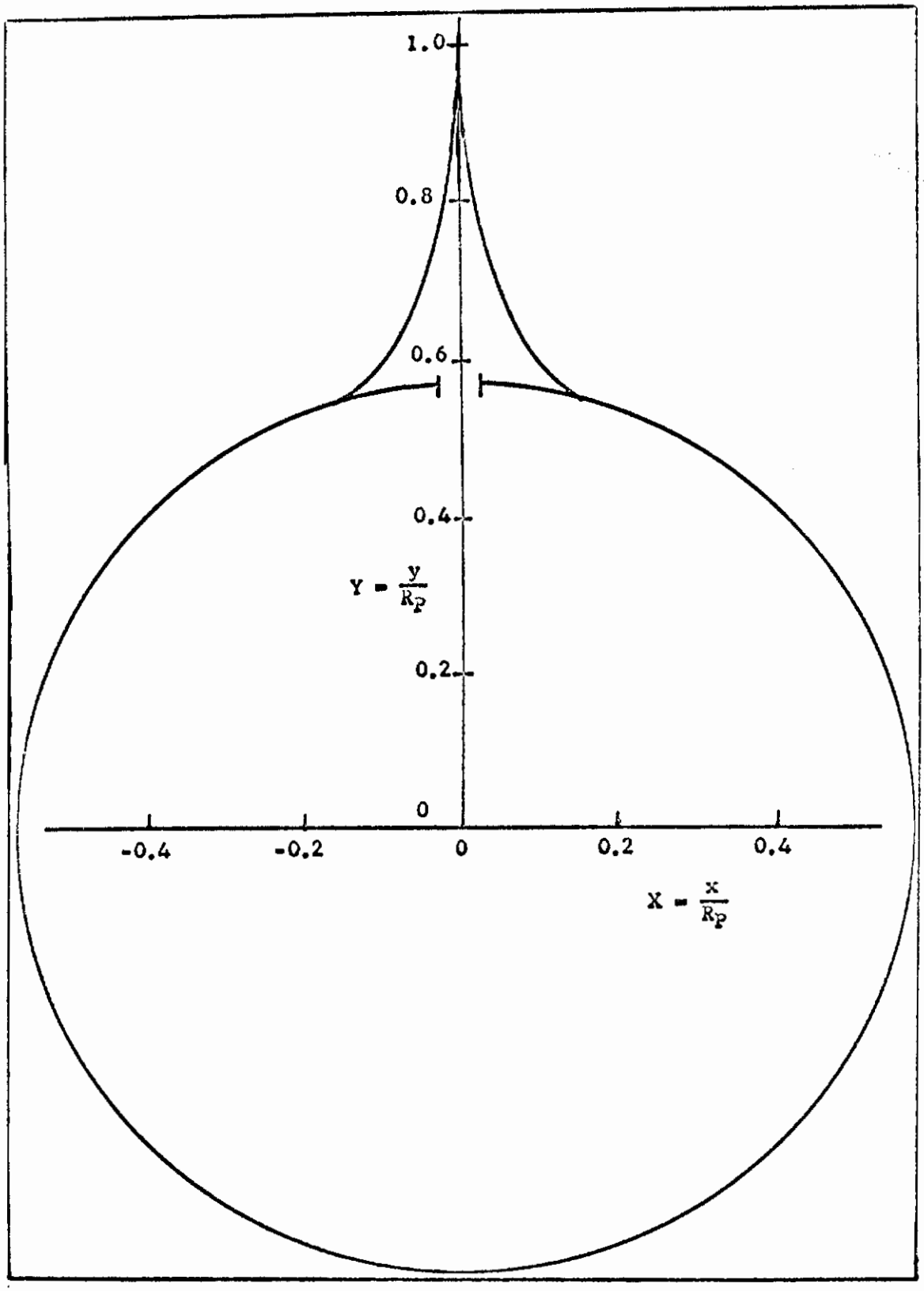

Fig. 15.--Natural Barriers for $\epsilon = 0.999$

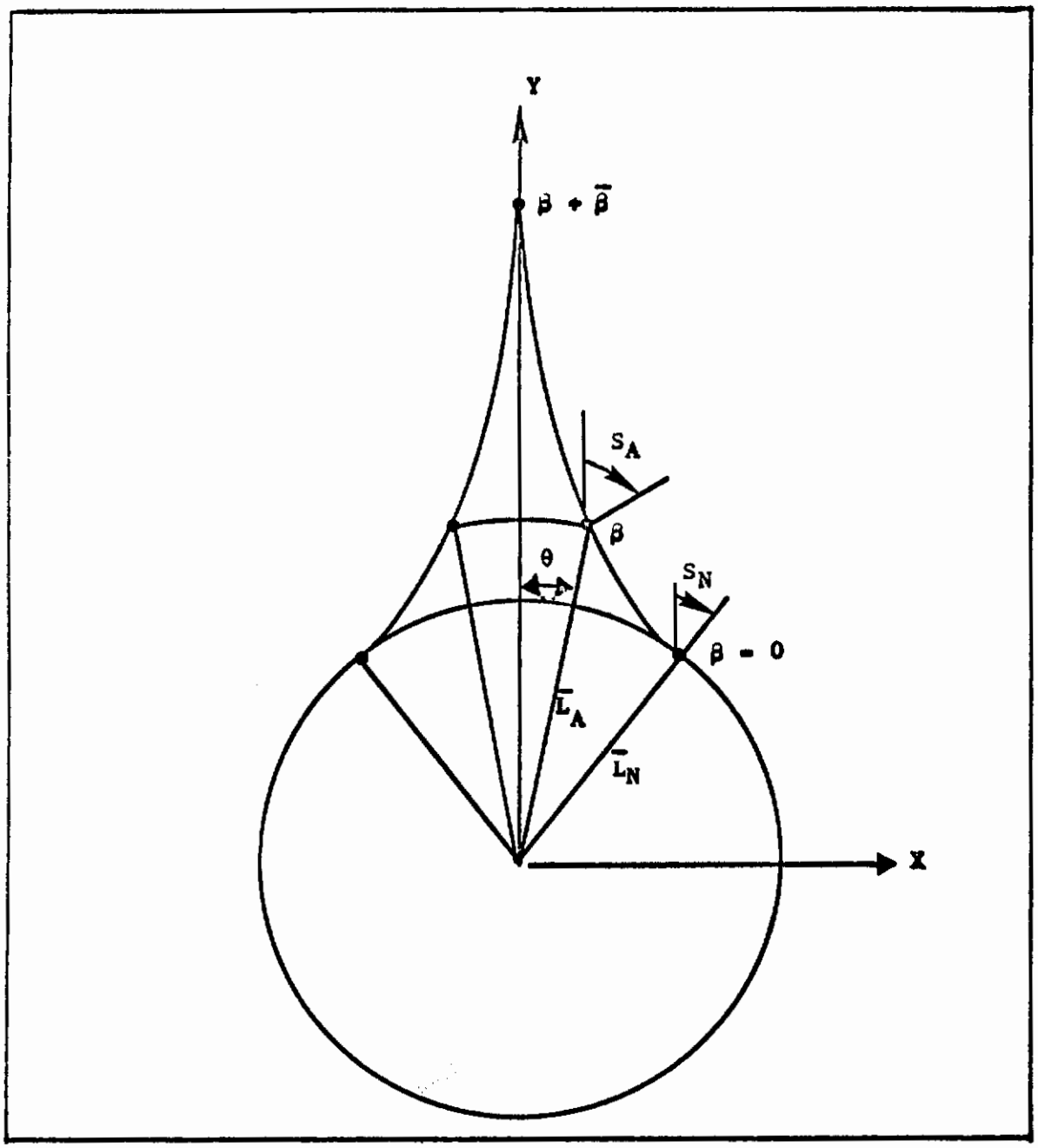

Fig. 16.--Natural Barrier Intersection

travel from the intersection to the Y-axis should be the same for both the natural and artificial barriers. Let subscript A and N correspond to the artificial and natural barrier, respectively. Since the trajectories are the same, it follows that

$$\beta + \bar{\beta} = \frac{\pi}{2} - S_N$$

$$S_A = S_N + \beta$$

$$X = \bar{L}_A \sin\theta$$

$$Y = \bar{L}_A \cos\theta$$

$$\bar{\beta} = \frac{\pi}{2} - S_A$$

$$X = (\bar{L}_N - \epsilon\beta) \sin(S_N + \beta) + 1 - \cos\beta$$

$$Y = (\bar{L}_N - \epsilon\beta) \cos(S_N + \beta) + \sin\beta$$

where $\bar{\beta}$ is the time to go from the intersection to the Y-axis and β is the time to travel on the natural barrier from the terminal surface defined by Eq (105) to the intersection X,Y. Substitution into Eq (85) gives

$$\begin{aligned}
&\epsilon - \cos S_A - \bar{L}_A \sin(S_A - \theta) \\
&\quad = \epsilon - \cos S_A - \bar{L}_A \sin S_A \cos\theta + \bar{L}_A \cos S_A \sin\theta \\
&\quad = \epsilon - \cos S_A - Y \sin S_A + X \cos S_A \\
&\quad = \epsilon - \cos S_A - [(\bar{L}_N - \epsilon\beta) \cos S_A + \sin\beta] \sin S_A \\
&\qquad + [(\bar{L}_N - \epsilon\beta) \sin S_A + 1 - \cos\beta] \cos S_A \\
&\quad = \epsilon - \cos(S_A - \beta) \\
&\quad = \epsilon - \cos S_N .
\end{aligned}$$

From Eq (102) we see that Eq (85) is satisfied. Substitution into Eq (100) gives

$$\begin{aligned}
&\bar{L}_A \sin\theta \cos\bar{\beta} + \bar{L}_A \cos\theta \sin\bar{\beta} + 1 - \cos\beta - \epsilon\bar{\beta} \\
&\quad = \left[(\bar{L}_N - \epsilon\beta)\sin S_A + 1 - \cos\beta\right]\cos\bar{\beta} \\
&\qquad + \left[(\bar{L}_N - \epsilon\beta)\cos S_A + \sin\beta\right]\sin\bar{\beta} + 1 - \cos\bar{\beta} - \epsilon\bar{\beta} \\
&\quad = (\bar{L}_N - \epsilon\beta)\sin(S_A + \bar{\beta}) - \cos(\beta + \bar{\beta}) + 1 - \epsilon\bar{\beta} \\
&\quad = \bar{L}_N - \epsilon(\beta + \bar{\beta}) - \cos(\beta + \bar{\beta}) + 1.
\end{aligned}$$

But

$$\beta + \bar{\beta} = \frac{\pi}{2} - S_N.$$

Thus Eq (100) becomes

$$\bar{L}_N - \epsilon\left(\frac{\pi}{2} - S_N\right) - \sin S_N + 1.$$

Substitution of Eq (105) shows that Eq (100) is satisfied. Substitution into Eq (101) gives

$$\begin{aligned}
&\bar{L}_A \cos(\theta - S_A + S_A + \bar{\beta}) + \sin\left(\frac{\pi}{2} - S_A\right) - \epsilon \\
&\quad = \bar{L}_A \cos\left(\theta - S_A + \frac{\pi}{2}\right) + \cos S_A - \epsilon \\
&\quad = -\bar{L}_A \sin(\theta - S_A) + \cos S_A - \epsilon.
\end{aligned}$$

But this is equivalent to Eq (85). Therefore the assumption that the natural and artificial barriers fall on each other is indeed correct.

Therefore, the artificial barrier solution, that is, $\bar{L}$ as a function of ϵ and θ, is obtained by first determining the natural barrier solution and then by constructing rays from the origin to the natural barrier at the angle-off of θ. If the natural barrier is like

that illustrated in Figure 15, then that portion of the natural barrier for which

$$\frac{X}{Y} > \tan \theta$$

is not used since these points result in reaching the natural barrier terminal surface. As a consequence, the relationship for the non-dimensional capture range $\bar{L}$ as a function of ϵ and θ may have discontinuities. The relationship is presented in Figure 17. The significance of the relationship is that it delineates between the capture and the escape sets in the playing space. If the evader is anywhere between the terminal surface and the barrier, as defined by Figure 17 and illustrated in Figure 16, then the pursuer can capture the evader, that is, eventually force the separation range to $\bar{L}$. Conversely, if the evader is initially outside the barrier, then the pursuer can never force the evader to reach $\bar{L}$ if the evader maneuvers optimally. Also, if the relationship is as illustrated in Figure 17, then the maximum initial separation with respect to τ corresponds to the point Y_c where the barrier meets the Y-axis. For capture with respect to time τ, ($\tau = 0$, initial time),

$$\begin{aligned} Y_c = Y(o) &< Y(\bar{\beta}) \\ &= \left[\bar{L}_N - \epsilon\left(\frac{\pi}{2} - S_N\right)\right] \cos\frac{\pi}{2} + \sin\left(\frac{\pi}{2} - S_N\right) \\ &= \cos S_N \\ &= \epsilon. \end{aligned}$$

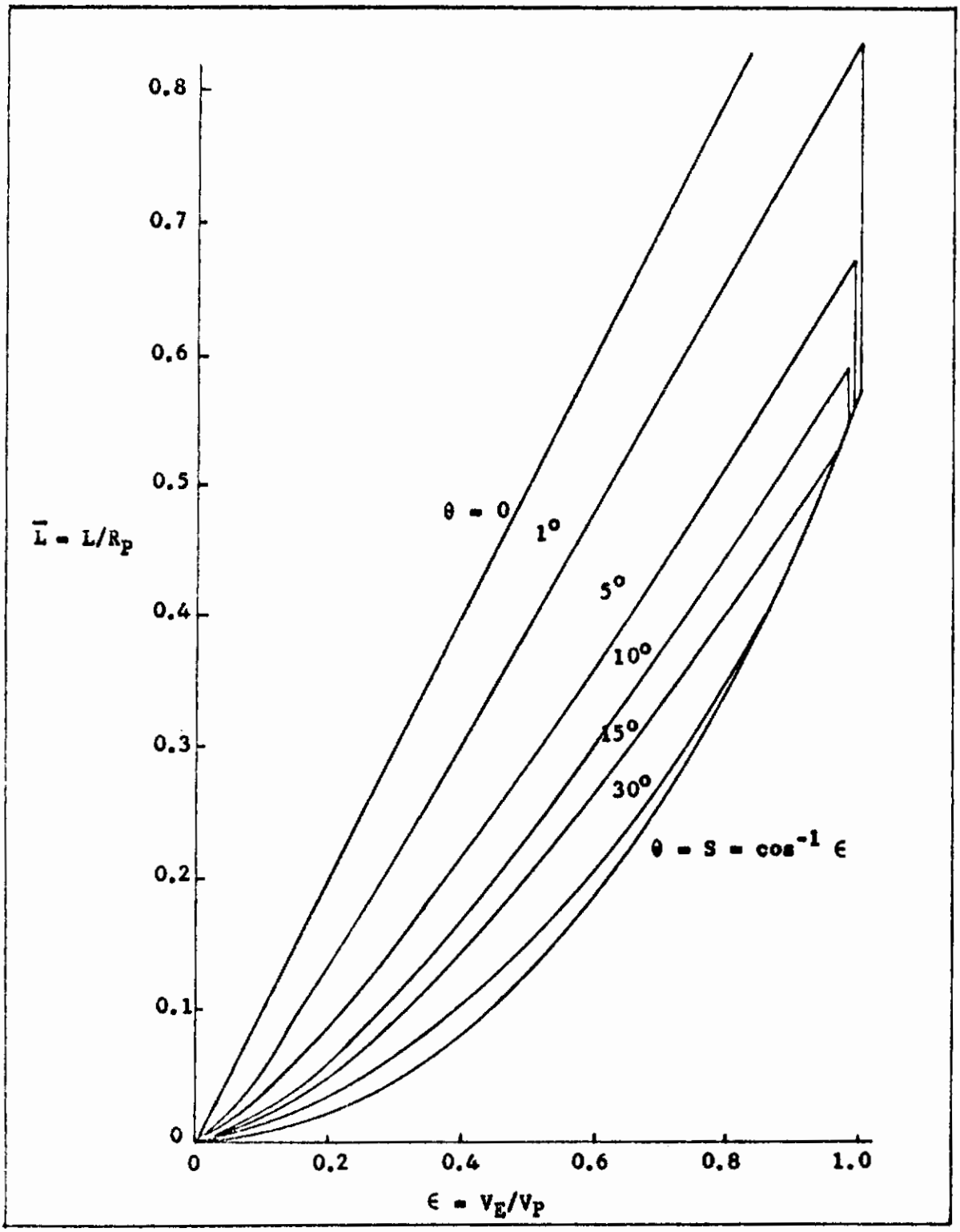

Fig. 17.--Problem I Capture Range

Consequently, if the pursuer captures the evader, then the separation at the beginning of the game must be less than or equal to ϵ. If the game starts at $Y = \epsilon$, $X = 0$, then under optimal play by both players, the minimum separation range is $\bar{L}$.

Capture Range Sensitivity

Consider next the sensitivity of the capture range to changes in the performance parameters. If costs can be assigned to changes in the performance parameters, then the optimal allocation of funds can be determined such that the improvement in $\bar{L}$ (or L, the dimensional capture range) is maximum. It should be clear that P wants to minimize $\bar{L}$ if he can. The evader speed will be held fixed, thus the changes in L are due only to changes in the pursuer's performance. Now L can be written as

$$L = \bar{L}\,(\epsilon,\theta)\; R_p \tag{106}$$

where R_p is the pursuer's minimum turning radius. The differential of L is

$$dL = R_p \frac{\partial \bar{L}}{\partial \theta}\, d\theta + R_p \frac{\partial \bar{L}}{\partial V_p}\, dV_p + \bar{L}\, dR_p$$

The previous equation is based upon the assumption that the pursuer could change θ, V_p, or R_p. Recall that

$$\epsilon = V_E/V_p$$

where V_E, V_p are the evader, pursuer speeds. Differentiation and substitution into Eq (106) gives

$$dL = R_p \frac{\partial \bar{L}}{\partial \theta} d\theta - R_p \epsilon \frac{\partial \bar{L}}{\partial \epsilon} \frac{dV_p}{V_p} + \bar{L}\, dR_p.$$

Dividing by R_p gives

$$\frac{dL}{R_p} = \frac{\partial \bar{L}}{\partial \theta} d\theta - \epsilon \frac{\partial \bar{L}}{\partial \epsilon} \frac{dV_p}{V_p} + \bar{L} \frac{dR_p}{R_p}$$

There are two different equations for R_p. This results from the relationship of maximum aerodynamic control as a function of speed which is illustrated in Figure 18. The aerodynamic control must be less than or equal to n_{MAX}. V_c is defined as the corner speed. Below the corner speed the control is limited by the stall angle-of-attack, that is, an aircraft would stall at higher angles of attack. Above the corner speed the control is limited by the acceleration that the pilot can stand or the structural load capability of the aircraft. The minimum turning radius R then has the following forms

$$R = \frac{2W}{g\rho S C_{L_{MAX}}} \qquad V < V_c$$
$$= \frac{V^2}{a_{N_{MAX}}} \qquad V > V_c \qquad (107)$$

where W is the weight, S is the reference area on which the maximum lift coefficient $C_{L_{MAX}}$ is based, g is the acceleration of gravity, ρ is the atmospheric density, and $a_{N_{MAX}}$ is the maximum normal acceleration. The relationships between $a_{N_{MAX}}$ and n_{MAX} is

$$a_{N_{MAX}} = g\, n_{MAX}.$$

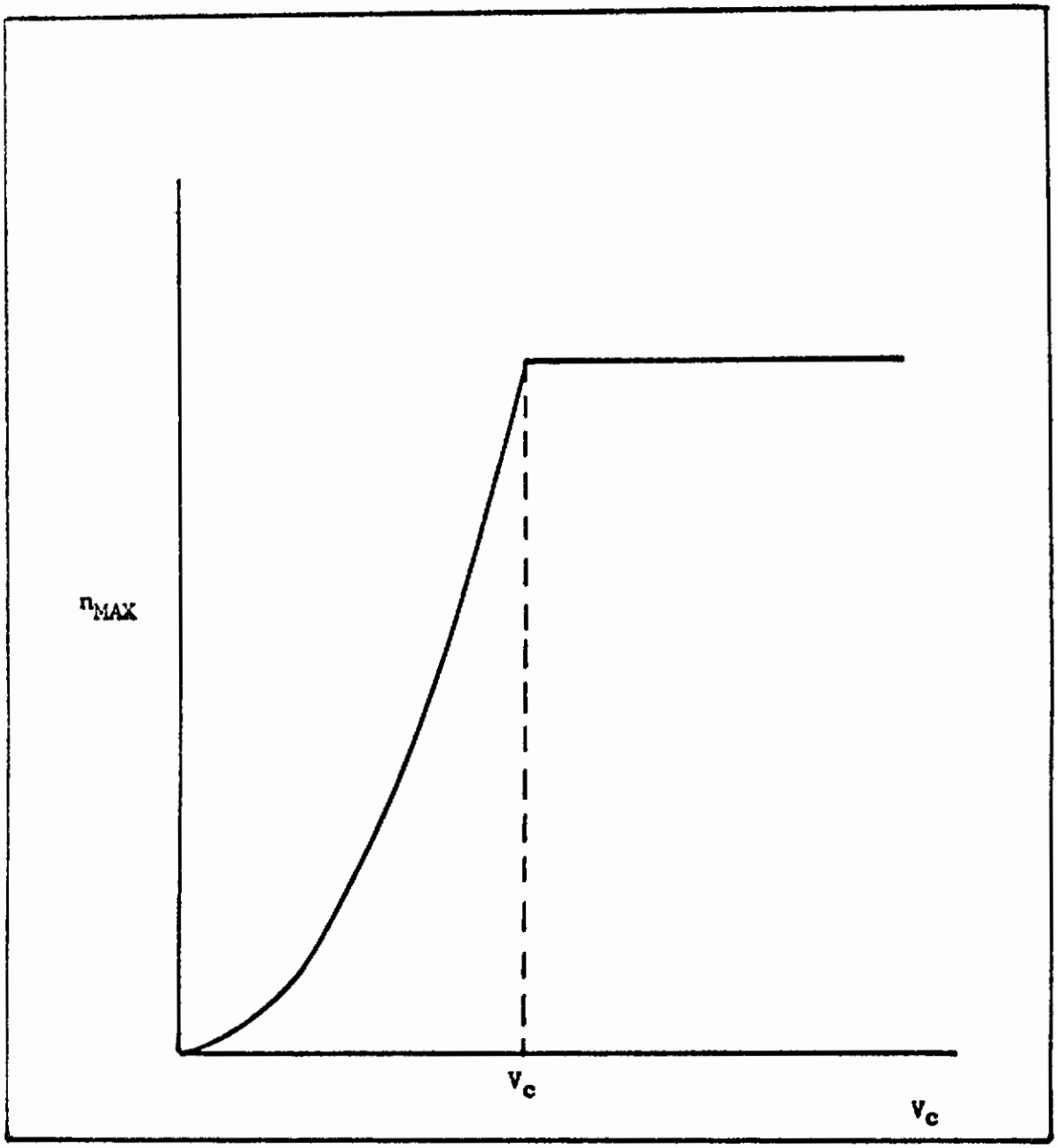

Fig. 18.--Maximum Allowable Control

The parameters which are of interest in aircraft design are W/S, $C_{L_{MAX}}$, and $a_{N_{MAX}}$ for constant speed aircraft. Differentiation of Eq (107) and substitution into Eq (106) gives

$$\frac{dL}{R_P} = \frac{\partial \bar{L}}{\partial \theta} d\theta - \epsilon \frac{\partial \bar{L}}{\partial \epsilon} \frac{dV_P}{V_P} + \bar{L} \frac{d(W/S)}{W/S} - \bar{L} \frac{dC_{L_{MAX}}}{C_{L_{MIN}}}, \qquad V < V_c$$

$$= \frac{\partial \bar{L}}{\partial \theta} d\theta + \left(2\bar{L} - \epsilon \frac{\partial \bar{L}}{\partial \epsilon}\right) \frac{dV_P}{V_P} - \bar{L} \frac{da_{N_{MAX}}}{a_{N_{MAX}}}, \qquad V > V_c.$$

In terms of sensitivity parameters, we can rewrite the previous equation as

$$\frac{dL}{R_P} = S_\theta \, d\theta + S_{V_P} \frac{dV_P}{V_P} + S_{W/S} \frac{d(W/S)}{W/S} + S_{C_{L_{MAX}}} \frac{dC_{L_{MAX}}}{C_{L_{MAX}}} + S_{a_{N_{MAX}}} \frac{da_{N_{MAX}}}{a_{N_{MAX}}},$$

where S_θ, S_{V_P}, $S_{W/S}$, $S_{C_{L_{MAX}}}$, and $S_{a_{N_{MAX}}}$ are the sensitivity parameters which are the multipliers on the differential changes in θ and P's performance characteristics. Clearly

$$S_{W/S} = -S_{C_L} = \bar{L}, \qquad V < V_c$$

$$S_{W/S} = S_{C_L} = 0, \qquad V > V_c$$

$$S_{a_{N_{MAX}}} = -\bar{L}, \qquad V > V_c$$

$$= 0, \qquad V < V_c.$$

Table 1 presents sensitivity data for selected values of ϵ and θ. The data were obtained from Figure 17.

TABLE 1

PROBLEM I SENSITIVITY DATA

ϵ	θ	$\bar{L}$	S_θ	$V < V_c$ S_{V_P}	$V > V_c$ S_{V_P}
0.5	1^o	.394	-.052	-.450	.338
0.5	5^o	.290	-.014	-.368	.212
0.5	10^o	.230	-.007	-.328	.132
0.5	15^o	.200	-.005	-.298	.102
0.5	30^o	.152	-.002	-.260	.044
0.9	1^o	.760	-.069	-.810	.620
0.9	5^o	.600	-.022	-.720	.480
0.9	10^o	.530	-.011	-.702	.358
0.9	15^o	.480	-.006	-.684	.276

There are several points to be made about the sensitivity of $\bar{L}$ the capture range to changes in the performance characteristics. First of all if $V_P < V_c$ then a decrease in $\bar{L}$ occurs if V_P can be increased up to V_c. Conversely if $V_P > V_c$ then $\bar{L}$ decreases if V_P can be decreased down to V_c. Thus in either case V_c is the best speed for the pursuer as long as $V_P > V_E$. The second point is that a one per cent decrease in wing loading W/S is equivalent to a one per cent increase in maximum lift coefficient if $V < V_c$. The same holds for a one per cent increase in $a_{N_{MAX}}$ if $V > V_c$. A direct comparison between S_θ and the other sensitivity parameters is

impossible due to the difference in units. S_θ is the partial of $\bar{L}$ with respect to θ, thus S_θ has units degree^{-1}.

The dimensional capture range L is important from a weapons standpoint. As an example consider the following aircraft parameters.

$W/S = 80$ pounds/square foot

$C_L = 1$

$\rho = 8.91 \times 10^{-4}$ slugs/cubic foot (corresponds to 30,000 feet altitude)

$n_{MAX} = 5.$

For this configuration

$V_c = 948$ feet/second

If

$V_P = V_c$

then the minimum turning radius is

$R = 5590$ feet.

We will consider two speed ratios, namely 0.5 and 0.9. If $\epsilon = 0.5$, $L = 2145$ feet for $\theta = 1^\circ$ and $L = 1590$ feet if $\theta = 5^\circ$. In order to reach these ranges, the game would start when E was directly ahead of P at a separation range of 2795 feet. This initial separation corresponds to $Y = \epsilon$ which is the point where the barrier reaches the Y-axis. If $\epsilon = 0.9$ the capture ranges are 4140 feet and 3350 feet for $\theta = 1^\circ$ and 5°, respectively. For this case the game would start at a separation of 4950 feet. For a fighter armed with machine guns, the gun is effective within approximately 2500 feet and an angle-off less than 1° to 3°. Consequently, the likelihood of achieving a kill when $\epsilon = 0.9$ is nil. The chances are good if $\epsilon = 0.5$ and P can reach 2750 feet from E before the latter starts maneuvering.

Problem I Conclusions

The solution to Problem I shows that P should operate as close to V_c as possible. In addition P must have a significant speed advantage, on the order of two to one, in order to achieve a kill using machine guns. These results, however, must be recognized as only a gross approximation to realistic air-to-air combat in light of E's being able to change directions instantaneously. We therefore turn our attention to Problem II which adds a little more realism.

SECTION V

PROBLEM II SOLUTION

Problem Definition

The differential equations of state and the control constraints were derived in Appendix A. Eqs (31) through (35) define the non-dimensional state equations and constraints

$$\dot{X} = \epsilon \sin \psi - \alpha_P Y \tag{31}$$

$$\dot{Y} = \epsilon \cos \psi - 1 + \alpha_P X \tag{32}$$

$$\dot{\psi} = - \alpha_P + \epsilon R \alpha_E \tag{33}$$

$$- 1 \leq \alpha_P \leq 1 \tag{34}$$

$$- 1 \leq \alpha_E \leq 1 \tag{35}$$

The control variables are α_P and α_E for P and E, respectively. The difference between this problem and the previous one is that whereas ψ was a control variable before, here it is a state variable. As a result, one additional state variable appears.

The Approximation of the Terminal Surface

The terminal surface is illustrated in Figure 9. For any value of ψ, the corners are smoothed like in Problem I and illustrated in Figure 12. The difference is that the corners are replaced with

cylinders of infinitesimal radius. On the right cylinder ($X > 0$) any point is defined by

$$\psi = s_2 \tag{109}$$

$$X = \bar{L} \sin\theta + r(\sin s_1 - \sin\theta - \cos\theta) \tag{110}$$

$$Y = \bar{L} \cos\theta + r(\cos s_1 + \sin\theta - \cos\theta) \tag{111}$$

where s_1 has the same interpretation as s did in Problem I. On the left infinitesimal cylinder ($X < 0$)

$$\psi = s_2 \tag{112}$$

$$X = -\bar{L} \sin\theta + r(-\sin s_1 + \sin\theta + \cos\theta) \tag{113}$$

$$Y = \bar{L} \cos\theta + r(\cos s_1 + \sin\theta - \cos\theta) \tag{114}$$

After developing the necessary conditions, the limit will be determined as r goes to zero.

The Necessary Conditions

Substitution of Eqs (31), (32) and (33) into the optimality condition, Eq (7) gives

$$\min_{\alpha_P} \max_{\alpha_E} [\nu_1(\epsilon \sin\psi - \alpha_P Y) + \nu_2(\epsilon \cos\psi - 1 + \alpha_P X) + \nu_3(-\alpha_P + \epsilon R \alpha_E)] = 0 \tag{115}$$

The optimal controls for P and E are therefore

$$\alpha_P^* = \text{sgn } B, \quad B = \nu_1 Y - \nu_2 X + \nu_3 \tag{116}$$

$$\alpha_E^* = \text{sgn } \nu_3 \tag{117}$$

Since $\bar{v}$ is perpendicular to the terminal surface, on the right cylinder

$$v_1 = \sin s_1 \tag{118}$$

$$v_2 = \cos s_1 \tag{119}$$

$$v_3 = 0 \tag{120}$$

and on the left cylinder

$$v_1 = -\sin s_1 \tag{121}$$

$$v_2 = \cos s_1 \tag{122}$$

$$v_3 = 0 \tag{123}$$

Clearly E's control is singular on the terminal surface in light of Eq (117). Expansion of B in Eq (116) on the right cylinder and letting r go to zero gives

$$B = \bar{L} \sin (s_1 - \theta) \tag{124}$$

Similarly on the left cylinder

$$B = -\bar{L} \sin (s_1 - \theta) \tag{125}$$

If $s_1 \leq \theta$, then the corner conditions do not hold and we set $\theta = s_1$ in which case $B = 0$ and P's control is undefined. This corresponds to the natural barrier, the solution for which will be derived later.

The boundary of the usable part (BUP) is derived from Eqs (7), (109) through (114), (118) through (123), (31), (32), and (33). In the limit as r goes to zero

$$\sin s_1(\epsilon \sin s_2 - \alpha_p^* \bar{L} \cos \theta) + \cos s_1(\epsilon \cos s_2 - 1 + \alpha_p^* \bar{L} \sin \theta) = 0 \tag{126}$$

on the right cylinder and

$$-\sin s_1(\epsilon \sin s_2 - \alpha_P^* \bar{L}\cos\theta) + \cos s_1(\epsilon \cos s_2 - 1 - \alpha_P^* \bar{L}\sin\theta) = 0 \quad (127)$$

on the left cylinder.

As in Problem I, introduce the nondimensional time β defined in Eq (88). The transformed differential equations of state are

$$X' = -\epsilon \sin\psi + \alpha_P^* Y \quad (128)$$

$$Y' = -\epsilon \cos\psi + 1 - \alpha_P^* X \quad (129)$$

$$\psi' = \alpha_P^* - \epsilon R \alpha_E^* \quad (130)$$

The differential equations for the ν_1 are

$$\nu_1' = \alpha_P^* \nu_2 \quad (131)$$

$$\nu_2' = -\alpha_P^* \nu_1 \quad (132)$$

$$\nu_3' = \epsilon(\nu_1 \cos\psi - \nu_2 \sin\psi) \quad (133)$$

The boundary conditions on the terminal surface, $\beta = 0$, are

$$X(0) = \bar{L}\sin\theta \quad \text{right corner} \quad (134)$$

$$= -\bar{L}\sin\theta \quad \text{left corner}$$

$$Y(0) = \bar{L}\cos\theta \quad (135)$$

$$\psi(0) = s_2 \quad (136)$$

$$\nu_1(0) = \sin s_1 \quad \text{right corner} \quad (137)$$

$$= -\sin s_1 \quad \text{left corner}$$

$$\nu_2(0) = \cos s_1 \quad (138)$$

$$\nu_3(0) = 0 \quad (139)$$

If $\theta \geq s_1$ then θ is replaced with s_1. The natural barrier solution will be determined first and then the artificial barrier problem will be addressed and solved.

Natural Barrier Solution

Set θ to s_1. Eqs (126) and (127) along with positive s_1 on both boundaries of the usable part shows that the boundaries are diametrically opposite since

$$\tan s_{1_L} = - \tan s_{1_R}$$

The relationship for s_1, as a function of s_2 and ϵ, is presented in Figure 19.

The optimal controls are undefined since both B and v_3 are zero on the BUP. However, differentiation of B gives

$$B' = v_1$$

On the terminal surface

$$B' = \sin s_1 > 0 \qquad \text{on the right barrier}$$

$$= - \sin s_1 < 0 \qquad \text{on the left barrier}$$

Consequently, P's controls are

$$\alpha_p^* = +1 \qquad \text{on the right barrier}$$

$$= -1 \qquad \text{on the left barrier.}$$

From Eq (133) evaluated on the terminal surface

$$v_3' = \epsilon(\sin s_1 \cos s_2 - \cos s_1 \sin s_2) \qquad \text{right barrier}$$

$$= \epsilon(- \sin s_1 \cos s_2 - \cos s_1 \sin s_2) \qquad \text{left barrier.}$$

Substitution of the relationship for s_1 gives

$$v_3' = \frac{\epsilon \sin s_1}{1-\epsilon \cos s_2} (\cos s_2 - \epsilon) \qquad \text{right barrier}$$

$$= - \frac{\epsilon \sin s_1}{1-\epsilon \cos s_2} (\cos s_2 - \epsilon) \qquad \text{left barrier.}$$

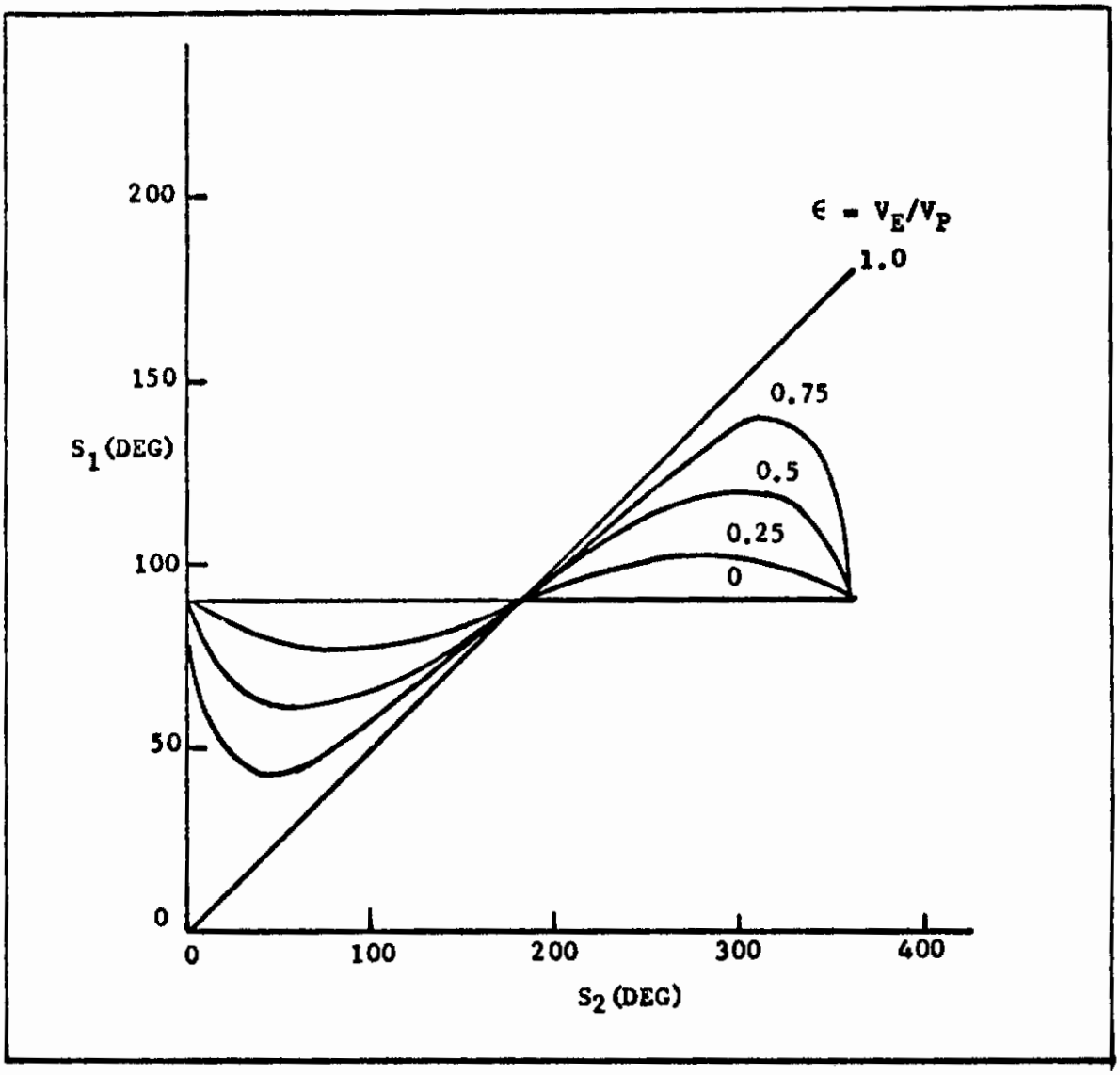

Fig. 19.--Right Natural Barrier BUP

From Figure 19 on the right BUP $\sin s_1 > 0$. By assumption $\epsilon < 1$. Since the two BUP are diametrically opposite, $\sin s_1 < 0$ on the left BUP. Consequently, v_3' is of opposite sign on the two BUP at the same value of s_2 and therefore α_E^* has opposite signs. Also, v_3' changes sign across $s_2 = \cos^{-1}\epsilon$ and $s_2 = 2\pi - \cos^{-1}\epsilon$. Thus on the two BUP E's optimal controls are as follows:

	Right BUP	Left BUP
$0 \le s_2 < \cos^{-1}\epsilon$	+1	-1
$\cos^{-1}\epsilon < s_2 < 2\pi - \cos^{-1}\epsilon$	-1	+1
$2\pi - \cos^{-1}\epsilon < s_2 < 2\pi$	+1	-1

Examination at $s_2 = \cos^{-1}\epsilon$ on the right BUP and $s_2 = 2\pi - \cos^{-1}\epsilon$ on the left BUP shows that gaps occur since ψ' in Eq (130) is discontinuous. These voids in the barrier are filled as follows. The relation for v_3' is repeatedly differentiated until α_E^* first appears, thus

$$\begin{aligned} v_3'' &= \epsilon(v_1' \cos\psi - \psi' v_1 \sin\psi - v_2' \sin\psi - \psi' v_2 \cos\psi) \\ &= \epsilon(\alpha_P^* - \psi')(v_1 \sin\psi + v_2 \cos\psi) \\ &= 0. \end{aligned}$$

Since $v_3' = 0$, $v_1 \sin\psi + v_2 \cos\psi \neq 0$, hence

$$\alpha_P^* - \psi' = 0.$$

Substitution for ψ' gives

$$\alpha_P^* - \psi' = \epsilon R \alpha_E^* = 0.$$

Thus on the singular arcs, E's optimal control is

$$\alpha_E^* = 0.$$

Right and left running arcs or tributaries emanating from the singular arc fill the void. Examination of Eqs (128), (129), and (130) shows that the trajectory for the singular arcs are the same as Problem I.

At the other switching point, $s_2 = \cos^{-1}\epsilon$ on the left BUP and $s_2 = 2\pi - \cos^{-1}\epsilon$ on the right BUP the trajectories on each side intercept each other. The arc of interception is determined by equating ψ, X, and Y. The trajectories are illustrated in Figure 20.

The differential equations of state, Eqs (128), (129), and (130) are nonlinear since sin ψ and cos ψ are nonlinear. They are integrable, however, if ψ is first integrated and then substituted into Eqs (128) and (129). The details are presented in Appendix B. The solution is

$$X = \bar{L} \sin \alpha_P^*(s_1+\beta) + \alpha_P^*(1-\cos\beta) - \frac{\alpha_E^*}{R}\left[\cos\psi - \cos(s_2+\alpha_P^*\beta)\right] \quad (140)$$

$$Y = \bar{L} \cos \alpha_P^*(s_1+\beta) + \sin\beta + \frac{\alpha_E^*}{R}\left[\sin\psi - \sin(s_2+\alpha_P^*\beta)\right] \quad (141)$$

$$\psi = s_2 + (\alpha_P^* - \epsilon R\,\alpha_E^*)\,\beta \quad (142)$$

$$\nu_1 = \sin \alpha_P^*(s_1+\beta)$$

$$\nu_2 = \cos \alpha_P^*(s_1+\beta) \quad (143)$$

$$\nu_3 = \frac{\alpha_E^*}{R}\left[\cos(s_1-s_2) - \cos(s_1-s_2+\epsilon R\,\alpha_E^*\beta)\right]$$

On the singular arcs

$$X = (\bar{L} - \epsilon\beta)\sin\alpha_P^*(S+\beta) + \alpha_P^*(1-\cos\beta) \quad (144)$$

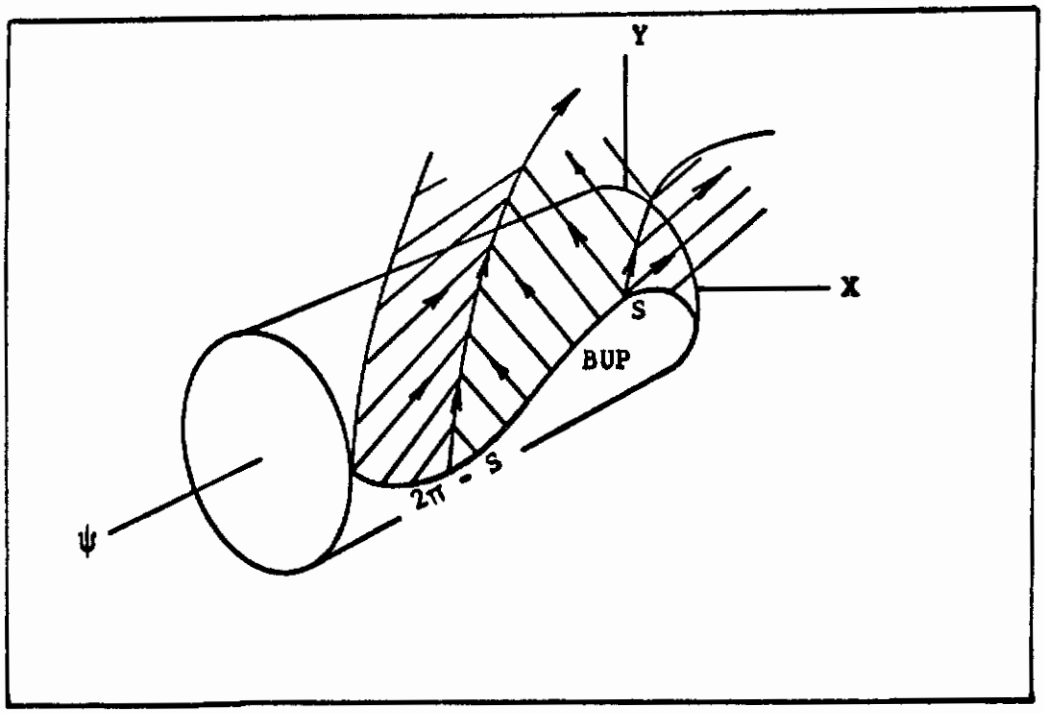

Fig. 20.--Terminal Surface, Boundary of the Usable Part, and the Barrier

$$Y = (\bar{L} - \epsilon\beta) \cos \alpha_p^*(S + \beta) + \sin \beta \tag{145}$$

$$\psi = \alpha_p^*(S + \beta) \tag{146}$$

$$\begin{aligned} \nu_1 &= \sin \alpha_p^* (S + \beta) \\ \nu_2 &= \cos \alpha_p^* (S + \beta) \\ \nu_3 &= 0 \\ S &= \cos^{-1} \epsilon \end{aligned} \tag{147}$$

For the tributaries

$$X = (\bar{L}-\epsilon \beta_o) \sin \alpha_p^*(S+ \beta)+ \alpha_p^*(1-\cos \beta)- \frac{\alpha_E^*}{R} [\cos \psi-\cos \alpha_p^*(S+ \beta)] \tag{148}$$

$$Y = (\bar{L}-\epsilon \beta_o)\cos \alpha_p^*(S+ \beta)+ \sin \beta + \frac{\alpha_E^*}{R} [\sin \psi-\sin \alpha_p^*(S+ \beta)] \tag{149}$$

$$\psi = \alpha_p^*(S+ \beta) - \epsilon R \alpha_E^* (\beta - \beta_o) \tag{150}$$

$$\begin{aligned} \nu_1 &= \sin \alpha_p^* (S+ \beta) \\ \nu_2 &= \cos \alpha_p^* (S+ \beta) \\ \nu_3 &= \frac{\alpha_E^*}{R} [1 - \cos \epsilon R \alpha_E^* (\beta - \beta_o)] \end{aligned} \tag{151}$$

where β_o corresponds to the time that the tributary leaves the singular arc.

It can be shown that the two barriers in the $\psi = 0$ plane are symmetrical about the Y-axis. Let subscripts R and L denote right and left barriers respectively. From Eq (142)

$$\psi_R = \psi_L = 0$$

or

$$S_{2_R} + (1 - \epsilon R)\beta = S_{2_L} + (-1 + \epsilon R)\beta = 0$$

Thus

$$S_{2_L} = - S_{2_R}$$

From the relationship for S_1, it follows that

$$S_{1_L} = S_{1_R}$$

Eqs (140), (141) become

$$X_L = \bar{L} \sin (-S_{1_R} - \beta) - (1 - \cos \beta) + \frac{1}{R}\left[1 - \cos(-S_{2_R} - \beta)\right]$$

$$= - X_R$$

$$Y_L = \bar{L} \cos (-S_{1_R} - \beta) + \sin \beta - \frac{1}{R}\left[0 - \sin (-S_{2_R} - \beta)\right]$$

$$= Y_R$$

Similarly on the singular arc, Eq (146) shows that

$$S_{2_L} = - S_{2_R} = S$$

Eqs (144) and (145) become

$$X_L = (\bar{L} - \epsilon\beta) \sin (-S - \beta) - (1 - \cos \beta)$$

$$= - X_R$$

$$Y_L = (\bar{L} - \epsilon\beta) \cos (S + \beta) + \sin \beta$$

$$= Y_R$$

For the tributaries, Eqs (148) and (149) become

$$X_L = (\bar{L} - \epsilon\beta_o) \sin (-S - \beta) - (1 - \cos \beta) + \frac{1}{R}\left[1 - \cos (S + \beta)\right]$$

$$= X_R$$

$$Y_L = (\bar{L} - \epsilon\beta_o) \cos (S+\beta) + \sin\beta - \frac{1}{R}[0 - \sin(-S-\beta)]$$
$$= Y_R$$

A sample trajectory is illustrated in the $\psi = 0$ plane in Figure 21.

Since the barriers are symmetric in the $\psi = 0$ plane, it suffices to examine the right barrier. The solution for $\bar{L}$ as a function of E and R can be determined from the simultaneous solution of

$$\nu_2(\bar{\beta}) = 0$$
$$X(\bar{\beta}) = 0$$
$$\psi(\bar{\beta}) = 0$$

where $\bar{\beta}$ corresponds to the time at which the barrier meets the Y-axis. Consider first the region $-S \leq S_2 \leq S$. From Eqs (142) and (143)

$$\bar{\beta} = \frac{\pi}{2} - S_1 \tag{152}$$

$$S_2 = (\epsilon R - 1)\bar{\beta} \tag{153}$$

Since From Eq (126)

$$\tan S_1 = \frac{1 - \epsilon \cos S_2}{\epsilon \sin S_2}$$

Substitution of S_2, rewriting, and combining terms gives

$$\epsilon \sin \epsilon R \left(\frac{\pi}{2} - S_1\right) = \cos S_1 \tag{154}$$

If $S_1 = S = \cos^{-1}\epsilon$

$$\epsilon \sin \epsilon R \left(\frac{\pi}{2} - S_1\right) = \cos S = \epsilon$$

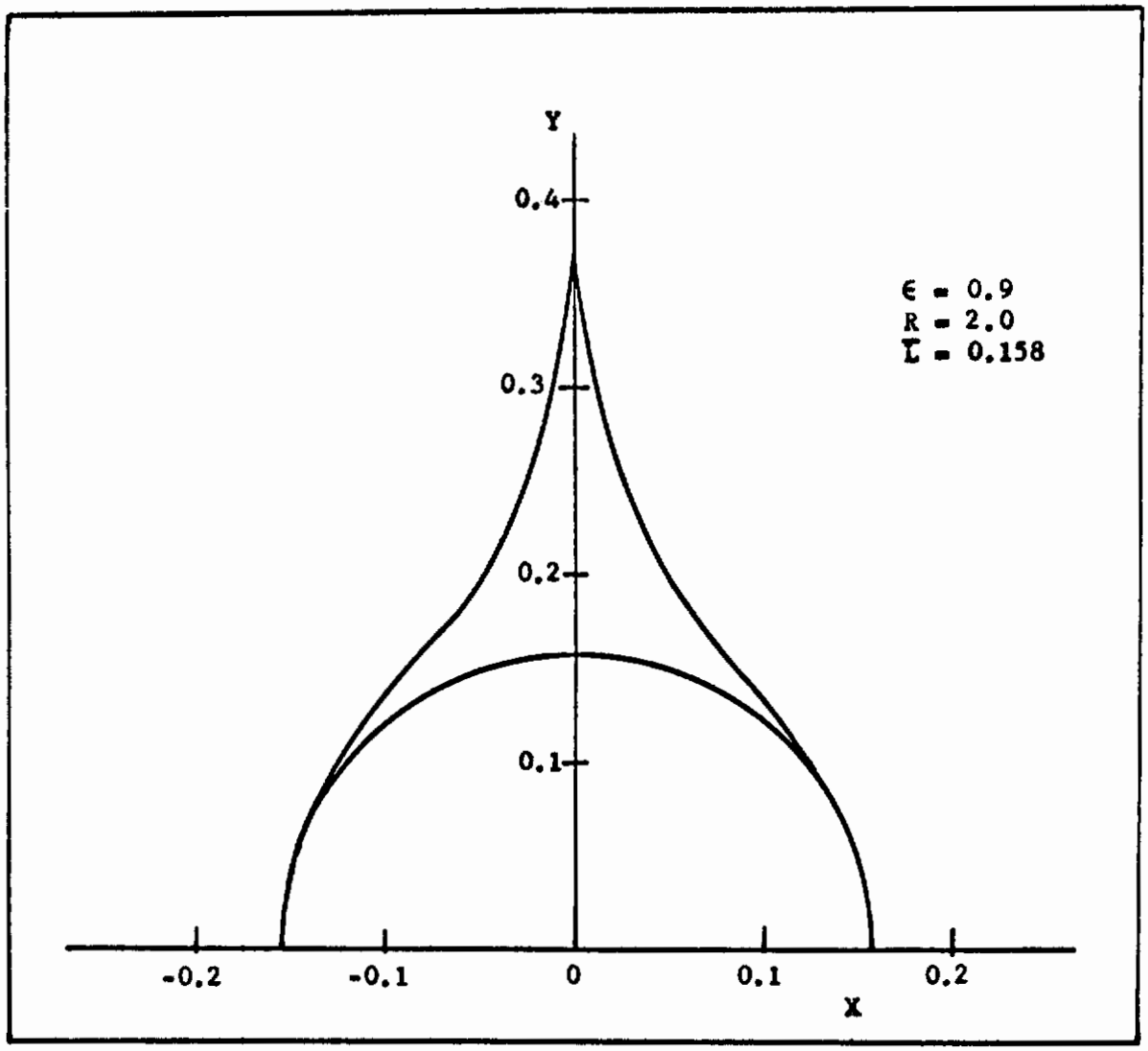

Fig. 21.--Problem II Sample Trajectory in $\psi = 0$ Plane

Hence

$$\epsilon R \left(\frac{\pi}{2} - S \right) = \frac{\pi}{2} \tag{155}$$

This is the singular arc solution. Substitution of Eqs (152) and (153) into $X(\bar{\beta}) = 0$ gives

$$\bar{L} + 1 - \sin S_1 - \frac{1}{R}\left[1 - \cos \epsilon R\left(\frac{\pi}{2} - S_1 \right)\right] = 0$$

Thus, if $-S < S_2 \leq S$, then the capture range is

$$\bar{L} = -1 + \sin S_1 + \frac{1}{R}\left[1 - \cos \epsilon R \left(\frac{\pi}{2} - S_1 \right)\right] \tag{156}$$

The iterative procedure is as follows:

1. Pick $R > 1$, $0 < \epsilon < 1$
2. Guess S_1
3. Substitute s_1 into the left side of Eq (154) and determine cos s_1. Repeat this step until convergence occurs.
4. Compute s_2 from Eqs (152) and (153).
5. Substitute s_1 into Eq (156) and compute $\bar{L}$.

For the tributaries, from Eq (151)

$$\bar{\beta} = \frac{\pi}{2} - S \tag{157}$$

From Eq (150)

$$S + \bar{\beta} - \epsilon R \left(\bar{\beta} - \beta_o \right) = 0$$

It follows that

$$\beta_o = \frac{\pi}{2} - S - \frac{\pi}{2\epsilon R} \tag{158}$$

Substitution of β_o and $\bar{\beta}$ into Eq (148) and solving for $\bar{L}$ gives

$$\bar{L} = \epsilon \left(\frac{\pi}{2} - S - \frac{\pi}{2\epsilon R} \right) + \sin S - 1 + \frac{1}{R}$$

Since $\cos S = \epsilon$

$$\bar{L} = \epsilon \left(\frac{\pi}{2} - \cos^{-1}\epsilon - \frac{\pi}{2\epsilon R} \right) + \sqrt{1-\epsilon^2} - 1 + \frac{1}{R}$$

Note that

$$\lim_{R \to \infty} \bar{L} = \epsilon \left(\frac{\pi}{2} - \cos^{-1} \epsilon \right) + \sqrt{1-\epsilon^2} - 1$$

which is the solution to Problem I. The relationship for $\bar{L}$ as a function of ϵ and R is presented in Figure 22.

There are several points to be made about the data in Figure 22. As the evader's turning radius increases, the capture range decreases. If the turning radius ratio R is one, then the pursuer can force the capture range to zero under optimal pursuer play. This physically makes sense because all the pursuer needs to do is maneuver until he is on the same circular arc as the evader. The pursuer due to his speed advantage and equal turning radius is then able to drive the capture range to zero. The third point about Figure 22 is that the nondimensional capture range is zero or increases with increasing speed ratio. Another point is that the capture range is zero for certain combinations of ϵ and R. The relationship between ϵ and R can be assessed from Eq (154). Rewriting gives

$$f(S_1) = \epsilon \sin \epsilon R \left(\frac{\pi}{2} - S_1 \right) - \cos S_1$$

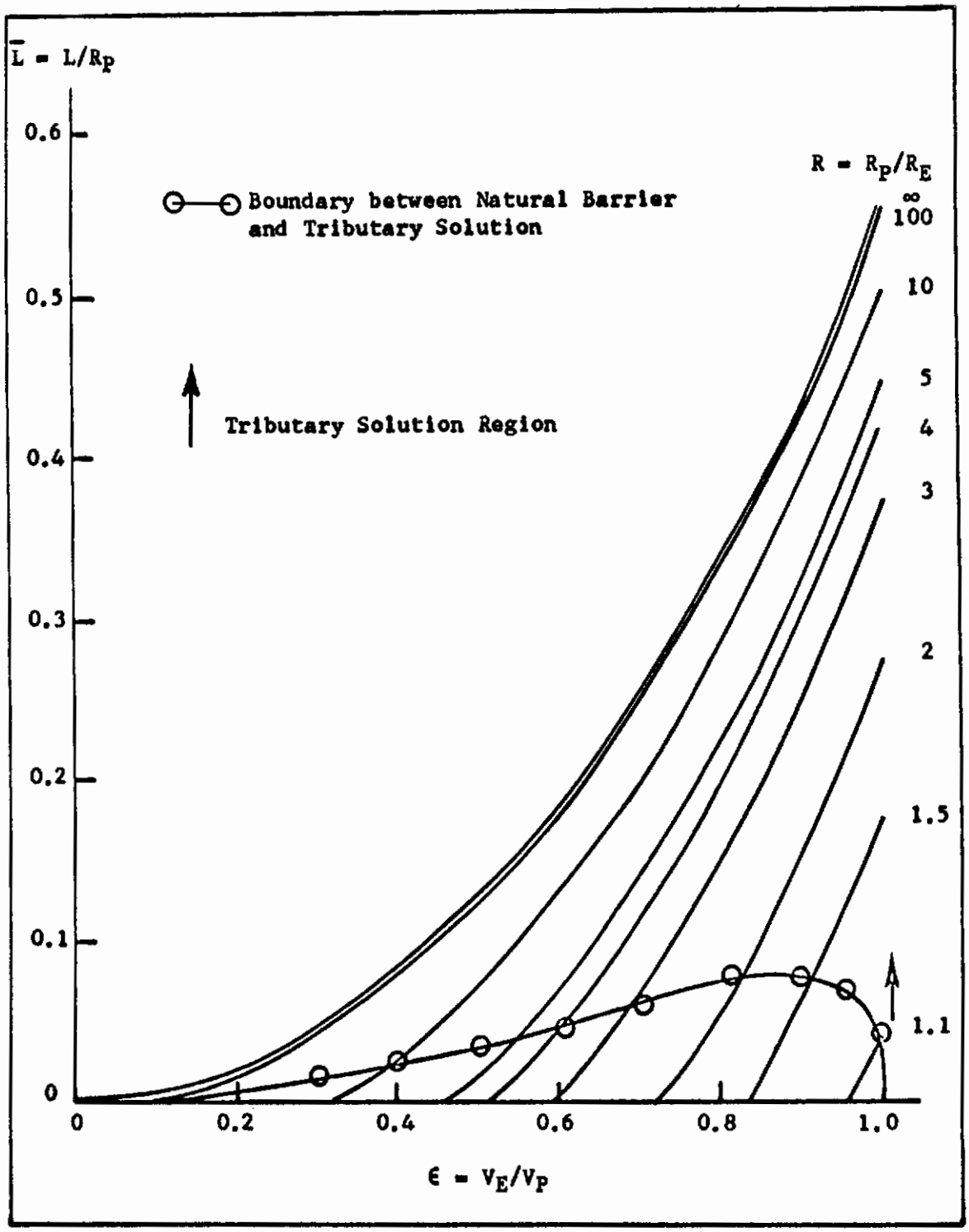

Fig. 22.--Problem II Natural Barrier Capture Range

We seek the value of S_1 for which $f(S_1) = 0$. Now from the BUP solution illustrated in Figure 19

$$0 \leq S_1 \leq \frac{\pi}{2}$$

between the $\psi = 0$ plane and the singular arc. Differentiation of $f(S_1)$ with respect to S_1 gives

$$\frac{df(S_1)}{dS_1} = -\epsilon^2 R \cos \epsilon R \left(\frac{\pi}{2} - S_1\right) + \sin S_1$$

Since

$$f(0) < 0$$

$$f\left(\frac{\pi}{2}\right) = 0$$

$$f'\left(\frac{\pi}{2}\right) = 1 - \epsilon^2 R$$

the relationship for $f(S_1)$ gives two roots if $\epsilon^2 R > 1$ and only one root if $\epsilon^2 R \leq 1$. The relationship is illustrated in Figure 23. Thus if $\epsilon^2 R \leq 1$, $S_1 = \pi/2$. Substitution of $S_1 = \pi/2$ into Eq (156) gives $\bar{L} = 0$; therefore, if $\epsilon^2 R \leq 1$, $\bar{L} = 0$. This solution has physical significance. Since the normal acceleration is V^2/R, substitution of the dimensional variables into $\epsilon^2 R \leq 1$ gives

$$\left(\frac{V_E}{V_P}\right)^2 \frac{R_P}{R_E} \leq 1$$

or

$$\frac{V_E^2}{R_E} \leq \frac{V_P^2}{R_P} .$$

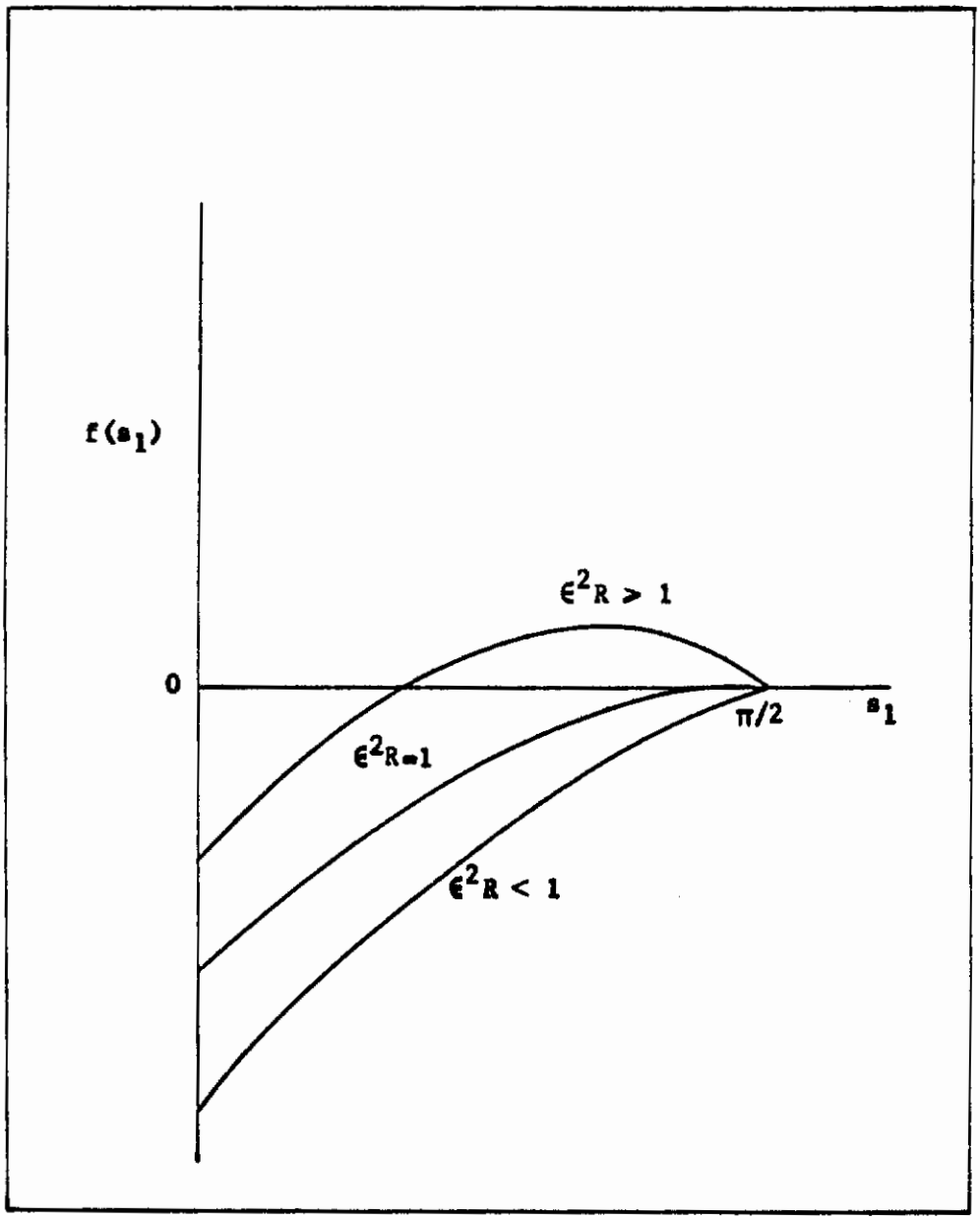

Fig. 23.--The $f(s_1)$ Relationship

Consequently, whenever the pursuer's normal acceleration equals or exceeds the evader's normal acceleration, the pursuer is assured of driving the capture range to zero under optimal control.

The sensitivity of $\bar{L}$ to variations in the performance parameters will be addressed after the artificial barrier solution is solved.

Artificial Barrier Solution

The optimal controls for P are obtained from Eqs (124) and (125). On the right barrier

$$0 \leq S_1 \leq \theta + \frac{\pi}{2}$$

It follows that $\alpha_P^* = 1$ on the right barrier and $\alpha_P^* = -1$ on the left barrier. Since $v_3(0) = 0$, E's optimal control is based upon $v_3'(0)$. From Eq (133) and the boundary conditions on the right barrier

$$v_3'(0) = \epsilon (\sin S_1 \cos S_2 - \cos S_1 \sin S_2)$$

$$= \frac{\epsilon \sin S_1}{1-\epsilon \cos S_2 - \bar{L} \sin \theta} [\cos S_2 - \epsilon - \bar{L} \sin (\theta - S_1)]$$

should be S_2

A similar result occurs for the left barrier. The singular arcs result when

$$\cos \bar{S}_2 - \epsilon - \bar{L} \sin (\theta - \bar{S}_2) = 0 \qquad (159)$$

For the natural barrier, a gap occurs on each barrier which is filled by a singular arc and tributaries. Between $S_2 = 0$ and the

solution of Eq (159), $S_2 = \bar{S}_2$, $\alpha_E^* = 1$ on the right barrier. Similarly $\alpha_E^* = -1$ between $S_2 = -\bar{S}_2$ and $S_2 = 0$ on the left barrier.

The evader optimal control on the singular arc is determined from differentiation of v_3 until α_E^* first appears. This occurs for v_3'' since

$$v_3'' = \epsilon(v_1 \sin\psi + v_2 \cos\psi)\, \epsilon R\, \alpha_E^*$$

$$= 0$$

Since $v_3' = 0$, the sum in the parentheses is not zero, hence $\alpha_E^* = 0$ on either singular arc. Tributaries run from the singular arcs and fill the gaps.

The trajectory equations are determined in Appendix B. For trajectories emanating from the BUP

$$X = \bar{L} \sin\alpha_P^*(\theta + \beta) + \alpha_P^*(1 - \cos\beta) - \frac{\alpha_E^*}{R}\left[\cos\psi - \cos(S_2 + \alpha_P^*\beta)\right] \tag{160}$$

$$Y = \bar{L} \cos\alpha_P^*(\theta + \beta) + \sin\beta + \frac{\alpha_E^*}{R}\left[\sin\psi - \sin(S_2 + \alpha_P^*\beta)\right]$$

$$\psi = S_2 + (\alpha_P^* - \epsilon R\, \alpha_E^*)\,\beta \tag{161}$$

$$v_1 = \sin\alpha_P^*(S_1 + \beta)$$

$$v_2 = \cos\alpha_P^*(S_1 + \beta) \tag{162}$$

$$v_3 = \frac{\alpha_E^*}{R}\left[\cos(S_1 - S_2) - \cos(S_1 - S_2 + \epsilon R\, \alpha_E^*\beta)\right]$$

On the right barrier singular arc, Eqs (126) and (159) are satisfied by

$$S_1 = \bar{S}_2$$

where $\bar{S}_2$ is the solution of Eq (159). On the left barrier

$$S_1 = -\bar{S}_2$$

The trajectory for the singular arc is

$$X = \bar{L} \sin \alpha_p^* (\theta + \beta) + \alpha_p^* (1 - \cos \beta) - \epsilon\beta \sin \alpha_p^* (\bar{S}_2 + \beta)$$

$$Y = \bar{L} \cos \alpha_p^* (\theta + \beta) + \sin \beta - \epsilon\beta \cos \alpha_p^* (\bar{S}_2 + \beta)$$

$$\psi = \alpha_p^* (\bar{S}_2 + \beta)$$

$$\nu_1 = \sin \alpha_p^* (S_1 + \beta)$$

$$\nu_2 = \cos \alpha_p^* (S_1 + \beta)$$

$$\nu_3 = 0$$

For the tributaries of the singular arcs, the trajectories are

$$X = \bar{L} \sin \alpha_p^* (\theta + \beta) + \alpha_p^* (1 - \cos \beta) - \epsilon\beta_o \sin \alpha_p^* (S_1 + \beta) - \frac{\alpha_E^*}{R} [\cos \psi - \cos \alpha_p^* (S_1 + \beta)] \quad (163)$$

$$Y = \bar{L} \cos \alpha_p^* (\theta + \beta) + \sin \beta - \epsilon\beta_o \cos (S_1 + \beta) + \frac{\alpha_E^*}{R} [\sin \psi - \sin \alpha_p^* (S_1 + \beta)]$$

$$\psi = \alpha_p^* (\bar{S}_2 + \beta) + (\alpha_p^* - \epsilon R \alpha_E^*)(\beta - \beta_o) \quad \text{Wrong} \quad (164)$$

$$\nu_1 = \sin \alpha_p^* (S_1 + \beta)$$

$$\nu_2 = \cos \alpha_p^* (S_1 + \beta) \quad (165)$$

$$\nu_3 = \frac{\alpha_E^*}{R} [1 - \cos \epsilon R \alpha_E^* (\beta - \beta_o)]$$

where β_o corresponds to the time that the tributary leaves the singular arc.

As for the natural barrier, it can be shown that the two barriers in the $\psi = 0$ plane are symmetric about the Y-axis, therefore it is sufficient to examine the right barrier in the $\psi = 0$ plane. The solution for $\bar{L}$ is derived in the same manner as before, namely, satisfaction of the BUP

$$\epsilon \cos (S_1 - S_2) - \cos S_1 + \bar{L} \sin (\theta - S_1) = 0 \qquad (166)$$

and

$$\psi(\bar{\beta}) = 0$$

$$v_2(\bar{\beta}) = 0$$

$$X(\bar{\beta}) = 0$$

The relationship for $\bar{L}$ consists of trajectories emanating from the terminal surface and tributaries emanating from the singular arc. Consider the former first. Eqs (160), (161), (162) give

$$\bar{\beta} = \frac{\pi}{2} - S_1$$

$$S_2 = (\epsilon R - 1)\,\bar{\beta}$$

$$\bar{L} \sin (\theta + \bar{\beta}) + 1 - \cos \bar{\beta} - \frac{1}{R}\left[1 - \cos (S_2 + \bar{\beta})\right] = 0 \qquad (167)$$

Substituting $\bar{\beta}$ and S_2 into Eqs (166) and (167) and then eliminating $\bar{L}$ gives

$$f(S_1) = -\cos\theta + \epsilon \sin\Lambda \cos(\theta - S_1) - \left[1 - \frac{1}{R}(1 - \cos\Lambda)\right] \sin(\theta - S_1)$$

$$= 0 \qquad (168)$$

where $\Lambda = \epsilon R \left(\frac{\pi}{2} - S_1 \right)$

The solution for S_1 as a function of ϵ and R results in $f(S_1) = 0$. Differentiation of $f(S_1)$ and evaluation at $S_1 = \pi/2$ gives

$$\frac{df(S_1)}{dS_1} = (1 - \epsilon^2 R) \cos \left(\theta - \frac{\pi}{2} \right)$$

The relationship for $f(S_1)$ is like that in Figure 23. If $\epsilon^2 R \leq 1$, $S_1 = \pi/2$ and Eq (167) shows that $\bar{L} = 0$. This is the same result as for the natural barrier. The solution for S_1 when $\epsilon^2 R > 1$ is determined by iteration using Newton's formula. The solution for S_1 substituted into Eq (167) gives $\bar{L}$ as a function of ϵ, R, and θ.

For the tributaries of the singular arc, Eqs (163), (164), (165) give

$$\bar{\beta} = \frac{\pi}{2} - S_1$$

$$\beta_o = \frac{\pi}{2} - S_1 - \frac{\pi}{2\epsilon R}$$

$$\bar{L} \sin (\theta + \bar{\beta}) + 1 - \cos \bar{\beta} - \epsilon \beta_o - \frac{1}{R} = 0 \qquad (169)$$

Substituting $\bar{\beta}$ and β_o into Eq ~~(163)~~, setting ~~$S_1 = S_2$~~ and eliminating $\bar{L}$ from the resulting equation and Eq ~~(169)~~ gives

$$f(S_1) = -\cos \theta + \epsilon \cos(\theta - S_1) - \left[1 - \epsilon \left(\frac{\pi}{2} - S_1 - \frac{\pi}{2\epsilon R} \right) \right] \sin (\theta - S_1)$$

$$= 0$$

The correct solution for S_1 yields $f(S_1) = 0$. The relationship for $\bar{L}$ is obtained from Eq (169). The solution for $\bar{L}$ as a function of

R, ϵ, and θ is presented in Figures 24 and 25. For large values of R, ($R \geq 1000$), the solution approaches that for Problem I. For R = 1.1, $\bar{L}$ is essentially the same for the natural and artificial barrier. For R = 1.5 there is also little difference between the natural and artificial barriers. The difference becomes more pronounced with increasing R. An important point to keep in mind is that the artificial and natural barrier solutions are approximately the same for small values of R, $R \leq 1.5$. This is likely to be the situation for aircraft engaged in air-to-air combat.

Capture Range Sensitivity

The dimensional capture range has the following form

$$L = \bar{L}\,(\epsilon, \theta, R)\, R_p$$

Only the sensitivity to changes in V_p, R_p, and θ will be considered since we are interested in the impact on the capture range due to changes in the pursuer's performance characteristics. The differential of L is

$$dL = R_p \frac{\partial \bar{L}}{\partial V_p} dV_p + R_p \frac{\partial \bar{L}}{\partial \theta} d\theta + \left(\frac{\partial \bar{L}}{\partial R_p} R_p + \bar{L} \right) dR_p$$

Substituting for ϵ and R gives

$$dL = -\frac{\epsilon}{V_p} R_p \frac{\partial \bar{L}}{\partial \epsilon} dV_p + R_p \frac{\partial \bar{L}}{\partial \theta} d\theta + \left(\frac{R_p}{R_E} \frac{\partial \bar{L}}{\partial R} + \bar{L} \right) dR_p$$

In nondimensional form

$$\frac{dL}{R_p} = -\epsilon \frac{\partial \bar{L}}{\partial \epsilon} \frac{dV_p}{V_p} + \frac{\partial \bar{L}}{\partial \theta} d\theta + \left(R \frac{\partial \bar{L}}{\partial R} + \bar{L} \right) \frac{dR_p}{R_p} \qquad (170)$$

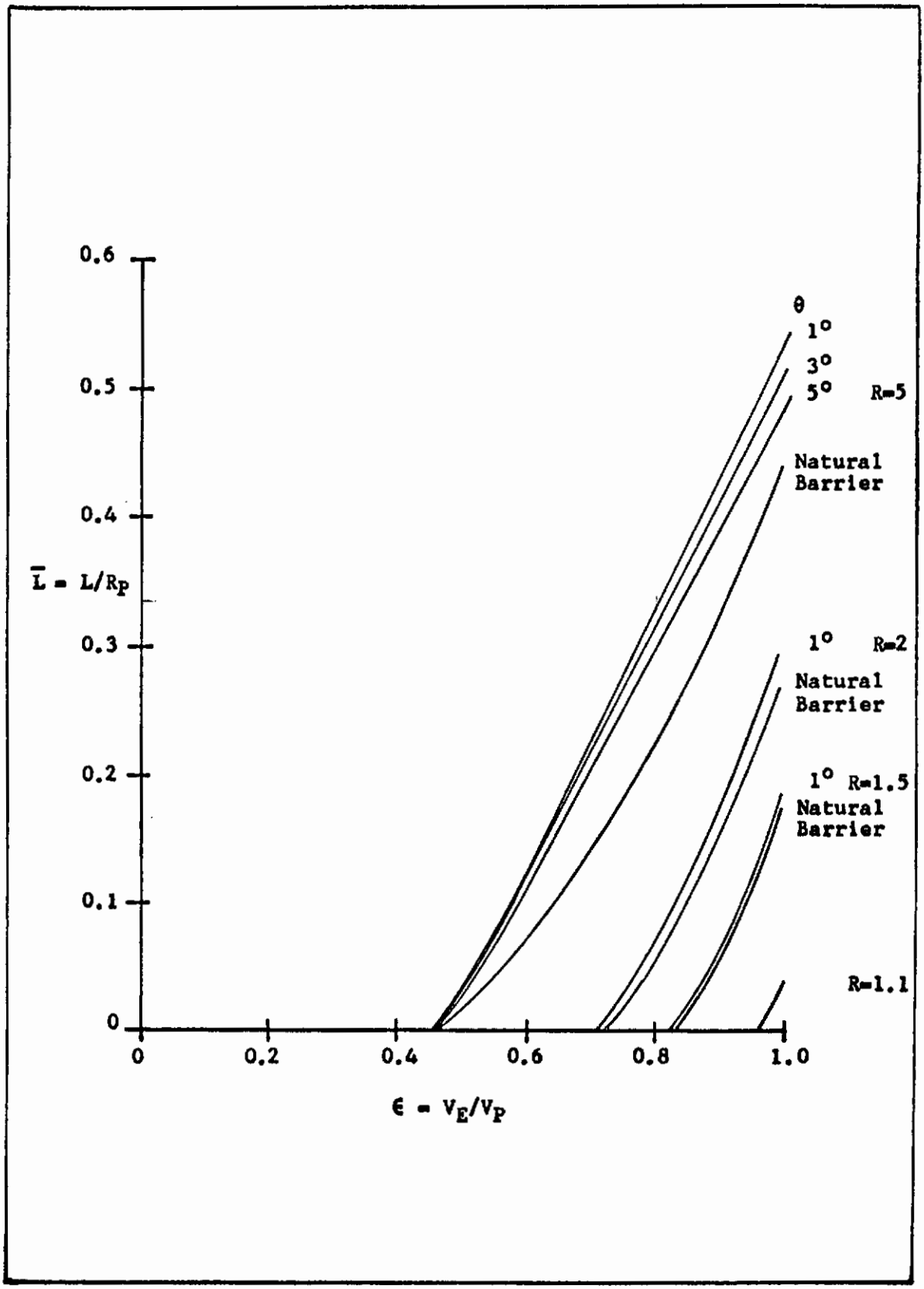

Fig. 24.--Problem II Artificial Barrier Capture Range

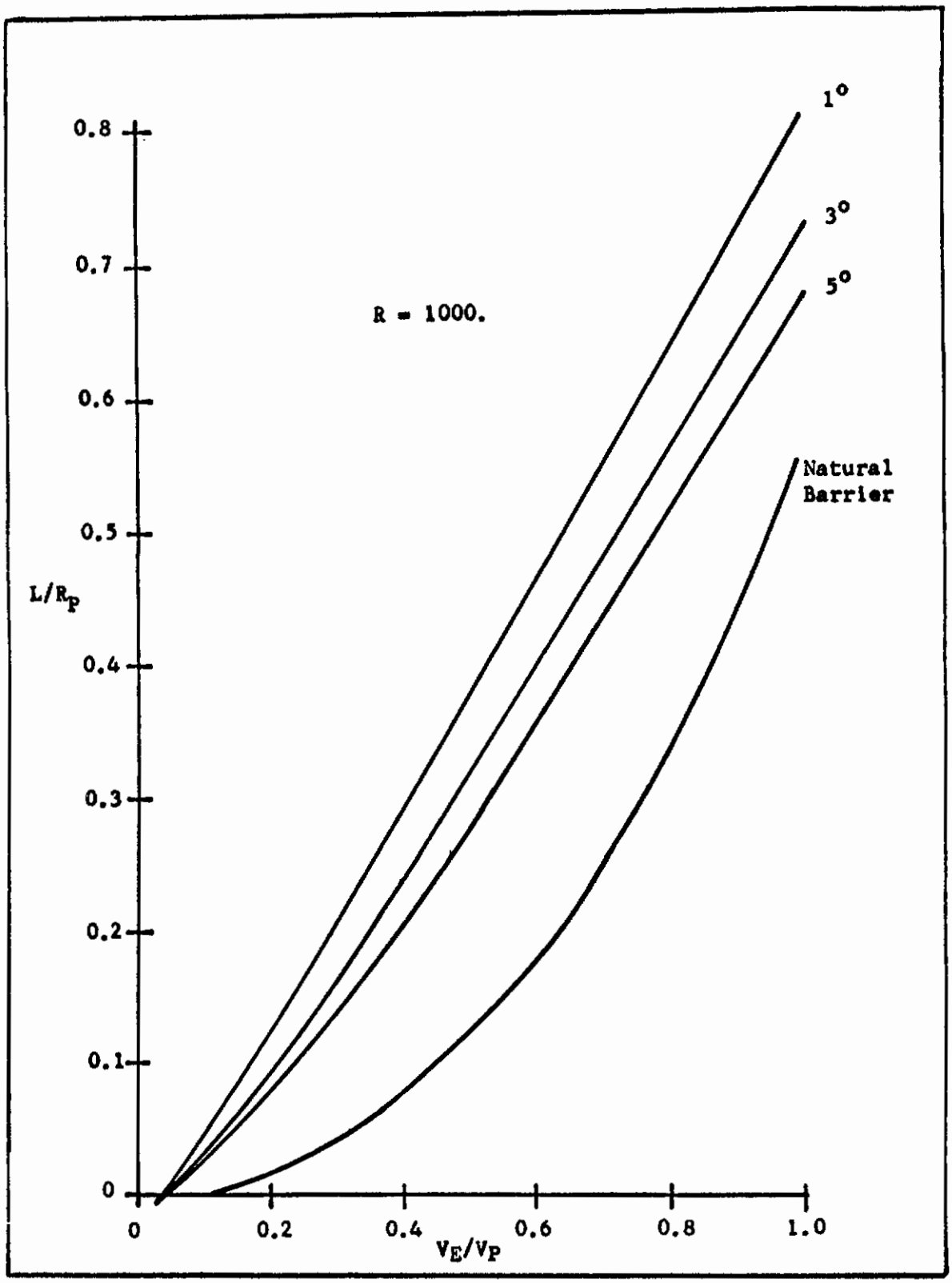

Fig. 25.--Problem II Artificial Barrier Capture Range

This form is slightly different from that derived for Problem I. The relationship between R_p and W/S, $C_{L_{MAX}}$ and $a_{N_{MAX}}$ was defined in Eq (107). Differentiation and substitution into Eq (170) gives

$$\frac{dL}{R_p} = -\epsilon \frac{\partial \bar{L}}{\partial \epsilon} \frac{dV_p}{V_p} + \frac{\partial \bar{L}}{\partial \theta} d\theta + \left(R \frac{\partial \bar{L}}{\partial R} + \bar{L}\right)\left(\frac{dW/S}{W/S} - \frac{dC_{L_{MAX}}}{C_{L_{MAX}}} \right) , \quad V < V_c$$

$$= \left[2\left(R \frac{\partial \bar{L}}{\partial R} + \bar{L}\right) - \epsilon \frac{\partial \bar{L}}{\partial \epsilon} \right] \frac{dV_p}{V_p} + \frac{\partial \bar{L}}{\partial \theta} d\theta - \left(R \frac{\partial \bar{L}}{\partial R} + \bar{L}\right) \frac{da_{N_{MAX}}}{a_{N_{MAX}}} , \quad V > V_c.$$

In terms of sensitivity parameters, dL/R_p can be rewritten as

$$\frac{dL}{R_p} = S_{V_p} \frac{dV_p}{V_p} + S_\theta \, d\theta + S_{W/S} \frac{dW/S}{W/S} + S_{C_{L_{MAX}}} \frac{dC_{L_{MAX}}}{C_{L_{MAX}}} + S_{a_{N_{MAX}}} \frac{da_{N_{MAX}}}{a_{N_{MAX}}}$$

By direct comparison, it follows that

$$S_{W/S} = - S_{C_{L_{MAX}}} = R \frac{\partial \bar{L}}{\partial R} + \bar{L} \qquad , V < V_c$$

$$S_{W/S} = S_{C_{L_{MAX}}} = 0, \; S_{a_{N_{MAX}}} = - \left(R \frac{\partial \bar{L}}{\partial R} + \bar{L}\right) , \; V > V_c$$

Table 2 presents sample sensitivity data for selected values of ϵ, θ, and R.

The discussion of the significance of the capture range to variations in the performance characteristics follows. For $V_p < V_c$, a one per cent increase in $C_{L_{MAX}}$ is equivalent to a one per cent decrease in W/S. For values of R less than or equal to 5.0 the biggest improvement in $\bar{L}$ occurs for an increase in V_p when $V_p < V_c$.

TABLE 2

PROBLEM II SENSITIVITY DATA

ϵ	R	θ	$\bar{L}$	S_θ	$R\frac{\partial \bar{L}}{\partial R} + \bar{L}$	$V_P < V_c$ S_{V_P}	$V_P > V_c$ S_{V_P}
0.99	1.1	1	.038	-.0001	.286	-1.32	-.75
		3	.037	-.0001	.278	-1.32	-.76
		5	.037	-.0001	.273	-1.33	-.78
0.9	1.5	1	.072	-.001	.412	-1.03	-.17
		3	.070	-.001	.399	-1.02	-.22
		5	.069	-.001	.391	-1.02	-.24
0.9	2.0	1	.184	-.002	.634	-1.03	.24
		3	.180	-.002	.618	-1.01	.23
		5	.176	-.002	.604	- .99	.22
0.9	5.0	1	.434	-.020	.662	- .92	.40
		3	.414	-.018	.619	- .89	.35
		5	.397	-.015	.517	- .86	.28

When $R \leq 2$, the capture range is relatively insensitive to the terminal surface constraint θ. Since $S_{V_P} < 0$ when $V_P < V_c$, the pursuer should operate as close to V_c as possible. This is not always the case when $V_P > V_c$. The data in Table 2 shows that if $V_P > V_c$ then S_{V_P} changes sign somewhere between $R = 1.5$ and $R = 2.0$. Below this value the pursuer should operate at maximum speed. Above it, and as in Problem I, the pursuer should fly at V_c. If $R = 1.1$ the biggest improvement results from an increase in V_P as evidenced by the S_θ data in Table 2. If $R \geq 2$, however, the biggest improvement results from an increase in $a_{N_{MAX}}$ rather than V_P. This is consistent with the results of Problem I.

We can make some direct comparisons with the dimensional range L computed for Problem I. Consider $\epsilon = 0.9$ and $\theta = 1^{\circ}$ and 5°. For the sample aircraft parameters in Problem I, the capture ranges were 4140 feet and 3350 feet, respectively. If $R = 1.1$, the corresponding capture range is zero for both values of θ. If $R = 1.5$, the capture ranges are 401 feet and 386 feet, respectively. For $R = 2.0$, $L = 1030$ feet and 980 feet. For $R = 5.0$, $L = 2420$ feet and 2220 feet. Consequently, if $R < 5.0$ the pursuer should be able to bring his machine guns to bear within the lethal range of the guns.

Problem II Conclusions

If $R \leq 1.5$, the pursuer should fly as fast as possible. If $R > 2.0$, the pursuer should fly at the corner speed. The capture range is relatively insensitive to θ if $R < 2.0$. If $V_p > V_c$ and $R \geq 1.5$ the biggest improvement in $\bar{L}$ results from an increase in $a_{N_{MAX}}$. Finally, if the pursuer's maximum normal acceleration equals or exceeds that for the evader, then under optimal play the pursuer can realize a collision, i.e., zero capture range, with the evader.

The previous results are based upon the assumption that the pursuer and evader can maintain constant speed while maneuvering. Since this is usually not the case in air-to-air combat, we next turn our attention to the variable speed problem.

SECTION VI

PROBLEM III SOLUTION

Problem Definition

The differential equations of state and control constraints were derived in Appendix A and presented in Chapter III. Eqs (60) through (69) define the problem to be addressed in this chapter, namely

$$\dot{X} = \alpha_1 \, v \sin\gamma \cos\delta_1 + \frac{n_P}{u} Y \sin\delta_2 \tag{60}$$

$$\dot{Y} = \alpha_1 \, v \cos\gamma - \alpha_1 \, u - \frac{n_P}{u} X \sin\delta_2 \tag{61}$$

$$\dot{\gamma} = -\frac{n_E}{v} \sin\phi_E + \frac{n_P}{u} \sin(\delta_2 - \delta_1) \tag{62}$$

$$\dot{\delta}_1 = \frac{n_E}{v} \sin\gamma \cos\phi_E - \alpha_1 \frac{Y}{X} \sin\gamma \sin\delta_1 + \frac{n_P}{u} \frac{Y}{X} \cos\delta_2 \tag{63}$$

$$\dot{v} = C_{T_E} - \alpha_2 \frac{n_E^2}{v^2} \tag{64}$$

$$\dot{u} = C_{T_P} - \alpha_3 \frac{n_P^2}{u^2} \tag{65}$$

$$\text{MIN } C_{T_E} \leq C_{T_E} \leq \text{MAX } C_{T_E} \tag{66}$$

$$\text{MIN } C_{T_P} \leq C_{T_P} \leq \text{MAX } C_{T_P} \tag{67}$$

$$0 \leq n_E \leq \text{MAX } n_E \tag{68}$$

$$0 \leq n_P \leq \text{MAX } n_P \tag{69}$$

The control variables are n_P, n_E, C_{T_P}, C_{T_E}, ϕ_E, and δ_2. This problem has six state and six control variables. As was pointed out in Chapter III, this problem reduces to Problem II under certain simplifying assumptions. Consequently, the solution to Problem II is a special solution to this problem.

Whereas the angle-off constraint held for the previous problems, it will not for this problem. The justification for this follows from the results of Problem II. For a speed ratio around 0.9 and a turning radius ratio of 1.5 or less, the capture range ratio was relatively insensitive to the angle-off. Consequently, if the speed variation is small, then the angle-off constraint can be dropped based upon the results of Problem II.

The Necessary Conditions

Substitution of Eqs (60) through (65) into the optimality condition, Eq (7) gives

$$\underset{(C_{T_P},n_P,\delta_2)}{\text{MIN}} \quad \underset{(C_{T_E},n_E,\phi_E)}{\text{MAX}} \quad [\nu_1(\alpha_1 v \sin\gamma \cos\delta_1 + \frac{n_P}{u} Y \sin\delta_2)$$

$$+ \nu_2 (\alpha_1 v \cos\gamma - \alpha_1 u - \frac{n_P}{u} X \sin\delta_2) + \nu_3(-\frac{n_E}{v} \sin\phi_E + \frac{n_P}{u} \sin(\delta_2-\delta_1))$$

$$+ \nu_4 (\frac{n_E}{v} \sin\gamma \cos\phi_E - \alpha_1 \frac{v}{x} \sin\gamma \sin\delta_1 + \frac{n_P}{u} \frac{Y}{X} \cos\delta_2)$$

$$+ \nu_5 (C_{T_E} - \alpha_2 \frac{n_E^2}{v^2}) + \nu_6(C_{T_P} - \alpha_3 \frac{n_P^2}{u^2})]$$

The optimal controls for C_{T_E} and C_{T_P} are

$$C_{T_E}^* = \text{MIN } C_{T_E} \qquad \text{if} \quad \nu_5 < 0 \qquad (171)$$

$$= \text{MAX } C_{T_E} \qquad \text{if} \quad \nu_5 > 0$$

$$C^*_{T_P} = \text{MIN } C_{T_P} \qquad \text{if} \quad \nu_6 > 0 \tag{172}$$

$$= \text{MAX } C_{T_P} \qquad \text{if} \quad \nu_6 < 0$$

The situation for $\gamma_5 = 0$ and $\gamma_6 = 0$ will be examined later. For optimal δ_2, minimization requires that δ_2 be the solution of

$$\underset{\delta_2}{\text{MIN}} \frac{n_P}{u} (B \sin \delta_2 + C \cos \delta_2) \tag{173}$$

where $B = \nu_1 Y - \nu_2 X + \nu_3 \cos \delta_1$

$$C = \nu_4 \frac{Y}{X} - \nu_3 \sin \delta_1 \tag{174}$$

B is the same variable that appeared in Problem II when $\delta_1 = 0$. The solution of Eq (173) is

$$\sin \delta_2^* = -\frac{B}{\sqrt{B^2 + C^2}} \quad , \quad \cos \delta_2^* = -\frac{C}{\sqrt{B^2 + C^2}} \tag{175}$$

provided that both B and C are not zero. The situation when $B = 0$ and $C = 0$ will be examined later. For optimal ϕ_E, the function to be maximized is

$$\underset{\phi_E}{\text{MAX}} (-\nu_3 \sin \phi_E + \nu_4 \sin \gamma \cos \phi_E)$$

The solution is

$$\sin \phi_E^* = -\frac{\nu_3}{\sqrt{\nu_3^2 + \nu_4^2 \sin^2 \gamma}} \quad , \quad \cos \phi_E^* = \frac{\nu_4 \sin \gamma}{\sqrt{\nu_3^2 + \nu_4^2 \sin^2 \gamma}} \tag{176}$$

if ν_3 and ν_4 are not zero. Again this situation will be examined later. The function to be minimized for optimal n_p is

$$\underset{n_p}{\text{MIN}} \left[\frac{n_p}{u} (B \sin \delta_2 + C \cos \delta_2) - \alpha_3 \nu_6 \frac{n_p^2}{u^2} \right] \tag{177}$$

The second partial derivative of this function with respect to n_p is

$$-2 \nu_6 \alpha_3 / u^2$$

Thus if $\nu_6 < 0$, the second partial is positive. If $\nu_6 > 0$, then it is negative and n_p is either equal to zero or MAX n_p. Consider first the case $\nu_6 < 0$. Let n_p^{**} denote the minimum solution of Eq (177), namely

$$n_p^{**} = - \frac{u \sqrt{B^2 + C^2}}{2 \nu_6 \alpha_3} > 0 \tag{178}$$

if B,C, and ν_6 are not zero. Then the solution for optimal n_p is

$$n_p^* = \text{MIN } (\text{MAX } n_p, n_p^{**}) \quad \text{if } \nu_6 < 0 \tag{179}$$

If $\nu_6 > 0$, then $n_p = 0$ substituted into Eq. (177) yields zero. If $\nu_6 > 0$ and $n_p = \text{MAX } n_p$, Eq (177) becomes upon substitution for optimal δ_2

$$\frac{\text{MAX } n_p}{u} \left(- \frac{B^2}{\sqrt{B^2 + C^2}} - \frac{C^2}{\sqrt{B^2 + C^2}} \right) - \alpha_3 \nu_6 \frac{(\text{MAX } n_p)^2}{u^2}$$

$$= - \frac{\text{MAX } n_p}{u} \sqrt{B^2 + C^2} - \alpha_3 \nu_6 \frac{(\text{MAX } n_p)^2}{u^2}$$

$$< 0$$

Since $n_p = 0$ gave zero for Eq (177), it follows that

$$n_p^* = \text{MAX } n_p \quad \text{if } \nu_6 > 0 \tag{180}$$

Eqs (179) and (180) define optimal n_p if B, C, and ν_6 are not zero. This possibility will be examined later. Finally, optimal n_E requires the maximization of

$$\underset{n_E}{\text{MAX}} \left[\frac{n_E}{v} \left(-\nu_3 \sin \phi_E + \nu_4 \sin \gamma \cos \phi_E \right) - \nu_5 \alpha_2 \frac{n_E^2}{v^2} \right] \tag{181}$$

The second partial of this function gives

$$-2 \nu_5 \alpha_2 / v^2 \tag{182}$$

Thus Eq (181) has a global maximum if $\nu_5 > 0$. If $\nu_5 < 0$ optimal n_E is either $n_E = 0$ or $n_E = \text{MAX } n_E$. Consider the situation where $\nu_5 = 0$. Define n_E^* as

$$n_E^{**} = \frac{v \sqrt{\nu_3^2 + \nu_4^2 \sin^2 \gamma}}{\partial \nu_5 \alpha_2} > 0 \tag{183}$$

if ν_3 and ν_4 are not zero. The solution for n_E^* maximizes Eq (181) if $\nu_5 > 0$, thus the optimal solution is

$$n_E^* = \text{MIN } (\text{MAX } n_E, n_E^{**}) \text{ if } \nu_5 > 0. \tag{184}$$

if $\nu_5 < 0$ substitution of $n_E = 0$ into Eq (181) gives zero. If $n_E = \text{MAX } n_E$, substitution along with optimal ϕ_E into Eq (181) gives

$$\frac{\text{MAX } n_E}{v}\left(\frac{v_3^2}{\sqrt{v_3^2 + v_4^2 \sin^2\gamma}} + \frac{v_4^2 \sin^2\gamma}{\sqrt{v_3^2 + v_4^2 \sin^2\gamma}}\right) - v_5\alpha_2 \frac{(\text{MAX } n_E)^2}{v^2}$$

$$= \frac{\text{MAX } n_E}{v}\sqrt{v_3^2 + v_4^2 \sin^2\gamma} - v_5\,\alpha_2 \frac{(\text{MAX } n_E)^2}{v^2}$$

$$> 0$$

since $v_5 < 0$. Thus

$$n_E^* = \text{MAX } n_E \quad \text{if} \quad v_5 < 0 \tag{185}$$

The situation when v_3, v_4, and v_5 are all zero will be examined later.

The boundary conditions for the state variables on the terminal surface are

$$X(0) = \bar{L} \sin s_1 \tag{186}$$

$$Y(0) = \bar{L} \cos s_1 \tag{187}$$

$$\gamma(0) = s_2 \tag{188}$$

$$\delta_1(0) = 0 \tag{189}$$

$$v(0) = \epsilon \tag{190}$$

$$u(0) = 1 \tag{191}$$

where nondimensional time zero is with respect to the variable β defined in Eq (88). The parameters $\bar{L}$, s_1, s_2, and ϵ have the same definition as they did in Problem II except that s_1 can take on both positive and negative values. The physical significance of Eq (189),

$\delta_1(0) = 0$, is that the velocities of P and E are in the same plane. Furthermore, the accelerations normal to and along the velocity vectors fall in this same plane. Since the normal acceleration is in the vertical plane of symmetry for fighter aircraft, E may be above or below P but not to the side of P. If δ_1 does not change with time, then the motion of P and E are in the same plane as that for the terminal surface. Consequently, E will not be to the side of P if $\delta_1 = 0$. From the definition of u in Eq (55), Eq (191) requires that the characteristic speed V_o be

$$V_o = V_P(0) \tag{192}$$

Consequently, ϵ is the speed ratio of the two players at the end of the game. The characteristic length R_o is now defined to be $R_P(0)$, the pursuer's minimum turning radius at the end of the game. In light of these definitions α_1, as defined by Eq (57), has a physical interpretation. Now

$$\alpha_1 = \frac{V_o^2}{gR_o} = \frac{V_P^2(0)}{g\ R_P(0)}$$

$$= \frac{a_{N_P}(0)}{g} = n_P(0) \tag{193}$$

Thus α_1 is the pursuer's maximum allowable load factor at the end of the game.

The vector $\bar{\nu}$ is perpendicular to the terminal surface, thus its components are taken to be

$$\nu_1(0) = \sin s_1 \tag{194}$$

$$\nu_2(0) = \cos s_1 \tag{195}$$

$$\nu_3(0) = 0 \tag{196}$$

$$\nu_4(0) = 0 \tag{197}$$

$$\nu_5(0) = 0 \tag{198}$$

$$\nu_6(0) = 0 \tag{199}$$

The rationale for Eqs (194), (195), and (196) is the same as that used in Problem II. The justification for Eqs (197), (198), and (199) is related to the boundary conditions for δ_1, u, and v as defined by Eqs (189), (190), and (191).

The optimal controls are undefined in light of the boundary conditions. But before addressing this problem, the boundary of the usable part will be determined since it will be used in establishing the initial controls. Substitution of the differential equations and boundary conditions into Eq (7) gives

$$\epsilon \sin s_1 \sin s_2 + \cos s_1 (\epsilon \cos s_2 - 1) = 0 \tag{200}$$

which is the same as the natural barrier in Problem II.

Next introduce the nondimensional time β as in Eq (88) which is zero on the terminal surface. The transformed differential equations of state are

$$X' = -\alpha_1 v \sin \gamma \cos \delta_1 - \frac{n_p^*}{u} Y \sin \delta_2^* \tag{201}$$

$$Y' = -\alpha_1 v \cos \gamma + \alpha_1 u + \frac{n_p^*}{u} X \sin \delta_2^* \tag{202}$$

$$\gamma' = \frac{n_E^*}{v} \sin \phi_E^* - \frac{n_P^*}{u} \sin(\delta_2^* - \delta_1) \tag{203}$$

$$\delta_1' = -\frac{n_E^*}{v} \sin\gamma \cos\phi_E^* + \alpha_1 \frac{v}{X} \sin\gamma \sin\delta_1 - \frac{n_P^*}{u} \frac{Y}{X} \cos\delta_2^* \tag{204}$$

$$v' = -C_{T_E}^* + \alpha_2 \frac{n_E^{*2}}{v^2} \tag{205}$$

$$u' = -C_{T_P}^* + \alpha_3 \frac{n_P^{*2}}{u^2} \tag{206}$$

where differentiation is with respect to β. Substitution of the differential equations of state into Eq (13) gives the differential equations for the ν_i. These differential equations differ in form dependent upon whether or not the speed is above the corner speed, as illustrated in Figure 18. The forms are different because MAX C_L is a constant below the corner speed and MAX n is a constant above V_c. If $V > V_c$, then

$$\nu_1' = -\nu_2 \frac{n_P^*}{u} \sin\delta_2^* - \nu_4 \frac{n_P^*}{u} \frac{Y}{X^2} \cos\delta_2^* + \nu_4 \frac{\alpha_1 v}{X^2} \sin\gamma \sin\delta_1 \tag{207}$$

$$\nu_2' = \nu_1 \frac{n_P^*}{u} \sin\delta_2^* + \nu_4 \frac{n_P^*}{u} \frac{1}{X} \cos\delta_2^* \tag{208}$$

$$\nu_3' = \nu_1 \alpha_1 v \cos\gamma \cos\delta_1 - \nu_2 \alpha_1 v \sin\gamma + \nu_4 \left(\frac{n_E^*}{v} \cos\gamma \cos\phi_E^* - \alpha_1 \frac{v}{X} \cos\gamma \sin\delta_1 \right) \tag{209}$$

$$\nu_4' = -\nu_1 \alpha_1 v \sin\gamma \sin\delta_1 - \nu_4 \frac{\alpha_1 v}{X} \sin\gamma \cos\delta_1 - \nu_3 \frac{n_P^*}{u} \cos(\delta_2^* - \delta_1) \tag{210}$$

$$\nu_5' = \nu_1 \alpha_1 \sin\gamma \cos\delta_1 + \nu_2 \alpha_1 \cos\gamma + \nu_3 \frac{n_E^*}{v^2} \sin\phi_E^* - \nu_4 \left(\frac{n_E^*}{v^2} \sin\gamma \cos\phi_E^* + \frac{\alpha_1}{X} \sin\gamma \sin\delta_1 \right) + 2\nu_5 \alpha_2 \frac{n_E^{*2}}{v^3} \tag{211}$$

$$\nu_6' = -\nu_1 \frac{n_P^*}{u^2} Y \sin\delta_2^* - \nu_2 \alpha_1 + \nu_2 \frac{n_P^*}{u^2} X \sin\delta_2^* \qquad (212)$$
$$-\nu_3 \frac{n_P^*}{u^2} \sin(\delta_2^* - \delta_1) - \nu_4 \frac{n_P^*}{u^2} \frac{Y}{X} \cos\delta_2^* + 2\nu_6 \alpha_3 \frac{n_P^{*2}}{u^3}$$

If $V \leq V_c$, then n is replaced with C_L where

$$C_L = \frac{nW}{\frac{1}{2} \rho S V^2} \qquad (213)$$

Since C_L is inversely proportional to V^2 the only changes when $V \leq V_c$ are in ν_5' and ν_6'

$$\nu_5' = \alpha_1 \nu_1 \sin\gamma \cos\delta_1 + \alpha_1 \nu_2 \cos\gamma - \nu_3 \frac{n_E^*}{V^2} \sin\phi_E^*$$
$$+ \nu_4 \left(\frac{n_E^*}{V^2} \sin\gamma \cos\phi_E^* - \frac{\alpha_1}{X} \sin\gamma \sin\delta_1 \right) - 2\alpha_2 \nu_5 \frac{n_E^{*2}}{V^3}$$

$$\nu_6' = \frac{n_P^*}{u^2} B \sin\delta_2^* - \alpha_1 \nu_2 + \nu_4 \frac{n_P^*}{u^2} \frac{Y}{X} \cos\delta_2^* - 2\alpha_3 \nu_6 \frac{n_P^{*2}}{u^3} - \nu_3 \frac{n_P^*}{u^2} \cos\delta_2^* \sin\delta_1$$

The aerodynamic constraints are

$$0 \leq n_E^* \leq \frac{\frac{1}{2} \rho_E S_E V_o^2 (\text{MAX } C_{L_E})}{W_E} \quad v^2 \quad \text{if} \quad V_E \leq V_c$$

$$0 \leq n_P^* \leq \frac{\frac{1}{2} \rho_P S_P V_o^2 (\text{MAX } C_{L_P})}{W_P} \quad u^2 \quad \text{if} \quad V_P \leq V_c$$

From the boundary conditions, Eqs (196) through (199), ν_3, ν_4, ν_5, and ν_6 are all zero on the terminal surface. Since ν_3, $\nu_4 = 0$, C = 0 from Eq (174). Substitution of the boundary conditions into B

as defined by Eq (174) gives B = 0 on the terminal surface. Thus the optimal controls are undefined or indeterminant on the terminal surface. The controls can be determined on the terminal surface however by examination of the derivatives of the appropriate variables. Substitution of the boundary conditions on the terminal surface gives the following results

$$B'(0) = \alpha_1 \sin s_1 \tag{214}$$

$$C'(0) = 0 \tag{215}$$

$$\nu_3'(0) = \alpha_1 \epsilon (\sin S_1 \cos S_2 - \cos S_1 \sin S_2) \tag{216}$$

$$\nu_4'(0) = 0 \tag{217}$$

$$\nu_5'(0) = \alpha_1 (\sin S_1 \sin S_2 + \cos S_1 \cos S_2) \tag{218}$$

$$\nu_6'(0) = -\alpha_1 \cos S_1 \tag{219}$$

From the solution for the boundary of the usable part, Eq (200), $B'(0)$ is positive (negative) on the right (left) barrier. Thus from Eq (175)

$$\begin{aligned} \delta_2^*(0) &= -\pi/2 \quad \text{on the right barrier} \\ &= \pi/2 \quad \text{on the left barrier} \end{aligned} \tag{220}$$

Substitution of the solution to Eq (200) into Eq (216) and combination with Eqs (176) and (217) gives the following results for ϕ_E^*:

Range of S_2	Right Barrier	Left Barrier
$0 < S_2 < S^*$	$-\pi/2$	$\pi/2$
$S^* < S_2 < 2\pi - S^*$	$\pi/2$	$-\pi/2$
$2\pi - S^* < S_2 < 2\pi$	$-\pi/2$	$\pi/2$

where cos $S^* = \epsilon$. These results are directly analogous with the evader's optimal control in Problem II. Substitution of the solution of Eq (200) into Eq (218) and combining with Eq (171) gives the following for optimal $C_{T_E}^*$:

Range of S_2	Right Barrier	Left Barrier
$0 < S_2 < \pi$	MAX C_{T_E}	MIN C_{T_E}
$\pi < S_2 < 2\pi$	MIN C_{T_E}	MAX C_{T_E}

Substitution for s_1 as a function of S_2 into Eq (219) and combining with Eq (172) gives optimal $C_{T_P}^*$, namely:

Range of S_2	Right Barrier	Left Barrier
$0 < S_2 < \pi$	MAX C_{T_P}	MIN C_{T_P}
$\pi < S_2 < 2\pi$	MIN C_{T_P}	MAX C_{T_P}

The combination of Eqs (214), (215), (219), and (177) defines optimal n_P^*:

Range of S_2	Right Barrier	Left Barrier
$0 < S_2 < \pi$	MIN (n_P^{**}, MAX n_P)	MAX n_P
$\pi < S_2 < 2\pi$	MAX n_P	MIN (n_P^{**}, MAX n_P)

where n_P^{**} is defined by Eq (178) except that B, C, and v_6 are replaced with their derivatives. Finally, optimal n_E^* is determined by the combination of Eqs (216), (217), and (182), namely:

Range of s_2	Right Barrier	Left Barrier
$0 < S_2 < \pi$	MIN (n_E^{**}, MAX n_E)	MAX n_E
$\pi < S_2 < 2\pi$	MAX n_E	MIN (n_E^{**}, MAX n_E)

where n_E^{**} is defined by Eq (183) with ν_3, ν_4, and ν_5 replaced by their derivatives. The previous results define the optimal controls on the boundary of the usable part on the terminal surface.

At $s_2 = S^*$ on the right barrier and $S_2 = 2\pi - S^*$ on the left barrier the trajectories diverge as they did in Problem II. It is easily verified, as it was in Problem II, that the voids are filled with a singular arc $\phi_E^* = 0$ and tributaries.

As in Problem II, it can be verified that the intercept of the two barriers and the $\gamma = 0$ plane are symmetrical. Let subscripts L and R denote the left and right barriers, respectively. In the range $-S^* < S_2 < S^*$ and analogous to Problem II, trajectories emanate from opposite sides of the $\gamma = 0$ plane for the two barriers, hence

$$\delta_{2_R}^*(0) = -\delta_{2_L}^*(0) = -\pi/2 \tag{221}$$

$$\phi_{E_R}^*(0) = -\phi_{E_L}^*(0) = -\pi/2 \tag{222}$$

$$C_{T_{E_R}}^*(0) = C_{T_{E_L}}^*(0) = \text{MAX } C_{T_E} \tag{223}$$

$$C_{T_{P_R}}^*(0) = C_{T_{P_L}}^*(0) = \text{MAX } C_{T_P} \tag{224}$$

$$n_{E_R}^*(0) = n_{E_L}^*(0) = \text{MIN } (n_E^{**}, \text{MAX } n_E) \tag{225}$$

$$n_{P_R}^*(0) = n_{P_L}^*(0) = \text{MIN } (n_P^{**}, \text{MAX } n_P) \tag{226}$$

If $S_{2_R} = -S_{2_L}$, then $S_{1_R} = -S_{1_L}$. From Eq (203)

$$\gamma_R' = -\frac{n_E^*}{v} + \frac{n_P^*}{u} = -\gamma_L'$$

The time to travel from the terminal surface to the $\gamma = 0$ plane given $S2_R = -S2_L$ is the same for the two barriers. Also, $\gamma_R = -\gamma_L$. From Eqs (204), (189), and the optimal controls

$$\delta_1(0) = 0$$

$$\delta_1'(0) = 0$$

thus δ_1 remains zero. Based upon the earlier description of the physical description of the physical significance of $\delta_1(0) = 0$, $\delta_1 = 0$ as a function of time means that E does not maneuver to the side of P. This will simplify the problem since if $\delta_1(0) = 0$, then δ_1 as a function of time is also zero. Eq (201), the optimal controls, and the boundary conditions, Eqs (187) and (188) show that

$$X_R'(0) = -X_L'(0)$$

Similarly it can be shown that

$$Y_R'(0) = Y_L'(0).$$

It can therefore be argued that

$$X_R = -X_L$$

$$Y_R = Y_L$$

and the conclusion is that the intercept of the two barriers and the $\gamma = 0$ plane are symmetrical about the Y-axis. Consequently, it suffices to examine only the right barrier for determining the relationship between the parameters in the problem which lead to the barrier

grazing the Y-axis. The optimal controls on the terminal surface are defined by Eqs (221) through (226).

Since $\delta_1 = 0$, Eqs (210) and (197) give $\nu_4 = 0$. Thus the number of differential equations reduces from twelve to ten. For the remaining ten differential equations u' and v' can be integrated analytically. Unfortunately, the resulting relations for u and v are implicit functions of β. It is impossible to solve for u and v explicitly in terms of β. Thus the remaining differential equations can not be integrated analytically. Recourse to numerical integration is required if the ten differential equations are to be integrated. Instead of this approach, however, two additional approximations will be made which will allow the resulting differential equations to be integrated analytically.

The Trajectory Solution

It will be assumed that both the pursuer's and evader's acceleration are constant. That is, u' and v' are constant with time. There are two reasons for assuming this. The first was mentioned previously, namely analytical solutions can be obtained. The second reason is that the results can be compared with the results from Problem II. Recall that in Problem II the evader's speed as well as the pursuer's speed was constant. Thus the impact of acceleration capability by the pursuer, $u' \neq 0$, can be compared with a constant speed pursuer. The constant in u' (or v') will be called C_{T_P} (or C_{T_E}) but it will be defined as the value of u'(0) (or v'(0)). If the change in u(v) is negligible, then this should be a reasonable approximation.

The differential equations become

$$X' = -\alpha_1 v \sin\gamma + \frac{n_P^*}{u} Y \tag{227}$$

$$Y' = -\alpha_1 v \cos\gamma + \alpha_1 u - \frac{n_P^*}{u} X \tag{228}$$

$$\gamma' = -\frac{n_E^*}{v} + \frac{n_P^*}{u} \tag{229}$$

$$v' = -C_{T_E} \tag{230}$$

$$u' = -C_{T_P} \tag{231}$$

$$\nu_1' = \nu_2 \frac{n_P^*}{u} \tag{232}$$

$$\nu_2' = -\nu_1 \frac{n_P^*}{u} \tag{233}$$

$$\nu_3' = \alpha_1 v (\nu_1 \cos\gamma - \nu_2 \sin\gamma) \tag{234}$$

$$\nu_5' = \alpha_1 (\nu_1 \sin\gamma + \nu_2 \cos\gamma) + \nu_3 \frac{n_E^*}{v^2} \tag{235}$$

$$\nu_6' = -\frac{n_P^*}{u^2} B - \alpha_1 \nu_2 \tag{236}$$

$$n_P^* = \alpha_5 (\text{MAX } C_{L_P}) u^2, \quad n_E^* = \alpha_4 (\text{MAX } C_{L_E}) v^2$$

The previous formulation is based upon the assumption that the pursuer and evader speeds are always less than or equal to the corner velocity which is representative of past air-to-air combat engagements. The equations are easier to integrate if u is taken to be the independent variable and the nondimensional time β is a dependent variable. Integration of Eq (231) along with the boundary condition gives

$$u = 1 - C_{T_P} \beta \tag{237}$$

Division of v' by u' gives

$$\frac{dv}{du} = \frac{C_{T_E}}{C_{T_P}} = C$$

Integration gives

$$v = \epsilon + C\,(u-1) \tag{238}$$

Division of γ' by u' gives

$$\frac{d\gamma}{du} = \frac{1}{C_{T_P}}\left[C_4\,(\epsilon - C) + (C_4 C - C_5)u\right]$$

where

$$C_4 = \alpha_4\ (\text{MAX}\ C_{L_E})$$

$$C_5 = \alpha_5\ (\text{MAX}\ C_{L_P})$$

$$\alpha_4 = \frac{.5\,\rho_E\,V_o^2}{W_E/S_E}$$

$$\alpha_4 = \frac{.5\,\rho_P\,V_o^2}{W_P/S_P}$$

Integration gives

$$\gamma = S_2 + \frac{1}{2C_{T_P}(C_4 C - C_5)}\left\{\left[C_4(\epsilon - C) + (C_4 C - C_5)u\right]^2 - (C_4\epsilon - C_5)^2\right\} \tag{239}$$

It is easily verified that γ satisfies the differential equation and boundary condition. Let

$$\lambda_0 = \frac{\alpha_1}{C_{T_P}} C$$

$$\lambda_1 = \frac{\alpha_1}{C_{T_P}} (\epsilon - C)$$

$$\lambda_2 = \frac{\alpha_1}{C_{T_P}}$$

$$\lambda_3 = \frac{C_5}{C_{T_P}}$$

Division of X' and Y' by u' gives

$$\frac{dX}{du} = (\lambda_1 + \lambda_0 u) \sin \gamma - \lambda_3 u Y \tag{240}$$

$$\frac{dY}{du} = (\lambda_1 + \lambda_0 u) \cos \gamma - \lambda_2 u + \lambda_3 u X \tag{241}$$

Both of these differential equations are linear. Hence the general solution is the sum of the homogeneous solution and the particular solution. Let subscripts H and L denote homogeneous and particular solutions, respectively. Then

$$\frac{dX_H}{du} = - \lambda_3 u Y_H \tag{242}$$

$$\frac{dY_H}{du} = \lambda_3 u X_H \tag{243}$$

Multiplying the first equation by X_H, the second equation by Y_H, and then adding gives

$$X_H \frac{dX_H}{du} + Y_H \frac{dY_H}{du} = 0$$

or

$$\frac{d}{du}\left(X_H^2 + Y_H^2\right) = 0$$

A solution is

$$X_H^2 + Y_H^2 = C_o^2 = \text{constant}$$

Solving for Y_H and substituting into Eq (242) gives

$$\frac{dX_H}{du} = -\lambda_3 u \left(\pm\sqrt{C_o^2 - X_H^2}\right)$$

This differential equation has two solutions, namely

$$X_H = \mp C_o \sin \tfrac{1}{2}\lambda_3 u^2$$

and

$$X_H = \pm C_o \cos \tfrac{1}{2}\lambda_3 u^2$$

We write therefore for the homogeneous solution for X_H and Y_H

$$X_H = A_1 \sin \tfrac{1}{2}\lambda_3 u^2 + B_1 \cos \tfrac{1}{2}\lambda_3 u^2 \qquad (244)$$

$$Y_H = -A_1 \cos \tfrac{1}{2}\lambda_3 u^2 + B_1 \sin \tfrac{1}{2}\lambda_3 u^2 \qquad (245)$$

Eq (245) was obtained by substitution of Eq (244) into Eq (242). Whether or not the solution is correct is determined by substitution of Eqs (244) and (245) into Eq (243), thus

$$\frac{dY_H}{du} = \lambda_3 u \left(A_1 \sin \tfrac{1}{2}\lambda_3 u^2 + B_1 \cos \tfrac{1}{2}\lambda_3 u^2\right)$$

The right side is equal to $\lambda_3 u X_H$; therefore Eqs (244) and (245) satisfy Eqs (242) and (243).

The particular solution to Eqs (240) and (241) can be obtained from the method of variation of parameters. The method replaces the constants A_1 and B_1 in Eqs (244) and (245) with unknown functions $v_1(u)$ and $v_2(u)$

$$X_p = v_1(u) \sin \tfrac{1}{2} \lambda_3 u^2 + v_2(u) \cos \tfrac{1}{2} \lambda_3 u^2 \tag{246}$$

$$Y_p = -v_1(u) \cos \tfrac{1}{2} \lambda_3 u^2 + v_2(u) \sin \tfrac{1}{2} \lambda_3 u^2 \tag{247}$$

Substitution of Eqs (246) and (247) into Eqs (240) and (241) gives

$$(\sin \tfrac{1}{2} \lambda_3 u^2) \frac{dv_1}{du} + (\cos \tfrac{1}{2} \lambda_3 u^2) \frac{dv_2}{du} = (\lambda_1 + \lambda_0 u) \sin \gamma$$

$$-(\cos \tfrac{1}{2} \lambda_3 u^2) \frac{dv_1}{du} + (\sin \tfrac{1}{2} \lambda_3 u^2) \frac{dv_2}{du} = (\lambda_1 + \lambda_0 u) \cos \gamma - \lambda_2 u$$

Solving these two equations for dv_1/du and dv_2/du gives

$$\frac{dv_1}{du} = -(\lambda_1 + \lambda_0 u) \cos (\gamma + \tfrac{1}{2} \lambda_3 u^2) + \lambda_2 u \cos \tfrac{1}{2} \lambda_3 u^2 \tag{248}$$

$$\frac{dv_2}{du} = (\lambda_1 + \lambda_0 u) \sin (\gamma + \tfrac{1}{2} \lambda_3 u^2) - \lambda_2 u \sin \tfrac{1}{2} \lambda_3 u^2 \tag{249}$$

From the solution for γ, Eq (239)

$$\gamma + \tfrac{1}{2} \lambda_3 u^2 = \lambda_4 + \lambda_5 u + \lambda_6 u^2 \tag{250}$$

where

$$\lambda_4 = s_2 + \frac{1}{2C_{T_p}(C_4 C - C_5)} \left\{ [C_4(\epsilon - C)]^2 - (C_4 \epsilon - C_5)^2 \right\}$$

$$\lambda_5 = \frac{C_4 (\epsilon - C)}{C_{T_P}}$$

$$\lambda_6 = \frac{C_4 C}{2C_{T_P}}$$

Since

$$\lambda_1 + \lambda_0 u = \frac{\lambda_0}{2\lambda_6} (\lambda_5 + 2\lambda_6 u)$$

$$= \frac{\lambda_0}{2\lambda_6} \frac{d}{du} (\lambda_4 + \lambda_5 u + \lambda_6 u^2) \qquad (251)$$

substitution into Eqs (248) and (249) gives

$$\frac{dv_1}{du} = - \frac{\lambda_0}{2\lambda_6} \frac{d}{du} (\lambda_4 + \lambda_5 u + \lambda_6 u^2) \cos (\lambda_4 + \lambda_5 u + \lambda_6 u^2)$$

$$+ \frac{\lambda_2}{\lambda_3} (\lambda_3 u \cos \tfrac{1}{2} \lambda_3 u^2)$$

$$\frac{dv_2}{du} = \frac{\lambda_0}{2\lambda_6} \frac{d}{du} (\lambda_4 + \lambda_5 u + \lambda_6 u^2) \sin (\lambda_4 + \lambda_5 u + \lambda_6 u^2)$$

$$- \frac{\lambda_2}{\lambda_3} (\lambda_3 u \sin \tfrac{1}{2} \lambda_3 u^2)$$

Both equations are integrable, thus

$$v_1 = - \frac{\lambda_0}{2\lambda_6} \sin (\lambda_4 + \lambda_5 u + \lambda_6 u^2) + \frac{\lambda_2}{\lambda_3} \sin \tfrac{1}{2} \lambda_3 u^2$$

$$v_2 = - \frac{\lambda_0}{2\lambda_6} \cos (\lambda_4 + \lambda_5 u + \lambda_6 u^2) + \frac{\lambda_2}{\lambda_3} \cos \tfrac{1}{2} \lambda_3 u^2$$

Substitution into Eqs (246) and (247) and then adding Eqs (244) and (245) gives the general solutions for X and Y

$$X = A_1 \sin \tfrac{1}{2}\lambda_3 u^2 + B_1 \cos \tfrac{1}{2}\lambda_3 u^2 - \frac{\lambda_0}{2\lambda_6} \cos \gamma + \frac{\lambda_2}{\lambda_3}$$

$$Y = -A_1 \cos \tfrac{1}{2}\lambda_3 u^2 + B_1 \sin \tfrac{1}{2}\lambda_3 u^2 + \frac{\lambda_0}{2\lambda_6} \sin \gamma$$

The constants A_1 and B_1 are determined from the boundary conditions, Eqs (186) and (187). Evaluation of A_1 and B_1 and substitution into the general solution gives

$$X = \bar{L} \sin(s_1 + \tfrac{1}{2}\lambda_3 - \tfrac{1}{2}\lambda_3 u^2) + \frac{\lambda_0}{2\lambda_6} \left[\cos(S_2 + \tfrac{1}{2}\lambda_3 u^2) - \cos \gamma\right] + \frac{\lambda_2}{\lambda_3} \left[1 - \cos \tfrac{1}{2}\lambda_3 (1 - u^2)\right] \qquad (252)$$

$$Y = \bar{L} \cos (S_1 + \tfrac{1}{2}\lambda_3 - \tfrac{1}{2}\lambda_3 u^2) - \frac{\lambda_0}{2\lambda_6} \left[\sin (S_2 + \tfrac{1}{2}\lambda_3 - \tfrac{1}{2}\lambda_3 u^2) - \sin \gamma\right] + \frac{\lambda_2}{\lambda_3} \sin \tfrac{1}{2}\lambda_3 (1-u^2) \qquad (253)$$

It was verified that the differential equations for X and Y and their respective boundary conditions are satisfied.

The transformed differential equations for ν_1 and ν_2 are

$$\frac{d\nu_1}{du} = -\lambda_3 u \nu_2$$

$$\frac{d\nu_2}{du} = \lambda_3 u \nu_1$$

These two differential equations have the same form as Eqs (242) and (243). Therefore, their solutions are

$$\nu_1 = A_2 \sin \tfrac{1}{2}\lambda_3 u^2 + B_2 \cos \tfrac{1}{2}\lambda_3 u^2$$

$$v_2 = -A_2 \cos \tfrac{1}{2} \lambda_3 u^2 + B_2 \sin \tfrac{1}{2} \lambda_3 u^2$$

Substitution of the boundary conditions determines the constants A_2 and B_2. Thus the solutions for v_1 and v_2 are

$$v_1 = \sin (S_1 + \tfrac{1}{2} \lambda_3 - \tfrac{1}{2} \lambda_3 u^2) \tag{254}$$

$$v_2 = \cos (S_1 + \tfrac{1}{2} \lambda_3 - \tfrac{1}{2} \lambda_3 u^2) \tag{255}$$

Both the boundary conditions and differential equations are satisfied by Eqs (254) and (255).

The transformed differential equations for v_3 is

$$\frac{dv_3}{du} = -\frac{\alpha_1 V}{C_{T_P}} (v_1 \cos \gamma - v_2 \sin \gamma)$$

Substituting v, v_1, and v_2 gives

$$\frac{dv_3}{du} = -(\lambda_1 + \lambda_0 u) \sin (S_1 + \tfrac{1}{2} \lambda_3 - \lambda_4 - \lambda_5 u - \lambda_6 u^2)$$

Substitution of Eq (251) gives

$$\frac{dv_3}{du} = -\frac{\lambda_0}{2\lambda_6} (\lambda_5 + 2\lambda_6 u) \sin (S_1 + \tfrac{1}{2} \lambda_3 - \lambda_4 - \lambda_5 u - \lambda_6 u^2)$$

$$= \frac{\lambda_0}{2\lambda_6} \frac{d}{du} (S_1 + \tfrac{1}{2} \lambda_3 - \lambda_4 - \lambda_5 u - \lambda_6 u^2) \sin (S_1 + \tfrac{1}{2} \lambda_3 - \lambda_4 - \lambda_5 u - \lambda_6 u^2)$$

This equation is integrable

$$v_3 = \frac{\lambda_0}{2\lambda_6} [\cos (S_1 + \tfrac{1}{2} \lambda_3 - \lambda_4 - \lambda_5 - \lambda_6) - \cos (S_1 + \tfrac{1}{2} \lambda_3 - \lambda_4 - \lambda_5 u - \lambda_6 u^2)] \tag{256}$$

It is easily verified that v_3 satisfies the differential equation and boundary condition.

The transformed differential equation for v_5 is

$$\frac{dv_5}{du} = -\frac{\alpha_1}{C_{Tp}} (v_1 \sin\gamma + v_2 \cos\gamma) - \frac{C_4}{C_{Tp}} v_3$$

Substitution for v_1, v_2, and v_3 gives

$$\frac{dv_5}{du} = -\lambda_2 \cos(S_1 + \tfrac{1}{2}\lambda_3 - \tfrac{1}{2}\lambda_3 u^2 - \gamma) - \frac{\lambda_0}{2\lambda_6}\frac{C_4}{C_{Tp}}[\cos(S_1 + \tfrac{1}{2}\lambda_3 - \lambda_4 - \lambda_5 - \lambda_6) - \cos(S_1 + \tfrac{1}{2}\lambda_3 - \lambda_4 - \lambda_5 u - \lambda_6 u^2)]$$

Since

$$\frac{\lambda_0}{2\lambda_6}\frac{C_4}{C_{Tp}} = \lambda_2$$

and

$$S_1 + \tfrac{1}{2}\lambda_3 - \tfrac{1}{2}\lambda_3 u^2 - \gamma = S_1 + \tfrac{1}{2}\lambda_3 - \lambda_4 - \lambda_5 u - \lambda_6 u^2$$

dv_5/du reduces to

$$\frac{dv_5}{du} = -\lambda_2 \cos(S_1 + \tfrac{1}{2}\lambda_3 - \lambda_6 - \lambda_7 - \lambda_8)$$

Integration gives

$$v_5 = -\lambda_2 (u-1) \cos(S_1 + \tfrac{1}{2}\lambda_3 - \lambda_6 - \lambda_7 - \lambda_8) \qquad (257)$$

which satisfies the differential equation and boundary condition.

In order to integrate dv_6/du we need B. The relation for B can be obtained either by substitution of X, Y, v_1, v_2, and v_3 into Eq (174) or by integration of dB/du. Since

$$B' = \alpha_1 v_1 u$$

$$\frac{dB}{du} = -\lambda_2 u \sin (S_1 + \tfrac{1}{2}\lambda_3 - \tfrac{1}{2}\lambda_3 u^2)$$

This equation is integrable

$$B = -\frac{\lambda_2}{\lambda_3}\left[\cos (S_1 + \tfrac{1}{2}\lambda_3 - \tfrac{1}{2}\lambda_3 u^2) - \cos S_1\right] \qquad (258)$$

Substitution into the transformed differential equation for v_6 gives

$$\frac{dv_6}{du} = \lambda_2 \cos (S_1 + \tfrac{1}{2}\lambda_3 - \tfrac{1}{2}\lambda_3 u^2) - \frac{\alpha_1 C_5}{\lambda_3 C_{T_P}^2}\left[\cos (S_1 + \tfrac{1}{2}\lambda_3 - \tfrac{1}{2}\lambda_3 u^2) - \cos S_1\right]$$

Since

$$\frac{\alpha_1 C_5}{\lambda_3 C_{T_P}^2} = \lambda_2$$

$$\frac{dv_6}{du} = \lambda_2 \cos S_1$$

this integrates to

$$v_6 = \lambda_2 (u-1) \cos S_1 \qquad (259)$$

Consequently, the assumptions that u' and v' are constants have led to an analytic solution. It was verified that Eqs (237),

(238), (239), (252), (253), (254), (255), (256), (257), and (259) satisfy Eqs (227) through (236). Also, all boundary conditions are satisfied.

Before determining the relationship between capture range and parameters in the problem, some comments are in order concerning the optimal controls. On the right barrier between $s_2 = 0$ and $s_2 = s^*$ it was derived in Eqs (227) through (236) that

$$C_{T_E} = \text{MAX } C_{T_E}$$

$$C_{T_P} = \text{MAX } C_{T_P}$$

$$\phi_E^* = -\pi/2$$

$$\delta_2^* = -\pi/2$$

$$n_E^* = \text{MAX } n_E$$

$$n_P^* = \text{MAX } n_P$$

It will be verified that the analytic solution yields the previous optimal controls. Clearly n_E^* and n_P^* are satisfied since $\alpha_3 = 0$ in Eq (178) and $\alpha_2 = 0$ in Eq (183). According to Eq (237) $u \leq 1$ if $C_{T_P} > 0$. Consequently, from Eqs (257) and (259), ν_5 and ν_6 do not change sign along a trajectory emanating on the terminal surface. It follows that C_{T_P} and C_{T_E} do not change along a trajectory. Furthermore, on the right barrier in the range $0 < s_2 < \pi$, $\nu_6 < 0$ and $\nu_5 \geq 0$, thus $C_{T_P} = \text{MAX } C_{T_P}$ and $C_{T_E} = \text{MAX } C_{T_E}$. From Eq (256)

$$S_1 + \tfrac{1}{2}\lambda_3 - \lambda_4 - \lambda_5 - \lambda_6 < S_1 + \tfrac{1}{2}\lambda_3 - \lambda_4 - \lambda_5 u - \lambda_6 u^2$$

if $0 < u < 1$. Thus ν_3 does not change sign between $s_2 = 0$ and $s_2 = s^*$ on the right barrier. This substantiates that $\phi_E^* = -\pi/2$ in this range. A similar argument using Eq (258) verifies that B does not change sign and therefore $\delta_2^* = -\pi/2$ everywhere on the right barrier.

The necessary conditions under which the two barriers graze but do not intercept in the $\gamma = 0$ plane will be derived next.

Barrier Closure Conditions

Recall that the intercept between the two barriers and the $\gamma = 0$ plane are symmetrical about the Y-axis. Barrier closure corresponds to the two barriers being tangent to each other in the $\gamma = 0$ plane. Attention will be focused on the right barrier in light of the symmetry. Let $\bar{\beta}$ be defined as the time that the trajectory emanating on the terminal surface reaches the $\gamma = 0$ plane. Then the necessary conditions are

$$\gamma(\bar{\beta}) = 0 \tag{260}$$

$$\nu_2(\bar{\beta}) = 0 \tag{261}$$

$$X(\bar{\beta}) = 0 \tag{262}$$

In addition the relation for the boundary of the usable part on the terminal surface must be satisfied. The necessary condition, Eq (200), can be rewritten as

$$\tan s_1 = \frac{1 - \epsilon \cos s_2}{\epsilon \sin s_2} \tag{263}$$

This is the equation for the boundary of the usable part on the terminal surface. Let $\bar{u}$ be defined by

$$\bar{u} = 1 - C_{T_p} \bar{\beta} \tag{264}$$

Then Eqs (260) and (261) along with Eqs (250) and (255) give

$$\lambda_4 + \lambda_5 \bar{u} + (\lambda_6 - \tfrac{1}{2}\lambda_3)\bar{u}^{-2} = 0 \tag{265}$$

$$s_1 + \tfrac{1}{2}\lambda_3 - \tfrac{1}{2}\lambda_3 \bar{u}^{-2} = 0 \tag{266}$$

Eliminating the $\bar{u}^{-2}$ terms in Eqs (265) and (266) gives a relation between s_1, s_2, and $\bar{u}$

$$s_1 = \Lambda_1 s_2 + \Lambda_2 + \frac{\Pi}{2} \tag{267}$$

where

$$\Lambda_0 = \frac{1}{2C_{T_p}(C_4C - C_5)} \left\{ [C_4(\epsilon - C)]^2 - (C_4\epsilon - C_5)^2 \right\}$$

$$\Lambda_1 = \frac{\tfrac{1}{2}\lambda_3}{\tfrac{1}{2}\lambda_3 - \lambda_6}$$

$$\Lambda_2 = \Lambda_1(\Lambda_0 + \lambda_5 \bar{u}) - \tfrac{1}{2}\lambda_3$$

Substituting Eq (267) into the left side of Eq (263) gives

$$\epsilon \sin(s_2 - \Lambda_1 s_2 - \Lambda_2) = -\sin(\Lambda_1 s_2 + \Lambda_2) \tag{268}$$

Since

$$\lambda_4 = s_2 + \Lambda_0$$

substitution into Eq (265) and solving for s_2 gives

$$s_2 = -\bigwedge_0 - \lambda_5\bar{u} - (\alpha_6 - \tfrac{1}{2}\lambda_3)\,\bar{u}^2 \qquad (269)$$

Substituting s_2 into Eq (268) results in an expression for the unknown $\bar{u}$. Rewrite Eq (268) as follows

$$F(\bar{u}) = \epsilon \sin(s_2 - \bigwedge_1 s_2 - \bigwedge_2) + \sin(\bigwedge_1 s_2 + \bigwedge_2) \qquad (270)$$

The solution of Eq (269) subject to $0 < \bar{u} < 1$ is the desired solution. This value substituted into Eq (269) gives s_2. Since $\gamma = 0$, Eqs (261) and (252) supply information for computing the capture range, namely

$$\bar{L} = \frac{\lambda_0}{2\lambda_6}\left[1 - \cos(s_2 + \tfrac{1}{2}\lambda_3 - \tfrac{1}{2}\lambda_3 u^2)\right] - \frac{\lambda_2}{\lambda_3}\left[1-\cos\tfrac{1}{2}\lambda_3(1-u^2)\right] \qquad (271)$$

An iterative approach is required for solving Eq (270). The approach employed here is to decrease $\bar{u}$ until Eq (270) is satisfied or $\bar{u} = 0$. The former leads to a solution for $\bar{L} > 0$. The latter is interpreted as $\bar{L} = 0$ or the solution results from trajectories emanating on the singular arc $\phi = 0$. The latter is not solved in this problem; the reason will be discussed later.

Having determined an analytic solution to the differential equations, we now turn our attention to deriving the relationship between capture range and the parameters in the problem. For the first example a constant speed evader, $C_{T_E} = 0$, is considered. Both pursuer and evader have equal wing loadings, W/S, of fifty pounds per square foot. The corner velocity for both is 1000 feet per second.

The altitude at which the engagement takes place is 20,000 feet. The pursuer's speed on the terminal surface is 800 feet per second which is less than the corner velocity. The remaining parameters are C_{T_P} and R_P/R_E. The following combinations will be considered in determining the capture range:

C_{T_P}	R_P/R_E
-.1	1.5
0	1.5
.1	1.5
.11	1.5
.1	1.35
.11	1.35

A value of C_{T_P} = .1 or .11 is representative of a high performance fighter. A value of C_{T_P} = -.1 is characteristic of a current fighter. The values of 1.35 and 1.5 for R_P/R_E fall within the turning performance capabilities of current and proposed fighter aircraft. The numerical results are displayed in Figure 26 as a function of V_E/V_P evaluated at time $\bar{\beta}$ which is the time that the barriers graze each other in the γ = 0 plane. The case C_{T_P} = 0 corresponds to the solution to Problem II. The agreement with the results of Problem II is excellent. The data in Figure 26 clearly shows an improvement from the pursuer's standpoint if either or both C_{T_P} is increased and R_P/R_E is decreased.

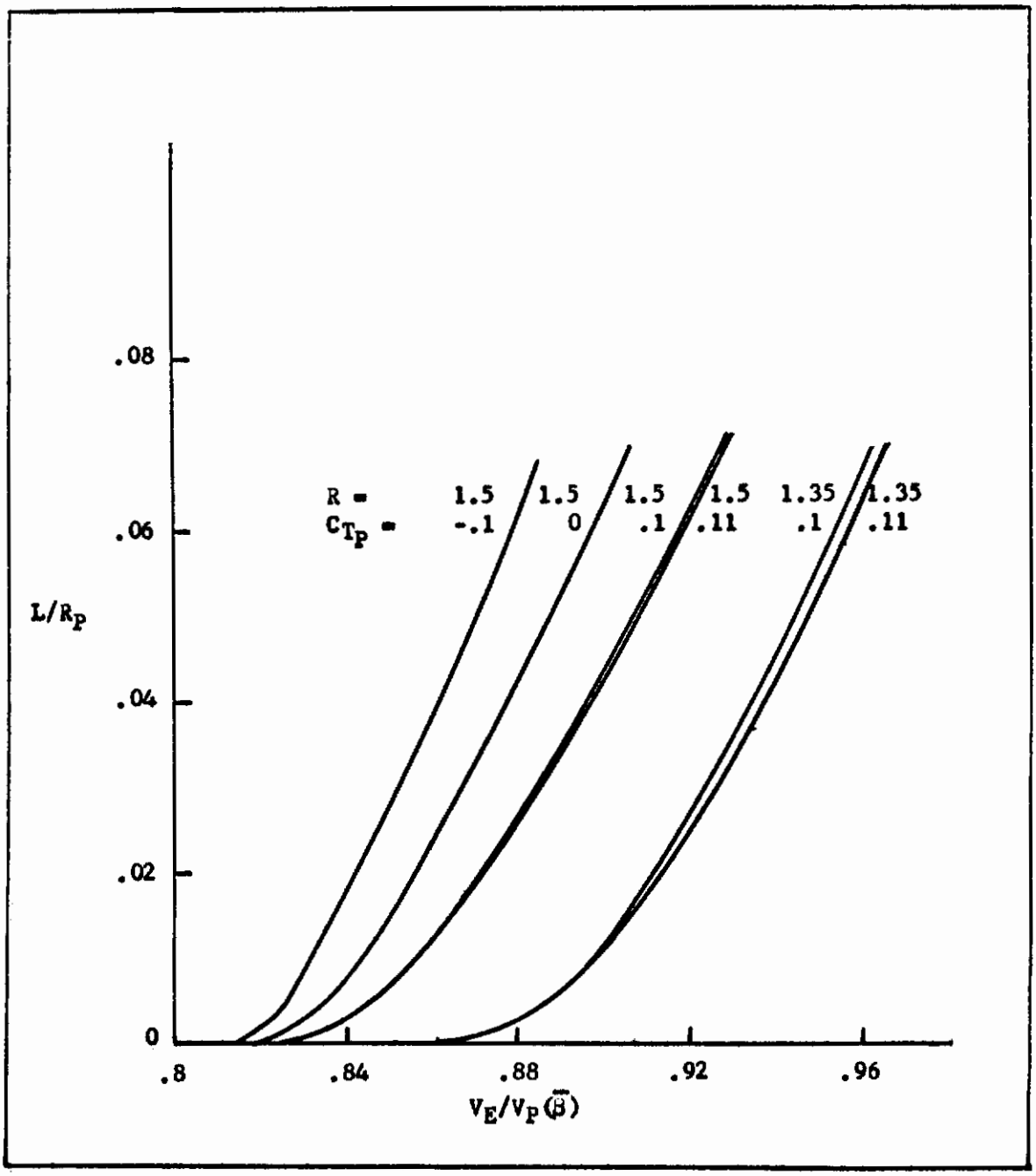

Fig. 26.--Problem III Capture Range, $C_{T_E} = 0$

For the second example the only change is that $C_{T_E} = .1$. The results are presented in Figure 27. The case $R = 1.5$, $C_{T_P} = 0$ falls between $R = 1.5$, $C_{T_P} = .1$ and $R = 1.5$, $C_{T_P} = .11$. The trends are the same as the trend for $C_{T_E} = 0$.

A comment is in order relative to the constant acceleration assumption for the pursuer and evader. Based upon the results obtained in Figures 26 and 27, the change in u or v was generally less than five per cent. Thus for the values of C_{T_P} and C_{T_E} considered here, the assumption appears well justified. Whether or not this holds for accelerations larger than those considered here remains to be determined.

Another comment is offered relative to the utility of the analytical solution derived in this research. The solution provides a method for assessing the outcome of the terminal part of an air-to-air engagement. For given evader and pursuer performance characteristics, the implementation of the trajectory solution determines the capture range under optimal control by both players. If the capture range exceeds the weapon lethal range, the evader escapes. Otherwise, the evader is subject to being destroyed. In addition, the trajectory solution can be employed to determine the performance characteristics of the pursuer necessary for capturing the evader. This is similar to designing a new fighter for engaging and defeating a given enemy. Consequently, the technology developed here can be used for designing new fighters.

We consider next the sensitivity of the capture range to changes in $V_E/V_P(\bar{\Theta})$, R, and C_{T_P}.

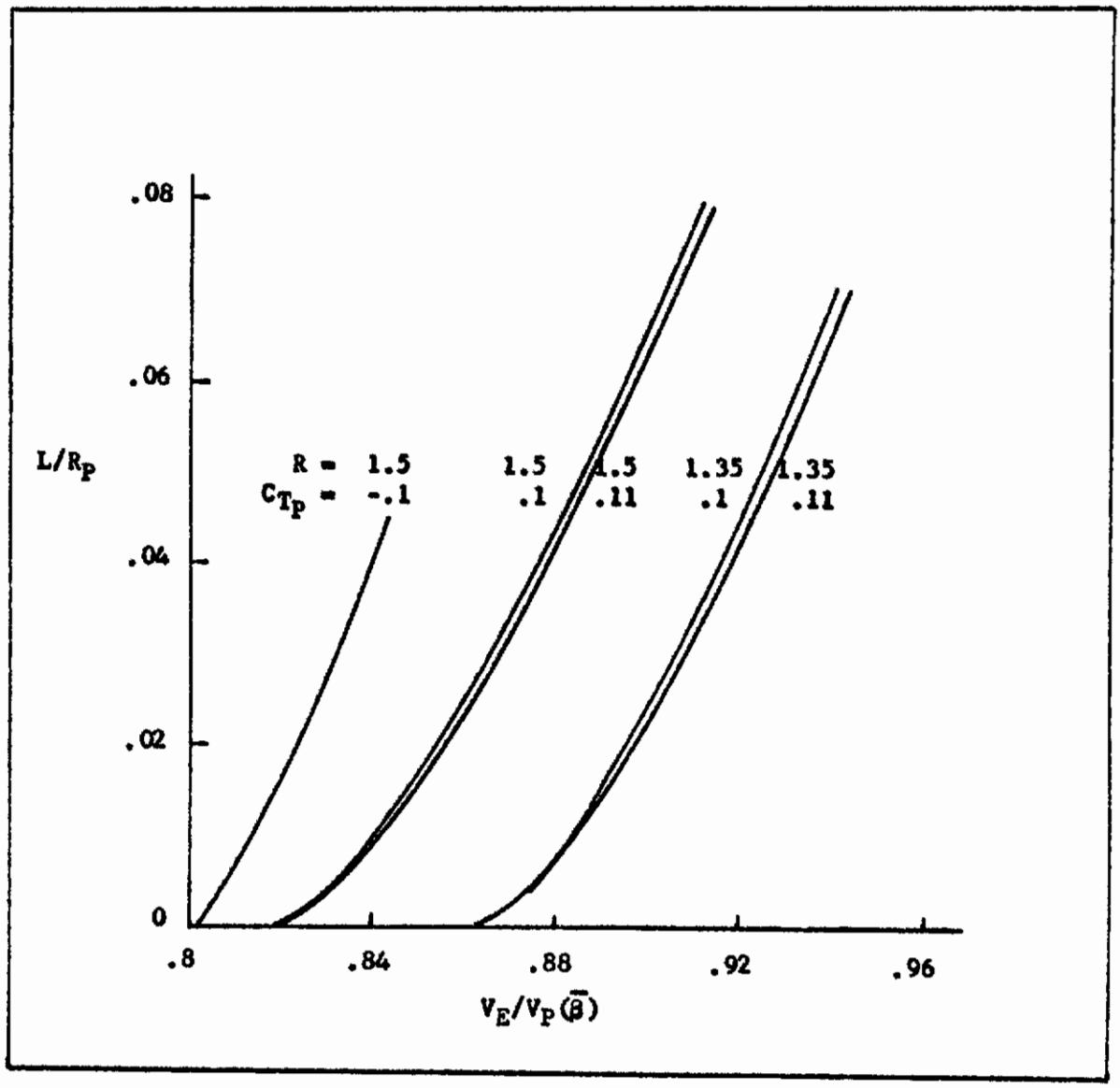

Fig. 27.--Problem III Capture Range, $C_{T_E} = 0.1$

Capture Range Sensitivity

The capture range L has the following functional form

$$L = \bar{L}\,(\bar{\epsilon},\ C_{T_P},\ R)\ R_P$$

where

$$\bar{\epsilon} = V_E/V_P(\bar{\beta}),\quad R = R_P(0)/R_E(0) \tag{272}$$

The differential of L is

$$dL = R_P \frac{\partial \bar{L}}{\partial V_P}\, dV_P + R_P \frac{\partial \bar{L}}{\partial C_{T_P}}\, dC_{T_P} + \left(\frac{\partial \bar{L}}{\partial R} \frac{\partial R}{\partial R_P} R_P + \bar{L} \right) dR_P \tag{273}$$

If $V_P < V_C$ which is characteristic of air-to-air combat, then

$$R_P = \frac{2\ W/S}{g\ \rho\ (\text{MAX}\ C_L)} \tag{274}$$

Substitution of Eqs (272) and (274) into Eq (273) gives

$$\frac{dL}{R_P} = -\bar{\epsilon} \frac{\partial \bar{L}}{\partial \bar{\epsilon}} \frac{dV_P}{V_P} + \frac{\partial \bar{L}}{\partial C_{T_P}}\, dC_{T_P} + \left(\bar{L} + R \frac{\partial \bar{L}}{\partial R}\right)\left(\frac{dW/S}{W/S} - \frac{d\ \text{MAX}\ C_L}{\text{MAX}\ C_L} \right) \tag{275}$$

In terms of sensitivity parameters, dL/R_P can be written as

$$\frac{dL}{R_P} = S_{V_P} \frac{dV_P}{V_P} + S_{C_{T_P}}\, dC_{T_P} + S_{W/S} \frac{dW/S}{W/S} + S_{\text{MAX}\ C_L} \frac{d\ \text{MAX}\ C_L}{\text{MAX}\ C_L}$$

where

$$S_{V_P} = -\bar{\epsilon} \frac{\partial \bar{L}}{\partial \bar{\epsilon}}$$

$$S_{C_{T_P}} = \frac{\partial \bar{L}}{\partial C_{T_P}}$$

$$S_{W/S} = - S_{MAX\ C_L} = \bar{L} + R \frac{\partial \bar{L}}{\partial R}$$

For $\bar{\epsilon} = 0.9$, $R = 1.5$, and $C_{T_P} = .1$ the sensitivity parameters are

$$S_{V_P} = 0.865$$

$$S_{C_{T_P}} = -0.200$$

$$S_{W/S} = -S_{MAX\ C_L} = 0.365$$

The data for determining the sensitivity coefficients were obtained by numerical differentiation of the data in Figure 26. As in Problems I and II, the biggest improvement in L results from an increase in V_P. A one per cent increase (decrease) in MAX C_L (W/S) results in a bigger improvement in L relative to the improvement realized by a one per cent increase in C_{T_P}.

We can make some direct comparisons of the capture range from Problems II and III. The solution for Problem II corresponds to $C_{T_P} = 0$. The pursuer's characteristics are W/S = 50 pounds per square foot, altitude is 20,000 feet, and his maximum allowable load factor is 4. This results in a minimum turning radius of 7750 feet. The dimensional capture ranges are as follows for $\bar{\epsilon} = 0.9$ and $C_{T_E} = 0$:

R_P/R_E	C_{T_P}	L(feet)
1.5	0	490
1.5	.1	334
1.5	.11	318
1.35	0	220
1.35	.1	86
1.35	.11	81

All combinations are within lethal gun range.

Although only a small combination of performance characteristics was considered, it is straightforward as far as determining the capture range to other performance characteristics. Thus, given any set of evader performance characteristics, the capture range can be computed as a function of the pursuer's characteristics. The solution for the tributaries from the singular $\phi_E = 0$ was not determined. However, the data of Figures 26 and 27 generally cover the speeds and accelerations of interest.

Problem III Conclusions

The original Problem III consisted of six state differential equations. Introduction of the assumption that the motion was planar, i.e., $\delta_1 = 0$, reduced the number to five. Assuming constant accelerations, $u' = -C_{T_P}$ and $v' = -C_{T_E}$, led to a set of differential equations that were analytically integrable. The solution defined the trajectories emanating on the barrier of the usable part and the components of the vector normal to the barrier. The barrier closure conditions were established and the capture range relation $\bar{L} = L/R_P$ was determined for selected combinations of the parameters ϵ, R_P/R_E, C_{T_P}, and C_{T_E}. For the particular combinations examined, it was demonstrated that significant decreases in the capture range occurred if the pursuer accelerated and decreased his turning radius.

The capture range sensitivity analysis demonstrated that for the performance characteristics examined, the biggest improvement in the capture range resulted from an increase in the pursuer's speed. A one per cent increase (decrease) in MAX C_L (W/S) resulted in a

bigger improvement in the capture range relative to the improvement realized by a one per cent increase in C_{T_P}.

The utility of the barrier solution is that it can be used for determining the capture range as a function of the pursuer and evader performance characteristics. In addition, the implementation of the trajectory solutions provides a means for determining fighter characteristics necessary to defeat a known enemy aircraft during the terminal part of an air-to-air combat engagement. In particular, the following characteristics can be assessed: thrust to weight ratio, weight to reference area ratio, maximum lift coefficient, and maximum normal acceleration.

SECTION VII

CONCLUSIONS

In this research the barrier theory of differential games was first presented and then applied to three pursuit-evasion problems approximating air-to-air combat engagements. The emphasis was on the terminal part of the engagement where armament like machine guns is the primary weapon. The objective of this research was the determination of the relationship between the capture range and the performance parameters in the problem. The capture range which in general is a function of the angle-off as well as the performance parameters corresponds to the minimum separation between the pursuer and evader during the course of the game. Whether or not the pursuer kills the evader is dependent upon how the capture range relates to the weapon envelope. If the capture range exceeds or falls outside the weapon envelope, then the pursuer can not kill the evader. If, however, the capture range falls on the boundary or within the weapon envelope, then the pursuer stands a good chance of destroying the evader.

The barrier is a surface within the playing space which is never crossed during optimal play. If the barrier is closed, then it separates the playing space into two parts - a capture set and an escape set. The outcome is neutral for initial states on the barrier

in that the terminal surface is only grazed. In other words, the closed barrier does not penetrate the terminal surface. This requirement leads to the establishment of the necessary conditions on the barrier. Consequently, the barrier solution for each particular problem provides the information for deriving the relationship for the capture range.

The three problems were formulated in a reduced coordinate frame. In this type of coordinate frame the evader's position and direction are measured relative to the pursuer's speed, location, and direction. The reason for using this coordinate frame is that a fighter's weapon effectiveness is measured in a reduced coordinate frame.

The first problem consisted of two differential equations representing the position of the evader relative to the pursuer's position and direction. The controls were the turning rate for the pursuer and for the evader, the direction of his velocity vector. The evader could change directions instantaneously. The speed ratio V_E/V_P was handled parametrically subject to the ratios being less than one. The relationship between the nondimensional capture range, $\bar{L} = L/R_P$, and the speed ratio, $\epsilon = V_E/V_P$, was originally determined by Isaacs for the natural barrier. In this research the angle-off constraint θ was addressed and the artificial barrier solution derived. It was proven that the natural and artificial barriers are coincident. As a consequence, the artificial barrier capture range was easily determined from the solution for the natural barrier. The sensitivity

analysis demonstrated that the pursuer should fly as close as possible to the corner velocity. The numerical results were that for a given speed ratio, the nondimensional capture range increased with decreasing angle-off. Also, for a given angle-off, the capture range increased with increasing speed ratio. In addition, the pursuer must have a speed advantage of at least twice the evader's speed in order to achieve a kill using guns.

The second problem consisted of three differential equations and one control for each player. The differential equations represented the position and direction of the evader's velocity vector measured relative to the pursuer's position and the direction of his velocity vector. The difference between this problem and the first problem was that the evader could not change directions instantaneously. Thus the angular difference between the directions of the two velocity vectors was a state variable whereas it was the evader's control variable in the first problem. Both pursuer and evader were constrained by their respective minimum radius of turn. The speeds were constant with the pursuer's speed greater than the evader's speed.

Isaacs originally derived the natural barrier trajectory solution. Miller determined the natural barrier capture range as a function of the speed ratio and turning radius ratio. In this research the angle-off constraint θ was introduced and the artificial barrier capture range relationship derived. Unlike the first problem, the closed artificial barrier and closed natural barrier are not coincident. Consequently, the artificial barrier capture range could not be determined from the natural barrier solution.

The relationship for the artificial barrier capture range as a function of the parameters ϵ, $R = R_P/R_E$, and θ was similar to the solution to the first problem. The difference was that the nondimensional capture range decreased as R decreased. If R_P decreases for fixed R_E or R_E increases for fixed R_P then R decreases. It was proven that if the pursuer's maximum normal acceleration equaled or exceeded the evader's maximum normal acceleration, then the capture range was zero. Also, the capture range was zero if the pursuer's minimum turning radius was less than or equal to the evader's minimum radius of turn.

The numerical results for the nondimensional capture range showed that for large values of R ($\geq$ 5), the capture range was sensitive to the value of the angle-off. Contrarily, when the ratio of the turning radii was less than 1.5, the capture range was relatively insensitive to the value of the angle-off. The sensitivity analysis indicated that if the speed ratio was 0.9 and the turning radius ratio less than or equal to 1.5, then the pursuer should fly as fast as possible. This is different from the first problem where the pursuer should fly as close as possible to the corner velocity.

The formulation of the third problem resulted in six state differential equations and three controls per player. This formulation was a reasonable formulation of the terminal portion of an air-to-air combat engagement. The six variables defined the position, the direction, and the magnitude of the velocity vector of the evader relative to the position, direction, and magnitude of the pursuer's velocity vector. The controls were the throttle setting for engine

thrust, aerodynamic load factor or lift coefficient, and the angular displacement that defines the direction of aerodynamic lift vector. It was demonstrated that if the velocity vectors were coplanar at the beginning of the engagement, then they remained coplanar thereafter under optimal control by both players. This assumption applied for the remainder of the study of the third problem. Additional assumptions were then introduced. First, the accelerations along the velocity vectors were assumed to be constant. Numerical results showed that the speeds changed by five per cent or less, hence the approximation was considered to be justified. The final assumption was that the difference between the artificial and natural barrier capture range relationship due to the angle-off constraint was negligible. The justification for this assumption was based upon the results of the second problem and the observation that the change in the speed was small. Thus for the speeds and minimum turning radii of interest for air-to-air combat, this assumption also appeared to be justified.

An analytic solution for the natural barrier was obtained subject to the assumptions regarding coplanar velocities, constant accelerations, and no angle-off constraint. The relationship for the nondimensional capture range followed a pattern similar to that for the first two problems. Increasing acceleration along the pursuer's velocity vector resulted in a decrease in the capture range. Consequently, an improvement in turning performance (decreasing minimum radius of turn) and acceleration potential gives a decrease in the capture range. The sensitivity analysis showed that for the sample

performance parameters that were considered, a decrease in wing loading or an increase in maximum lift coefficient was more significant in decreasing the capture range when measured relative to the improvement gained by increasing only the pursuer's acceleration.

Uncertainty has existed up to the present time relative to the derivation of the necessary performance characteristics for new fighter systems engaging a known enemy aircraft. In other words, even though the performance characteristics of an enemy aircraft were known, there was no sound technical basis for deriving new system performance characteristics. The solution to the third problem offers potential for being able to define such characteristics as wing loading, thrust to weight ratio, and the relation between maximum load factor and speed for the terminal part of the engagement. The solution can be employed for situations where the new system is either the pursuer or evader. If the new system is the evader, then he must be able to stay outside the enemy's weapon envelope. The opposite holds if he is the pursuer. Thus the utility of this solution will be in assessing performance characteristics for the terminal part of air-to-air combat engagements.

APPENDIX A

DERIVATION OF THE DIFFERENTIAL STATE EQUATIONS

Problem I. Differential Equations of State

Refer to the geometry in Figure 7 for Problems I and II. An x y coordinate frame is attached to the pursuer with the y axis co-linear with the pursuer's velocity vector. This coordinate frame translates and rotates with time. Let $\bar{X}_P$, $\bar{X}_E$, and $\bar{X}$ denote vectors where $\bar{X}_P$ and $\bar{X}_E$ are measured relative to the fixed coordinate frame X'Y' and $\bar{X}$ is the relative position of E as seen by P. By vector addition

$$\bar{X}_E = \bar{X}_P + \bar{X} \tag{A-1}$$

Differentiating gives

$$\dot{\bar{X}}_E = \dot{\bar{X}}_P + \dot{\bar{X}} + \bar{\omega} \times \bar{X} \tag{A-2}$$

where $\dot{\bar{X}}$ is the relative velocity of E as observed by P and $\bar{\omega}$ is the angular velocity vector of the x y coordinate frame. Since $\bar{\omega}$ is perpendicular to the x y and (X'Y') coordinate plane, let

$$\bar{\omega} = \omega \, \bar{e}_z \tag{A-3}$$

where $\bar{e}_z$ is a unit vector normal to the x y plane. The magnitude of $\bar{\omega}$ is

$$\omega = -\dot{\sigma}_P$$

$$= -\frac{V_P}{R_P}\alpha_P, \qquad -1 \le \alpha_P \le 1 \tag{A-4}$$

Where R_P is the minimum radius of turn for P and α_P is his control. Hard right and left turns correspond to $\alpha_P = 1$ and $\alpha_P = -1$, respectively. The velocities of E and P are

$$\dot{\bar{X}}_E = V_E\,(\bar{e}_x \sin\psi + \bar{e}_y \cos\psi)$$

$$\dot{\bar{X}}_P = V_P\,\bar{e}_y \tag{A-5}$$

where $\bar{e}_x$ and $\bar{e}_y$ are unit vectors along the x and y axes and

$$\psi = \sigma_E - \sigma_P \tag{A-6}$$

Solving Eq (A-2) for $\dot{\bar{X}}$ and then substituting Eqs (A-3), (A-4), and (A-5) gives

$$\dot{\bar{X}} = \dot{\bar{X}}_E - \dot{\bar{X}}_P - \bar{\omega} \times \bar{X}$$

$$= V_E(\bar{e}_x \sin\psi + \bar{e}_y \cos\psi) - V_P\bar{e}_y + \frac{V_P}{R_P}\alpha_P\,\bar{e}_z \times (\bar{e}_x x + \bar{e}_y y)$$

$$= \bar{e}_x\left(V_E \sin\psi - \frac{V_P}{R_P}\alpha_P\, y\right) + \bar{e}_y\left(V_E \cos\psi - V_P + \frac{V_P}{R_P}\alpha_P\, x\right)$$

Equating scalar components yields

$$\dot{x} = V_E \sin\psi - \frac{V_P}{R_P}\alpha_P\, y$$

$$\dot{y} = V_E \cos\psi - V_P + \frac{V_P}{R_P}\alpha_P\, x \tag{A-7}$$

$$-1 \le \alpha_P \le 1$$

P and E controls are α_P and ψ, respectively. Eq (A-7) defines the state differential equations for Problem I.

Problem II. Differential Equations of State

If E's turning performance is constrained by a nonzero radius of turn, as in Problem II, then

$$\dot{\sigma}_E = \frac{V_E}{R_E}\alpha_E, \quad -1 \le \alpha_E \le 1$$

where α_E is E's control. Then from Eq (A-6)

$$\dot{\psi} = \frac{V_E}{R_E}\alpha_E - \frac{V_P}{R_P}\alpha_P$$

Consequently for Problem II, the state differential equations and control constraints are

$$\begin{aligned}
\dot{x} &= V_E \sin\psi - \frac{V_P}{R_P}\alpha_P\, y \\
\dot{y} &= V_E \cos\psi - V_P + \frac{V_P}{R_P}\alpha_P\, x \qquad \text{(A-8)} \\
\dot{\psi} &= \frac{V_E}{R_E}\alpha_E - \frac{V_P}{R_P}\alpha_P \\
&-1 \le \alpha_P \le 1 \\
&-1 \le \alpha_E \le 1
\end{aligned}$$

Problem III. Differential Equations of State

The situation for Problem III is considerably more complicated. The approach here is very similar to that employed by Lynch (4). Figure 10 illustrates some of the variables in the problem. The acceleration components along and normal to $\bar{V}$ are $\bar{a}_V$ and $\bar{a}_N$.

The angular velocity $\bar{\omega}$ is normal to the acceleration components and $\bar{V}$ and is produced by $\bar{a}_N$. The magnitudes of the accelerations are

$$\left|\bar{a}_V\right| = \dot{V} \tag{A-9}$$

$$\left|\bar{a}_N\right| = \frac{V^2}{R}\alpha , \qquad 0 \leq \alpha \leq 1 \tag{A-10}$$

The angular velocity vector of the reduced coordinate frame is

$$\bar{\omega} = \frac{V_P}{R_P}\alpha_P \left(\bar{e}_x \cos \phi_P + \bar{e}_z \sin \phi_P\right) \tag{A-11}$$

where ϕ_P is an angle controlled by the pursuer and defines the orientation of $\bar{\omega}$ in the x z plane.

The evader's velocity is obtained by two angular transformations relative to the x y z reduced coordinate frame. Let σ denote the angle of the first transformation as illustrated in Figure 28. The linear transformation from the x y z coordinate frame to the $x_\sigma y_\sigma z_\sigma$ coordinate frame is

$$\begin{vmatrix} x_\sigma \\ y_\sigma \\ z_\sigma \end{vmatrix} = \begin{vmatrix} \cos\sigma & 0 & \sin\sigma \\ 0 & 1 & 0 \\ -\sin\sigma & 0 & \cos\sigma \end{vmatrix} \begin{vmatrix} x \\ y \\ z \end{vmatrix} \tag{A-12}$$

As a result of this transformation, $\bar{V}_E$ falls in the $x_\sigma y_\sigma$ plane. A rotation about z_σ of angle γ relative to y_σ as illustrated in Figure 29 results in $\bar{V}_E$ falling along y_γ. The transformation from $x_\sigma y_\sigma z_\sigma$ to $x_\gamma y_\gamma z_\gamma$ is defined by

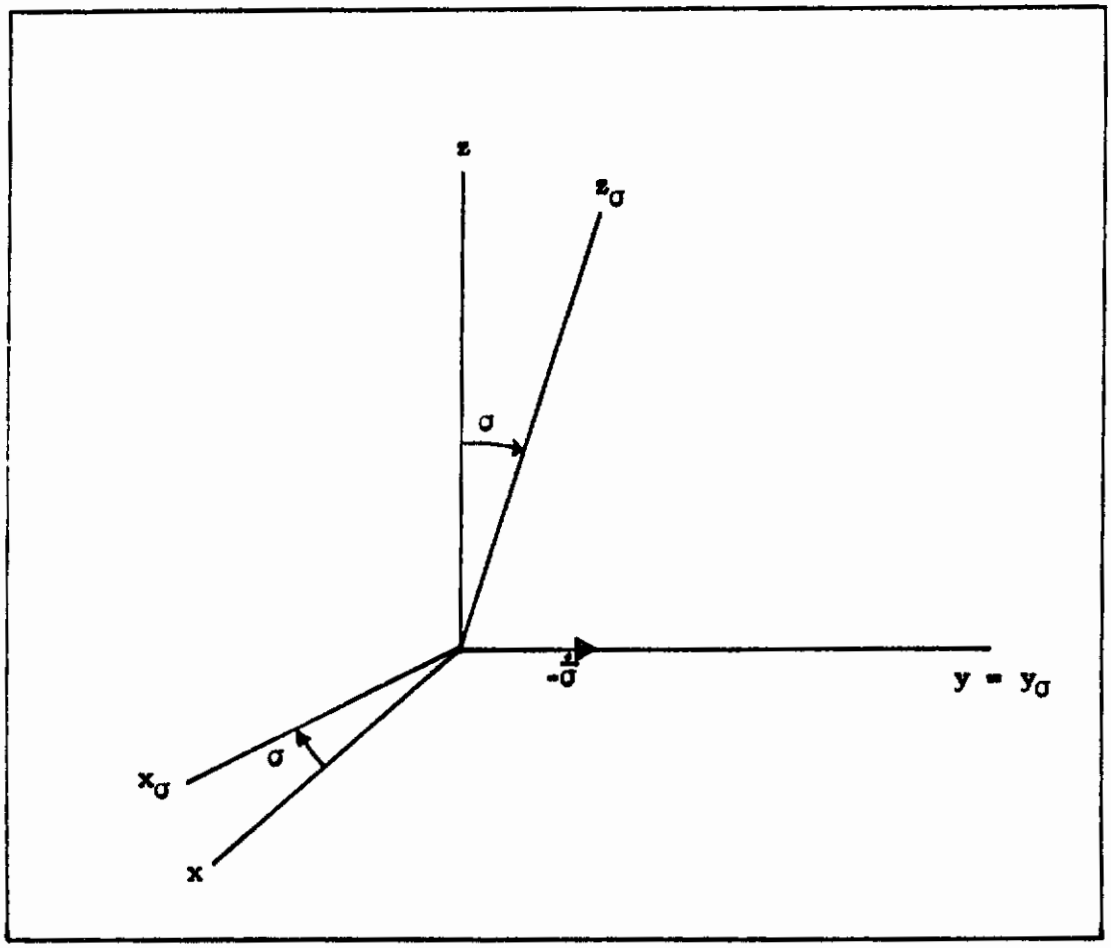

Fig. 28.--The σ Angular Transformation

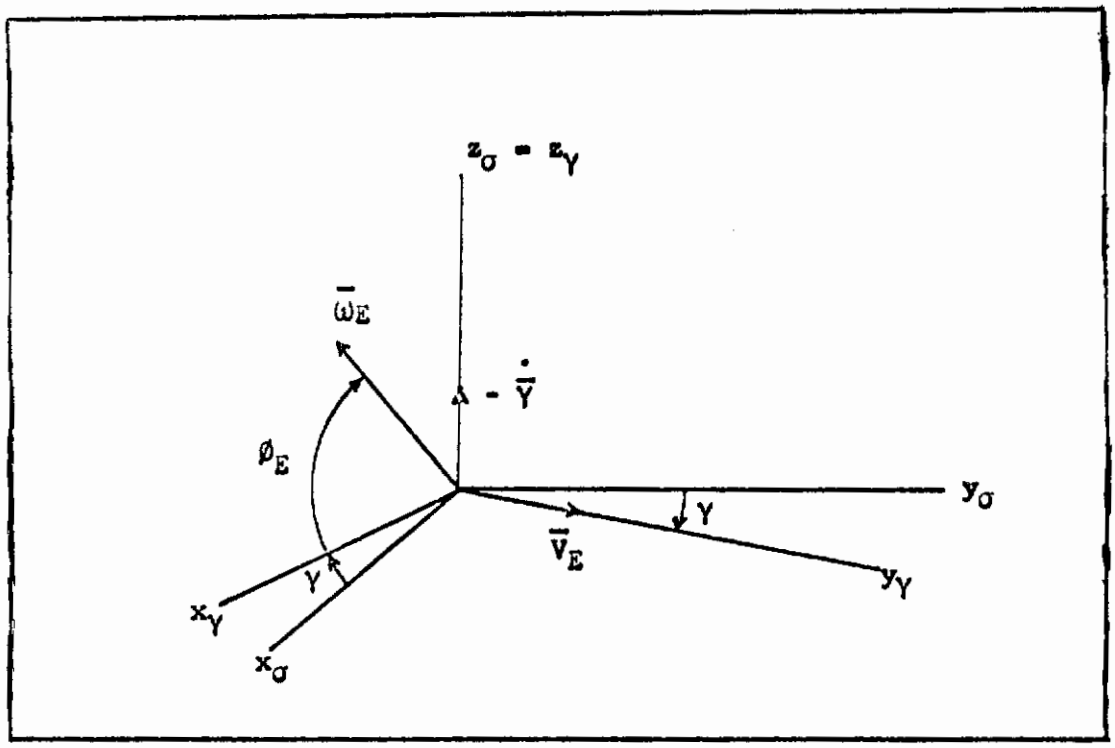

Fig. 29.--The γ Angular Transformation

$$\begin{vmatrix} x_\gamma \\ y_\gamma \\ z_\gamma \end{vmatrix} = \begin{vmatrix} \cos\gamma & -\sin\gamma & 0 \\ \sin\gamma & \cos\gamma & 0 \\ 0 & 0 & 1 \end{vmatrix} \begin{vmatrix} x_\sigma \\ y_\sigma \\ z_\sigma \end{vmatrix} \qquad \text{(A-13)}$$

The velocity vector $\bar{V}_E$ is

$$\bar{V}_E = V_E \bar{e}_{y_\gamma}$$

$$= V_E (\bar{e}_x \sin\gamma \cos\sigma + \bar{e}_y \cos\gamma + \bar{e}_z \sin\gamma \sin\sigma) \qquad \text{(A-14)}$$

Now the evader's angular velocity vector can be written in two different forms; the reason for doing so is to obtain differential state equations for γ and σ. The first form is

$$\bar{\omega}_E = \frac{V_E}{R_E} \alpha_E (\bar{e}_{x_\gamma} \cos\phi_E + \bar{e}_{z_\gamma} \sin\phi_E) \qquad \text{(A-15)}$$

where α_E and ϕ_E are controls available to the evader. The other form for $\bar{\omega}_E$ results from the rotations σ and γ

$$\bar{\omega}_E = \dot{\bar{\sigma}} + \dot{\bar{\gamma}} + \bar{\omega}$$

$$= -\dot{\sigma}\,\bar{e}_y - \dot{\gamma}\,\bar{e}_{z_\sigma} + \bar{\omega} \qquad \text{(A-16)}$$

Eq (A-16) follows from the relative rotations σ and γ in the rotating coordinate frame x y z which is rotating at the angular velocity, $\bar{\omega}$. Substitution of the transformations Eqs (A-12) and (A-13) and Eq (A-11) into Eqs (A-15) and (A-16) gives

$$\bar{\omega}_E = \frac{V_E}{R_E} \alpha_E \left[(\bar{e}_x \cos\gamma \cos\sigma - \bar{e}_y \sin\gamma + \bar{e}_z \cos\gamma \sin\sigma) \cos\phi_E \right.$$

$$\left. + (-\bar{e}_x \sin\sigma + \bar{e}_z \cos\sigma) \sin\phi_E \right] \qquad \text{(A-17)}$$

and

$$\bar{\omega}_E = -\dot{\sigma}\,\bar{e}_y - \dot{\gamma}\,(-\bar{e}_x \sin\sigma + \bar{e}_z \cos\sigma) + \frac{V_P}{R_P}\alpha_P\,(\bar{e}_x \cos\phi_P + \bar{e}_z \sin\phi_P) \qquad \text{(A-18)}$$

Equating components in Eqs (A-17) and (A-18) gives

$$\frac{V_E}{R_E}\alpha_E\,(\cos\gamma\cos\sigma\cos\phi_E - \sin\sigma\sin\phi_E) = \dot{\gamma}\sin\sigma + \frac{V_P}{R_P}\alpha_P\cos\phi_P$$

$$-\frac{V_E}{R_E}\alpha_E\sin\gamma\cos\phi_E = -\dot{\sigma}$$

$$\frac{V_E}{R_E}\alpha_E\,(\cos\gamma\sin\sigma\cos\phi_E + \cos\sigma\sin\phi_E) = -\dot{\gamma}\cos\sigma + \frac{V_P}{R_P}\alpha_P\sin\phi_P$$

Multiplying the first equation by sin σ and the third equation by -cos σ and then adding gives

$$\dot{\gamma} = -\frac{V_E}{R_E}\alpha_E\sin\phi_E + \frac{V_P}{R_P}\alpha_P\sin(\phi_P - \sigma)$$

Eq (A-19) and the equation for $\dot{\sigma}$, namely

$$\dot{\sigma} = \frac{V_E}{R_E}\alpha_E\sin\gamma\cos\phi_E \qquad \text{(A-19)}$$

then provide the state differential equations for defining the evader's velocity vector in the reduced coordinate frame.

Eqs (A-1) and (A-2) still hold, thus solving for relative positional rates gives

$$\dot{\bar{X}} = \bar{V}_E - \bar{V}_P - \bar{\omega} \times \bar{X}$$

Since

$$\bar{X} = X\,\bar{e}_x + y\,\bar{e}_y + z\,\bar{e}_z$$

it follows that

$$\dot{\bar{X}} = V_E(\bar{e}_x \sin\gamma \cos\sigma + \bar{e}_y \cos\gamma + \bar{e}_z \sin\gamma \sin\sigma) - V_P \bar{e}_y$$

$$- \frac{V_P}{R_P} \alpha_P \begin{vmatrix} \bar{e}_x & \bar{e}_y & \bar{e}_z \\ \cos\phi_p & 0 & \sin\phi_p \\ x & y & z \end{vmatrix}$$

$$= \bar{e}_x(V_E \sin\gamma \cos\sigma + \frac{V_P}{R_P} \alpha_P \, y \sin\phi_p)$$

$$+ \bar{e}_y \left[V_E \cos\gamma - V_P - \frac{V_P}{R_P} \alpha_P \, (x \sin\phi_p - z \cos\phi_p)\right]$$

$$+ \bar{e}_z \, (V_E \sin\gamma \sin\sigma - \frac{V_P}{R_P} \alpha_P \, y \cos\phi_p)$$

Equating scalar components gives

$$\dot{x} = V_E \sin\gamma \cos\sigma + \frac{V_P}{R_P} \alpha_P \, y \sin\phi_p$$

$$\dot{y} = V_E \cos\gamma - V_P - \frac{V_P}{R_P} \alpha_P \, (x \sin\phi_p - z \cos\phi_p) \qquad \text{(A-20)}$$

$$\dot{z} = V_E \sin\gamma \sin\sigma - \frac{V_P}{R_P} \alpha_P \, y \cos\phi_p$$

Let Δ denote the angle that the projection of $\bar{x}$ onto the x z plane makes with the x-axis. The angle Δ and the projection r are illustrated in Figure 30. The goal is to replace x and z with r and Δ. Since

$$x = r \cos\Delta$$

$$z = r \sin\Delta$$

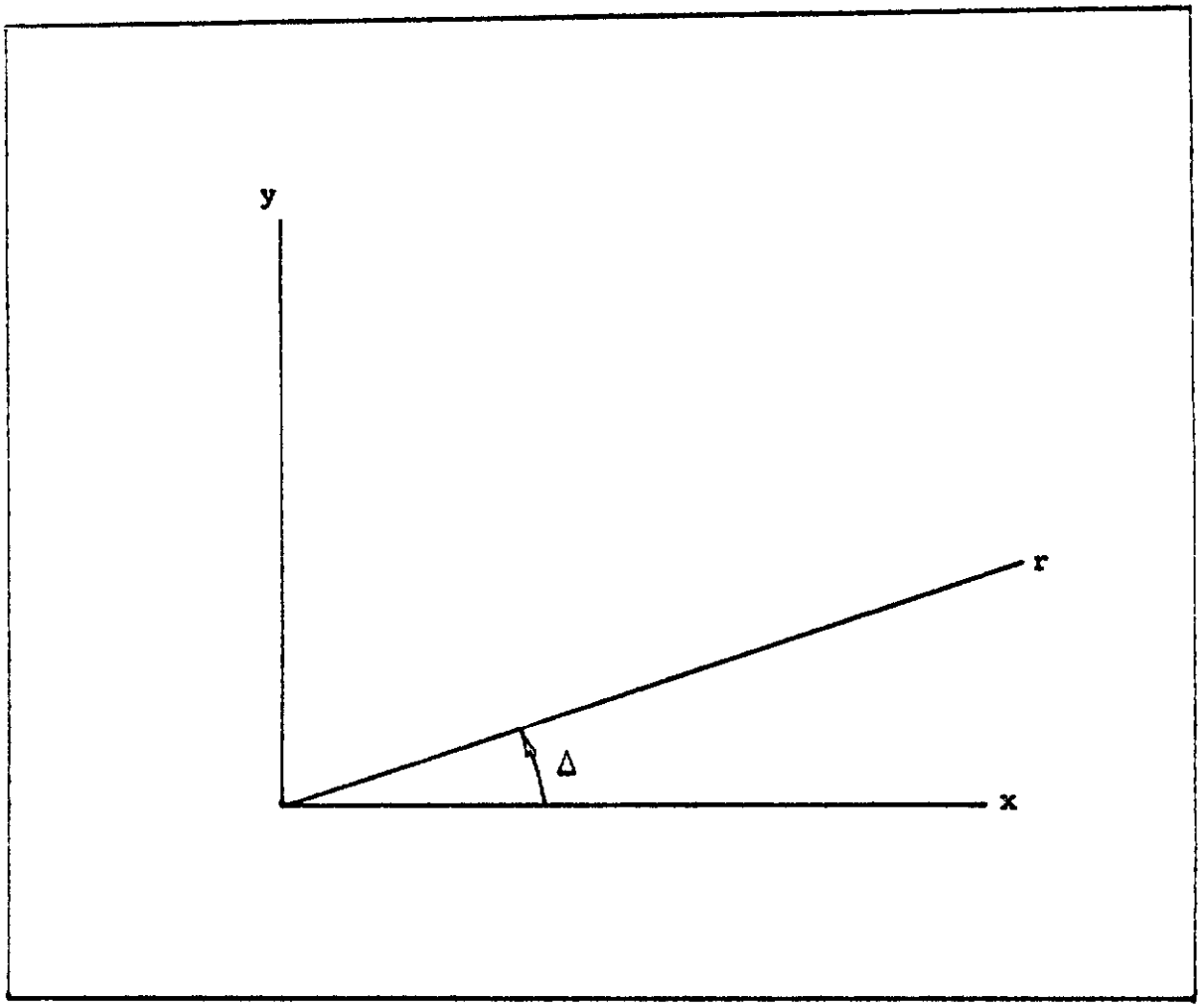

Fig. 30.--The Projection r and Angle Δ

differentiation gives

$$\dot{x} = \dot{r} \cos \Delta - r \dot{\Delta} \sin \Delta$$

$$\dot{z} = \dot{r} \sin \Delta + r \dot{\Delta} \cos \Delta$$

solving for $\dot{r}$ and $r \dot{\Delta}$ gives

$$\dot{r} = \dot{x} \cos \Delta + \dot{z} \sin \Delta$$

$$r \dot{\Delta} = - \dot{x} \sin \Delta + \dot{z} \cos \Delta$$

Substitution of Eq (A-20) gives

$$\begin{aligned} \dot{r} &= V_E \sin \gamma \cos (\sigma - \Delta) + \frac{V_P}{R_P} \alpha_P y \sin (\phi_P - \Delta) \\ r \dot{\Delta} &= V_E \sin \gamma \sin (\sigma - \Delta) - \frac{V_P}{R_P} \alpha_P y \cos (\phi_P - \Delta) \\ \dot{y} &= V_E \cos \gamma - V_P - \frac{V_P}{R_P} \alpha_P r \sin (\phi_P - \Delta) \end{aligned} \qquad \text{(A-21)}$$

Introduce the angular transformations

$$\delta_1 = \sigma - \Delta$$

$$\delta_2 = \phi_P - \Delta$$

Differentiating δ_1 and substituting Eqs (A-19) and (A-21) gives

$$\begin{aligned} \dot{\delta}_1 &= \dot{\sigma} - \dot{\Delta} \\ &= \frac{V_E}{R_E} \alpha_E \sin \gamma \cos \phi_E - \frac{1}{r} (V_E \sin \gamma \sin \delta_1 - \frac{V_P}{R_P} \alpha_P y \cos \delta_2) \end{aligned}$$

The differential equations for r, y, γ, and δ_1, are therefore

$$\begin{aligned}
\dot{r} &= V_E \sin\gamma \cos\delta_1 + \frac{V_P}{R_P}\alpha_P\, y \sin\delta_2 \\
\dot{y} &= V_E \cos\gamma - V_P - \frac{V_P}{R_P}\alpha_P\, r \sin\delta_2 \\
\dot{\gamma} &= -\frac{V_E}{R_E}\alpha_E \sin\phi_E + \frac{V_P}{R_P}\alpha_P \sin(\delta_2 - \delta_1) \\
\dot{\delta}_1 &= \frac{V_E}{R_E}\alpha_E \sin\gamma \cos\phi_E - \frac{1}{r}\left(V_E \sin\gamma \sin\delta_1 - \frac{V_P}{R_P}\alpha_P\, y \cos\delta_2\right)
\end{aligned} \tag{A-22}$$

The pursuer controls are α_P and δ_2 and the evader controls are α_E and ϕ_E.

In addition to Eq (A-22), V_E and V_P are state variables. Their differential equations can be approximated by

$$\begin{aligned}
\dot{V}_E &= g\left(\frac{T_E}{W_E} - \frac{D_E}{W_E}\right) \\
\dot{V}_P &= g\left(\frac{T_P}{W_P} - \frac{D_P}{W_P}\right)
\end{aligned} \tag{A-23}$$

where g is the acceleration of gravity, T is the thrust, D is the aerodynamic drag, and W is the weight. The weight is assumed to be constant, the thrust is controllable between minimum and maximum engine throttle settings, and the drag is a function of the normal acceleration, the speed, the altitude and speed brake drag. The rates $\dot{V}_E$ and $\dot{V}_P$ are the longitudinal accelerations identified in Eq (A-9). In general the equation for $\dot{V}$ contains an additional term which is a function of the weight and the flight path angle relative to the

horizontal plane. This term is negligible for small flight path angles, however. Therefore this analysis is restricted to situations wherein the difference T-D is dominant. The aerodynamic drag is related to the normal acceleration in the following way

$$D = \frac{1}{2} \rho S V^2 (C_{D_o} + k C_L^2) \qquad \text{(A-24)}$$

where ρ is the atmospheric density, S is a reference area on which C_{D_o} (the zero lift drag coefficient) and k (the induced drag parameter) are based and C_L is the aerodynamic lift coefficient. The normal acceleration is controlled by the magnitude of C_L. Rewriting Eq (A-24) gives

$$D = D_o + \frac{k}{QS} (QS\ C_L)^2$$

$$D_o = QS\ C_{D_o}$$

where Q is the dynamic pressure defined by

$$Q = \frac{1}{2} \rho V^2$$

The aerodynamic lift L is defined by

$$L = QS\ C_L$$

L is related approximately to the normal acceleration by

$$L = \frac{W}{g} a_N$$

D becomes

$$D = D_o + \frac{k}{QS} \left(\frac{W}{g} a_N \right)^2$$

Substitution into $\dot{V}$ gives

$$\dot{V} = g\left(\frac{T}{W} - \frac{D_o}{W} - \frac{kW}{g^2 QS} a_N^2\right)$$

$$= g\, C_T - \frac{kW}{gQS} a_N^2 \qquad \text{(a-25)}$$

where

$$C_T = \frac{T}{W} - \frac{D_o}{W}$$

is a control function dependent upon the throttle setting and speed brake setting. C_T is constrained by

$$C_{T_{MIN}} \leq C_T \leq C_{T_{MAX}} .$$

The normal acceleration and α are related according to Eq (A-10). Solving for α gives

$$\alpha = \frac{R}{V^2} a_N$$

Substitution into Eq (A-22) gives the following set of state differential equations:

$$\dot{r} = V_E \sin\gamma \cos\delta_1 + \frac{a_{N_P}}{V_P} y \sin\delta_2$$

$$\dot{y} = V_E \cos\gamma - V_P - \frac{a_{N_P}}{V_P} r \sin\delta_2$$

$$\dot{\gamma} = -\frac{a_{N_E}}{V_E} \sin\phi_E + \frac{a_{N_P}}{V_P} \sin(\delta_2 - \delta_1) \qquad \text{(A-26)}$$

$$\dot{\delta}_1 = \frac{a_{N_E}}{V_E} \sin\gamma \cos\phi_E - \frac{1}{r}\left(V_E \sin\gamma \sin\delta_1 - \frac{a_{N_P}}{V_P} y \cos\delta_2\right)$$

$$\dot{V}_E = g\, C_{T_E} - \frac{k_E W_E}{g\, Q_E S_E}\, a_{N_E}^2$$

$$\dot{V}_P = g\, C_{T_P} - \frac{k_P W_P}{g\, Q_P S_P}\, a_{N_P}^2$$

The control constraints are

$$0 \leq a_N \leq a_{N_{MAX}}$$

$$C_{T_{MIN}} \leq C_T \leq C_{T_{MAX}} \qquad \text{(A-27)}$$

Eqs (A-26) and (A-27) constitute the state variable differential equations and control constraints for Problem III.

APPENDIX B

PROBLEM II TRAJECTORY SOLUTION

The differential equations are

$$X' = -\epsilon \sin\psi + \alpha_p^* Y$$

$$Y' = -\epsilon \cos\psi + 1 - \alpha_p^* X$$

$$\psi' = \alpha_p^* - \epsilon R \alpha_E^*$$

Let X_o, Y_o, ψ_o correspond to initial or reference values.

Integration of ψ' gives

$$\psi = \psi_o + (\alpha_p^* - \epsilon R \alpha_E^*) \beta$$

Application of Laplace transforms to X' and Y' gives

$$zL(X) - \alpha_p^* L(Y) = -\epsilon L(\sin\psi) + X_o$$

$$\alpha_p^* L(X) + zL(Y) = -\epsilon L(\cos\psi) + \frac{1}{z} + Y_o$$

The solutions for $L(X)$ and $L(Y)$ are easily obtained

$$L(X) = \frac{z}{z^2+\alpha_p^{*2}}\left[-\epsilon L(\sin\psi) + X_o\right] + \frac{\alpha_p^*}{z^2+\alpha_p^{*2}}\left[-\epsilon L(\cos\psi) + \frac{1}{z} + Y_o\right]$$

$$L(Y) = \frac{z}{z^2+\alpha_p^{*2}}\left[-\epsilon L(\cos\psi) + \frac{1}{z} + Y_o\right] - \frac{\alpha_p^*}{z^2+\alpha_p^{*2}}\left[-\epsilon L(\sin\psi) + X_o\right]$$

For the natural barrier, set $\theta = S_1 = S = \cos^{-1} \epsilon$.

On the tributaries replace β with $\beta - \beta_o$ where β_o is the time of travel on the singular arc. The values X_o and Y_o are $X(\beta_o)$ and $Y(\beta_o)$ on the singular arcs. Substitution of the singular arc solution gives

$$X_o = \bar{L} \sin \alpha_P^* (\theta + \beta_o) + \alpha_P^*(1 - \cos \alpha_P^* \beta_o) - \epsilon\beta_o \sin \alpha_P^* (S_1 + \beta_o)$$

$$Y_o = \bar{L} \cos \alpha_P^* (\theta + \beta_o) + \alpha_P^* \sin \alpha_P^* \beta_o - \epsilon\beta_o \cos \alpha_P^*(S_1 + \beta_o)$$

$$\psi_o = \alpha_P^* (S_1 + \beta_o)$$

The tributary trajectory equations are

$$X = \bar{L} \sin \alpha_P^*(\theta + \beta) + \alpha_P^*(1 - \cos \alpha_P^* \beta) - \epsilon\beta_o \sin \alpha_P^* (S_1 + \beta)$$
$$- \frac{\alpha_E^*}{R} [\cos \psi - \cos \alpha_P^* (S_1 + \beta)]$$

$$Y = \bar{L} \cos \alpha_P^* (\theta + \beta) + \alpha_P^* \sin \alpha_P^* \beta - \epsilon\beta_o \cos \alpha_P^* (S_1 + \beta)$$
$$+ \frac{\alpha_E^*}{R} [\sin \psi - \sin \alpha_P^* (S_1 + \beta)]$$

$$\psi = \alpha_P^* (S_2 + \beta) - \epsilon R \alpha_E^*(\beta - \beta_o) \qquad OK$$

For the natural barrier set $\theta = S_1 = S$.

Laplace inversion formulas and the convolution property give

$$X = X_o \cos \alpha_P^*\beta + Y_o \sin \alpha_P^* \beta + \alpha_P^*(1 - \cos \alpha_P^* \beta)$$
$$- \frac{\alpha_E^*}{R} [\cos \psi - \cos (\psi_o + \alpha_P^* \beta)]$$

$$Y = -X_o \sin \alpha_P^* \beta + Y_o \cos \alpha_P^* \beta + \alpha_P^* \sin \alpha_P^* \beta + \frac{\alpha_E^*}{R} [\sin \psi - \sin (\psi_o + \alpha_P^* \beta)]$$

The situation on the singular arc is different since $\alpha_E^* = 0$. The convolution property gives

$$X = X_o \cos \alpha_P^* \beta + Y_o \sin \alpha_P^* \beta + \alpha_P^*(1 - \cos \alpha_P^* \beta) - \epsilon \beta \sin (\psi_o + \alpha_P^* \beta)$$

$$Y = -X_o \sin \alpha_P^* \beta + Y_o \cos \alpha_P^* \beta + \alpha_P^* \sin \alpha_P^* \beta - \epsilon \beta \cos (\psi_o + \alpha_P^* \beta)$$

The boundary conditions for the artificial barrier can be written as follows for trajectories emanating on the BUP.

$$X_o = \bar{L} \sin \alpha_P^* \theta$$

$$Y_o = \bar{L} \cos \alpha_P^* \theta$$

$$\psi_o = S_2$$

The equations for X, Y, and ψ become

$$X = \bar{L} \sin \alpha_P^* (\theta + \beta) + \alpha_P^*(1 - \cos \alpha_P^* \beta) - \frac{\alpha_E^*}{R} [\cos \psi - \cos(S_2 + \alpha_P^* \beta)]$$

$$Y = \bar{L} \cos \alpha_P^*(\theta + \beta) + \alpha_P^* \sin \alpha_P^* \beta + \frac{\alpha_E^*}{R} [\sin \psi - \sin (S_2 + \alpha_P^* \beta)]$$

$$\psi = S_2 + (\alpha_P^* - \epsilon R \alpha_E^*) \beta$$

For the natural barrier simply set $\theta = S_1$. On the singular arcs

$$X_o = \bar{L} \sin \alpha_p^* \theta$$

$$Y_o = \bar{L} \cos \alpha_p^* \theta$$

$$\psi_o = \alpha_p^* S_2 = \alpha_p^* S_1$$

The trajectory equations are

$$X = \bar{L} \sin \alpha_p^* (\theta + \beta) + \alpha_p^* (1 - \cos \alpha_p^* \beta) - \epsilon \beta \sin \alpha_p^* (S_1 + \beta)$$

$$Y = \bar{L} \cos \alpha_p^* (\theta + \beta) + \alpha_p^* \sin \alpha_p^* \beta - \epsilon \beta \cos \alpha_p^* (S_1 + \beta)$$

$$\psi = \alpha_p^* (S_1 + \beta)$$

REFERENCES

1. Isaacs, Rufus. Differential Games: A Mathematical Theory with Applications to Warfare and Pursuit, Control and Optimization. New York: John Wiley and Sons, Inc., 1965.

2. Breakwell, J. V., and Merz, A. W. "Towards a Complete Solution of the Homocidal Chauffeur Game." Proceedings of the First International Conference on the Theory and Applications of Differential Games. Amherst, Mass., 1969.

3. Miller, L. E. Tactics Optimization Study: Constant Speed Case. Report ASBES WP 68-8, Wright-Patterson Air Force Base, Ohio, 1968.

4. Lynch, U. H. D. Differential Game Barriers and Their Applications in Air-to-Air Combat. Ph.D. Dissertation, DS/ML/73-1, Air Force Institute of Technology, School of Engineering, Wright-Patterson Air Force Base, Ohio, 1973.

5. Othling, W. L. Application of Differential Game Theory to Pursuit-Evasion Problems of Two Aircraft. Ph.D. Dissertation, DS/MC/67-1, Air Force Institute of Technology, School of Engineering, Wright-Patterson Air Force Base, Ohio, 1970.

6. Miller, L. E. "Tactics Optimization Study: Variable Speed Case." Proceedings of the First International Conference on the Theory and Applications of Differential Games. Amherst, Mass., 1969.

7. Starr, A. W. Nonzero - Sum Differential Games: Concepts and Models. Technical Report No. 590, Harvard University, Cambridge, Mass., 1969.

8. Case, J. H. "Toward a Theory of Many Player Differential Games." SIAM Journal Control, Vol. 7, No. 2 (May 1969), 179-197.

9. Prasad, U. R. N-Person Differential Games and Multicriterion Optimal Control Problems. Ph.D. Dissertation, Indian Institute of Technology Kanpur, Kanpur, India, 1969.

10. Leatham, A. L. Some Theoretical Aspects of Nonzero Sum Differential Games and Applications to Combat Problems. Ph.D. Dissertation, DS/MC/71-3, Air Force Institute of Technology, School of Engineering, Wright-Patterson Air Force Base, Ohio, 1971.

11. Roberts, D. A., and Montgomery, R. C. Development and Application of a Gradient Method for Solving Differential Games. NASA TN D-6502, Langley Research Center, National Aeronautics and Space Administration, Hampton, Va., 1971.

12. Graham, R.G. Quasilinearization Solutions of Differential Games and Evaluation of Suboptimal Strategies. UCLA-ENG-7128, School of Engineering and Applied Science, University of California Los Angeles, California, 1971.

13. Lin, H. S. Contributions to the Theory and Applications of Pursuit-Evasion Games. Report No. 70-22, School of Engineering and Applied Science, University of California Los Angeles, California, 1970.

14. McFarland, W. W. New Techniques for the Solution of Differential Games. Ph.D. Dissertation, Massachusetts Institute of Technology, Cambridge, Massachusetts, 1970.

☆ U. S. GOVERNMENT PRINTING OFFICE: 1975 — 657-630/180